Galactose-Decorated Polymers and Nanogels Synthesized via Reversible Addition-Fragmentation Chain Transfer Polymerization for *in vitro* Tumor Targeted Drug Delivery and Gene Knockdown

by

Stephen Quan

A thesis submitted in partial fulfillment of the requirements for the degree of

Master of Science

in

Chemical Engineering

Department of Chemical and Materials Engineering
University of Alberta

Abstract

The first part of this thesis focuses on the synthesis and development of thermosensitive galactose-based nanogels, evaluating their potential in encapsulating and releasing Iodoazomycin Arabinofuranoside (IAZA), a clinical drug for imaging solid hypoxic tumors, for its hypoxia-selective theranostic (therapy + diagnostic) potential in the management of hepatocellular carcinoma. The shell of the nanogels is decorated with galactose molecules to facilitate asialoglycoprotein receptor (ASGPR)-mediated uptake in HepG2 cells. The nanogels were synthesized *via* reversible-addition fragmentation chain transfer (RAFT) polymerization having a temperature responsive core and permanently hydrophilic shell. The molecular size of the nanogel, cross-linker concentration and the presence of cationic/anionic moieties impacted the encapsulation efficiency of IAZA. The release profile of IAZA from the nanogels' core demonstrated a stable, non-burst release of IAZA over time with excellent biocompatibility. The radiosensitization studies with *nanogel-IAZA* demonstrated that IAZA in encapsulated form offers superior radiosensitization capacity of hypoxic cells as compared to the parent IAZA drug.

The second part of the thesis describes the synthesis of a series of statistical and block glycopolymers composed of 2-lactobionamidoethyl methacrylamide (LAEMA) and cationic monomer 2-aminoethylmethacrylamide hydrochloride (AEMA) for the delivery of epidermal growth factor receptor (EGFR)-small interfering RNA (siRNA) knockdown in HeLa cells. The colloidal stability of the glycopolymer-siRNA complexes was assessed by dynamic light scattering (DLS) and gel electrophoresis in the presence and absence of serum proteins. Their cytotoxicity, cellular uptake and transfection efficiencies were examined in HeLa cells. The shortest AEMA diblock glycopolymer was the most effective in EGFR gene silencing, however

it exhibited a higher toxicity profile in comparison to its statistical counterpart at higher weight/weight ratios. Regardless of the presence or absence of serum proteins, the glycopolymer-siRNA polyplexes demonstrated excellent knockdown efficacies.

Preliminary *in vitro* studies indicate that delivering IAZA drug in encapsulated form enhanced the radiosensitization of hypoxic hepatocellular cancer cells. Additional studies with EGFR gene knockdown in HeLa cells was achieved using EGFR siRNA complexed with galactose-based diblock glycopolymers synthesized *via* RAFT polymerization. In future studies, galactose-decorated nanogels will be used to assess the delivery and radiotherapeutic potential of radioiodinated IAZA to hypoxic HepG2 cells, along with *in vivo* biological evaluation of galactose-based nanogels in physiological organs for their capacity in targeting liver carcinoma and delivering IAZA for radiotherapeutic treatments. Future studies with cationic galactose-based polymers will be pursed and evaluated *in vivo* to demonstrate their potential as polymeric macromolecule carriers for increased sensitivity, biocompatibility and targeting in gene knockdown using mammalian models. Furthermore, additional studies to evaluate the efficacy and capacity of galactose-based nanogel to deliver other nitroimidazole-derived radiosensitization agents and small molecule drug compounds will also be useful. Finally, other monosaccharide carbohydrate-based polymer systems, such as glucose and mannose, should be evaluated for their *in vivo* and *in vitro* applications in drug delivery and gene knockdown.

Acknowledgment

Health, wealth and happiness to everyone who joined me for this endeavor. I would like to give appreciation to my supervisors Dr. Ravin Narain and Dr. Piyush Kumar for investing their time, nurturing my academic progressions and giving me the opportunity to work under their guidance. Harmonizing my knowledge and insights, I have gained many experiences which have helped me grow academically and personally.

I would also like to express my appreciation to lab colleagues who helped me progress my research during tough times. I sincerely wish them all the best in their future ingenuities and endeavors.

Engaged in funding my research, I would like to thank the Natural Sciences and Engineering Research Council of Canada (NSERC), Discovery CREATE Molecular Imaging Probes and Alberta Innovates Health Solutions CRIO Program grant (PK).

Last, but not least, I would like to thank my family and Hanhmi for their support and love through this entire journey.

Table of Contents

List of Tables

List of Figures

Abbreviations

AEMA: 2-Aminoethyl Methacrylamide Hydrochloride

ACVA: 4-Cyanovaleric acid

ASGPR: Asialoglycoprotein Receptor

CL: Crosslinker

CTA: Chain Transfer Agent

CTP: 4-Cyanopentanoic acid dithiobenzoate

DEGMA: Di(ethylene glycol)methylethylmethacrylate

DLS: Dynamic Light Scattering

DMEM: Dulbecco`s Modified Eagle Medium

DMF: *N,N`*-Dimethyl Formaldehyde

DMSO: Dimethyl Sulfoxide

DNA: Deoxyribonucleic Acid

EGFR: Epidermal Growth Factor Receptor

FAZA: 1-α-(5-Deoxy-5-fluoroarabinofuranosyl)-2-nitroimidazole

FBS: Fetal Bovine Serum

FITC: Fluorescein Isothiocyanate

FMISO: Fluoromisonidazole

GPC: Gel Permeation Chromatography

HeLa: Cervical Adenocarcinoma

Hep G2: Hepatocellular Carcinoma

HPLC: High Pressure Liquid Chromatography

HRP: Horse Radish Peroxidase

IAZA- 1-α-(5-Deoxy-5-iodoarabinofuranosyl)-2-nitroimidazole

IgG: Immunoglobulin G

LAEMA: 2-Lactobionamidoethyl Methacrylamide Hydrochloride

LALLS: Low Angle Laser Light Scattering

LCST: Lower Critical Solution Temperature

LET: Linear Energy Transfer

MA: Methacylamide

MALLS: Multi Angle Laser Light Scattering

MBam: N,N'-Methylenebisacrylamide

MCF-7: Human Breast Cancer

MFI: Mean Fluorescence Intensity

MRC-5: Human Fetal Lung Fibroblast

MTT: 3-(4,5-Dimethylthiazol-2-yl)-2,5-diphenyltetrazolium Bromide

*M*n: Number Average Molecular Weight

*M*w: Weight Average Molecular Weight

*M*n/*M*w: Molecular Weight Distribution

NG: Nanogel

NMR: Nuclear Magnetic Resonance

OMEM: Eagles Minimal Essential Medium

PEI: Polyethylenimine

PET: Position Emission Tomography

PDI: Polydispersity Index

PBS: Phosphate Buffered Saline

RAFT: Reversible Addition-Fragmentation Chain Transfer Polymerization

RITC: Rhodamine Isothiocyanate

RI: Refractive Index

Rh: Hydrodynamic Radius

SEC: Size Exclusion Chromatography

SER: Sensitization Enhancement Ratio

siRNA: Small Interfering Ribonucleic Acid

SPECT: Single Photon Emission Computed Tomography

TAE: Tris-Acetate-EDTA TBS: Tris Buffered Saline

TEM: Transmission Electron Microscopy

TMB: 3,3′, 5,5′-tetramethylbenzidine

UV-VIS Spec- Ultraviolet-Visible Spectroscopy

Ve: Elution Volume

Vh: Hydrodynamic Volume

Vi: Interstitial Volume

Vp: Pore Volume

W/w: Weight/Weight

General Introduction

This thesis is comprised of five chapters:

Chapter 1 introduces the general concept of polymerization and more specifically, it elaborates on the reversible addition-fragmentation chain transfer (RAFT) polymerization technique and its versatile suitability in biomedical applications. The characteristics of stimuli-responsive monomers and their general properties are explained with brief details about the temperature responsive monomer di(ethylene glycol) methyl ethyl methacrylate (DEGMA) and its role in thermo-responsive nanogels. The general biological concept of tissue hypoxia and its significance in cancer management are reviewed. The role of the asialoglycoprotein receptor (ASGPR) expressed in hepatocellular carcinoma (HCC) and its importance in mediating galactose binding and endocytosis are discussed. The development of nanogel-encapsulated hypoxia-selective drug Iodoazomycin Arabinofuranoside (IAZA) that has been used in clinical imaging (as a radioiodinated pharmaceutical) in cancer patients diagnosed with solid hypoxic tumors is deliberated. The impacts of parent IAZA drug and nanogel-encapsulated IAZA in enhancing the radiosensitization potential of hypoxic HCC is discussed. The aim of this project was to characterize and evaluate the efficacy of galactose-decorated thermo-responsive nanogels for the delivery of IAZA to demonstrate its potential as a radiosensitizer in theranostic (therapy +diagnostic) management of hypoxic HCC.

Chapter 2 introduces the techniques used in determining statistical chemical analysis of small molecules and characterize the polymers/nanogels synthesized by RAFT polymerization. Gel permeation chromatography (GPC) was used to determine the polymer molecular weights and

molecular weight distributions. Dynamic light scattering (DLS) was used to evaluate the hydrodynamic size of the polymers and nanogels in aqueous solutions. Nuclear magnetic resonance (NMR) was used to determine the chemical composition and structure of the polymer chain. Flow cytometry utilizing light scattering methods and fluorescence detection allows for the physical and chemical characterizations of single particles, usually cells, as they pass through a laser-based detection system. Gel electrophoresis allows us to determine the binding capacity of polymers with DNA or RNA to form stable polyplex structures. (3-(4,5-Dimethylthiazol-2-yl)-2,5-diphenyltetrazolum bromide)) (MTT) assay facilitates the determination of cytotoxicity of polymeric and small molecule in cell culture. Enzyme-linked immunosorbent assay (ELISA) offers the determination of the presence of antigens or ligands by application of highly-specific antibody detection agents.

Chapter 3 is focused on the detailed study of thermosensitive nanogels synthesized by RAFT polymerization that was used for the encapsulation and delivery of IAZA to hypoxic HCC. The nanogels have a cross-linked temperature responsive core that has a multivalent display of galactose on the outer shell. The thermo-responsive nature allows for the controlled encapsulation of IAZA above the lower critical solution temperature (LCST) and the galactose shell mediates uptake via the ASGPR pathway. The nanogel-IAZA system demonstrated a stable, non-burst release of IAZA with a maximum loading capacity of IAZA within the core. The cytotoxicity was found to be highly biocompatible in multiple cell lines. The radiosensitization studies indicated that IAZA in the encapsulated form offers a superior radiosensitization of hypoxic cells compared to free form (sensitization enhancement ratio [SER] of 1.33 and 1.62 for free IAZA and nanogel encapsulated IAZA, respectively).

Chapter 4 discusses the synthesis of a series of block and statistical copolymers composed of 2-lactobionamidoethyl methacrylamide (LAEMA) and cationic monomer 2-aminoethylmethacrylamide hydrochloride (AEMA) by RAFT polymerization, and their applications in delivering epidermal growth factor receptor (EGFR) small interfering RNA (siRNA) to cervical adenocarcinoma cells. The colloidal stability of the polyplexes was evaluated by dynamic light scattering (DLS) and gel electrophoresis in the presence and absence of serum proteins. The transfection studies indicated that the shortest AEMA diblock glycopolymer was the most effective at silencing EGFR expression in HeLa cells, but was considerably more toxic as compared to its statistical counterpart at higher W/w ratios. The glycopolymer-siRNA complexes demonstrated excellent knockdown efficacies in the absence and presence of serum proteins.

Chapter 5 summarizes the research findings and elaborates on future insights, directions and the experiments that can be pursued to evolve the biomedical applications of these nanogels and glycopolymers. The application of thermosensitive nanogels are reported for the targeted drug delivery of IAZA to hypoxic HCC cells. Cationic glycopolymers are evaluated for gene delivery purposes in EGFR-siRNA knockdown in cervical adenocarcinoma cells.

1 Introduction

1.1 Techniques of Polymerization

Polymers are incredibly versatile materials that can be functionally tuned to enable the properties required for specialized tasks. Over the past decade, the applications of polymers have expanded from their typical industrial bulk material production to more advanced forms of research in nanotechnology, biomaterials and health care [1-3]. The overall process of polymerization creates polymer chains and three-dimensional networks by the subsequent addition reaction of monomeric subunits. Polymerization can be classified into two main categories: chain growth polymerization and step growth polymerization [4]. Free radical polymerization, a chain growth method, is one of the most versatile methods and compatible with a broad range of monomer units. However some limitations such as low control over polydispersity, lack of control over polymer growth kinetics and the inability to synthesise block copolymers hinder its effectiveness [4, 5]. On the other hand, living radical polymerization, also known as controlled free radical polymerization, allows unprecedented control over the simultaneous growth of all polymer chains through the absence of chain transfer and termination, thus resulting in a narrow molecular weight distribution of the synthesized polymers. Additionally, living radical polymerization has negligible chain transfer and termination reactions, and propagation resumes upon the introduction of additional monomers, thus providing the opportunity to control the properties and composition of the bulk material at a molecular level [6]. In particular, RAFT polymerization is a very effective type of chain-growth polymerization, and will be focussed here (Figure 1-1).

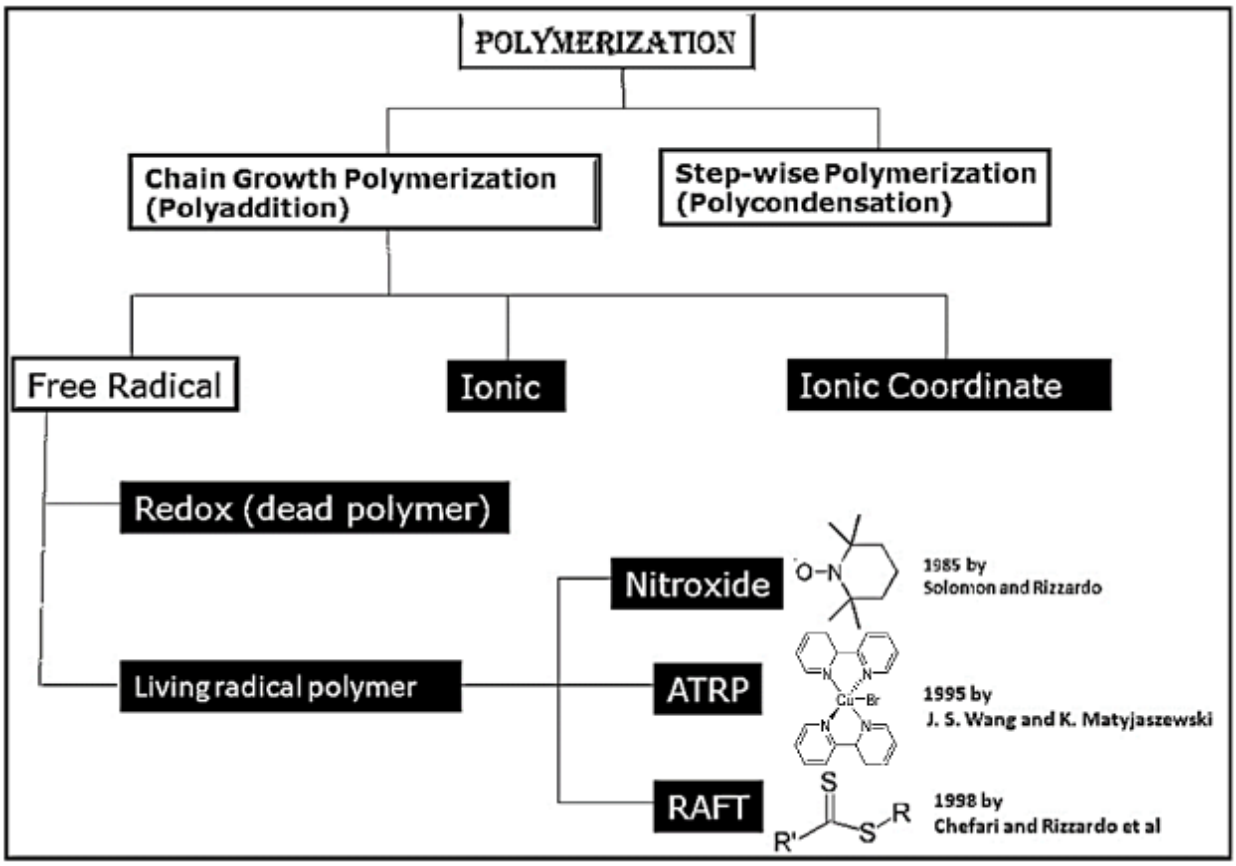

Figure 1-1. Overview of polymerization techniques by chain growth and step-wise polymerization [6].

In free radical polymerization, the polymer is synthesized in a linear fashion by the successive addition of monomeric units. The growth of polymer molecules is governed by a kinetic chain of reactions depicted by three distinct steps [7]:

1. *Initiation:* an active radical site is formed at a vinyl double bond on a monomer after the initiator is activated (thermal decomposition, photolysis, redox, etc.)
2. *Propagation*: activated monomer reacts with free monomer on the vinyl double bond thus successively adding monomers on the polymer chain and regenerating the active radical site (radical stability and steric hindrance governs radical generating on 3^o or 2^o carbon)

3. *Termination*: Under steady state assumption, propagation reactions should occur until all free monomeric units are polymerized, however the growth of polymer chains are usually terminated by combination or disproportionation reactions. Combination terminations occur when two polymer radical species react to form a single bonded product without radicals. Disproportionation terminations occur when a radical species abstracts a proton from another primary carbon on a polymer, thus generating a polymer with a newly formed double bond and another polymer with a regenerated single bond.

1.2 Reversible Addition-Fragmentation Chain Transfer (RAFT) Mechanism

RAFT is a type of living polymerization technique that was first reported in 1998 by Rizzardo and colleagues [4]. The RAFT technique has gained significant importance in the field of polymer chemistry due to its unprecedented control over molecular weight distributions, architecture, compositions and versatility to polymerize a variety of monomers (methacrylamide, methacrylates, acrylates, acrylamides and styrene) in a one-step process using various solvents [8]. Most notably, RAFT technique does not utilize any toxic metal or carcinogenic substrate as catalyst, resulting in its wide acceptance and preference in biomedical applications. Figure 1-2 outlines the mechanism of the RAFT polymerization process.

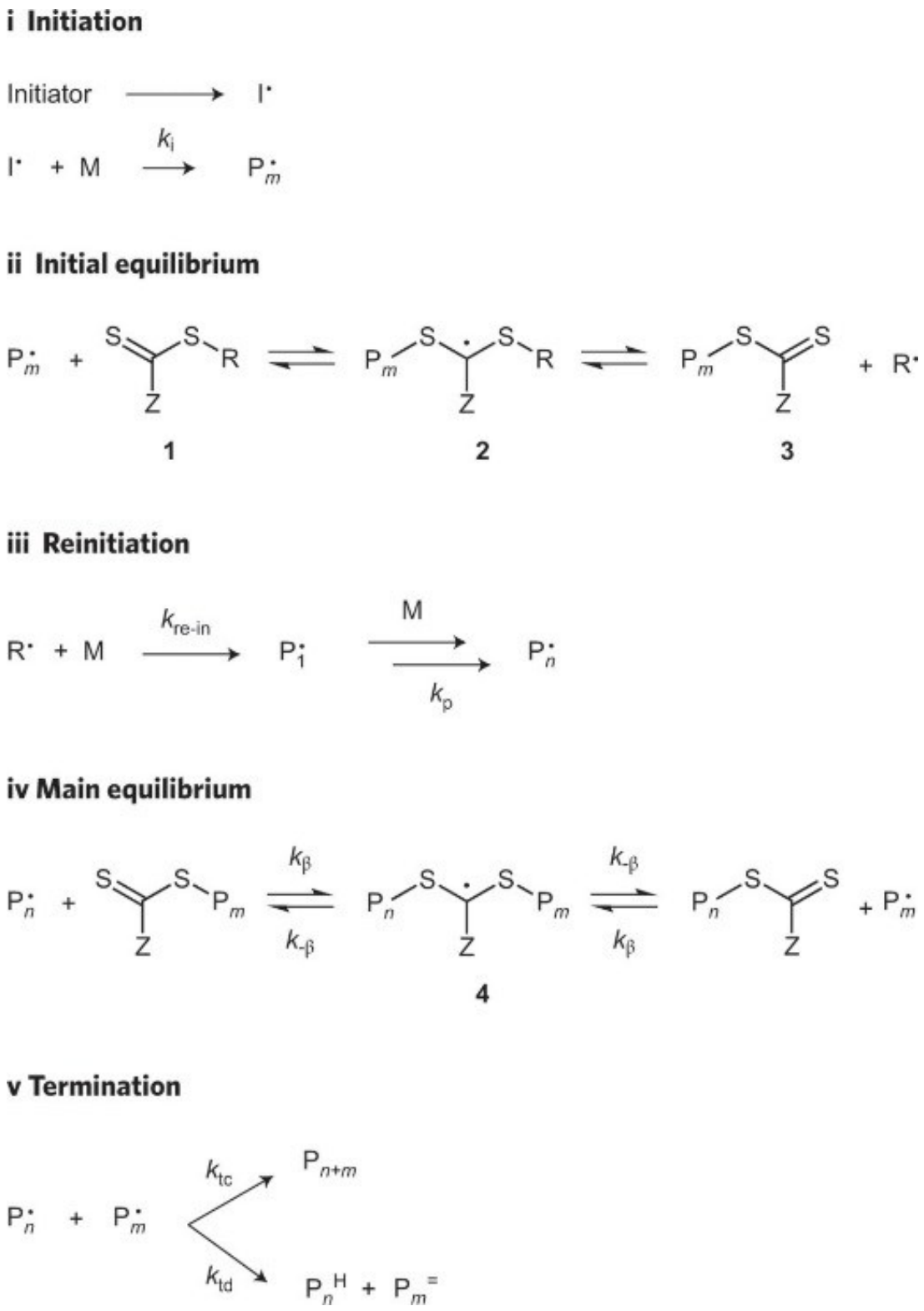

Figure 1-2. Mechanism of RAFT polymerization technique [9].

Step 1 Initiation: The initiator decomposes to form two radical species which react with free monomeric units to generate a propagating radical monomer P_m.

Step 2 Pre-equilibrium: The propagating radical monomer P_m. reacts with the C=S double bond, creating a radical intermediate and rearranging to generate a leaving group R.

Step 3 Reinitiation: The radical leaving group reacts with another free monomer to generate the propagating radical monomer P_n. Kinetically, all chain transfer agents (CTAs) should be activated and reacted with P_m before propagation takes place since the C=S bond is highly reactive, and the rate of addition/fragmentation are faster than the rate of propagation.

Step 4 Main Equilibrium: The newly generated $P_{n\cdot}$ radical monomer reacts with growing polymer chains on C=S double bond creating a radical intermediate and rearranging to generate $P_{m\cdot}$ as a leaving group to reinitiate another monomer. Ideally, the radicals are generated equally and thus causing equal opportunities for polymer chains to grow and control the polydispersity.

Step 5 Termination: Once all free monomers are polymerized, active radicals site on polymer chains combine by proportionation or disproportionation to quench the radical species.

RAFT uses dithioester-based compounds as chain transfer agents (CTA), also known as RAFT agents, to control uniform growth of polymer chains and prevent chain termination. An effective RAFT agent polymerization requires that (1) both rates of addition and fragmentation must be fast relative to the rate of propagation, and (2) the expelled radical must be capable of reinitiating polymerization [10] (Figure 1-3).

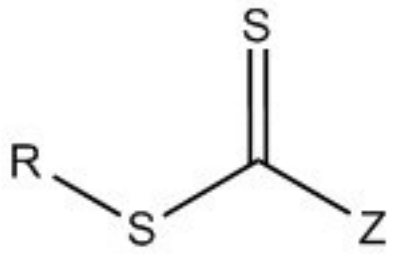

Figure 1-3. Structure of RAFT chain transfer agent

In essence, CTAs modulate the lifetime of a growing polymer chain and create more polymer chains than would be forming in their absence, leading to lower degrees of polymerization. The moles of CTA required for the synthesis of a polymers target molecular weight can be calculated as follows:

$$M_n(theory) = \left(\frac{[Monomer]_o}{[CTA]_o}\right) x\ M_w(monomer)$$

The solubility and reactivity of RAFT agents depend on the substituent R and Z groups, which can be classified as dithiobenzoates, trithiocarbonates and dithiocarbamates based on the pendent groups. The Z groups modulate the rates of addition and fragmentation during polymerizations, while the R group should have a weak S-R bond so it can act as a good leaving group and react with free monomers [7].

1.3 Thermosensitive Polymers

Stimuli-responsive polymers mimic biological systems in which an external stimulus can modify the size and solubility of the material. These external stimuli include pH, temperature, heat, sound and the concentration [11-13]. Stimuli-responsive behaviour is extremely advantageous for the preparation of "smart delivery systems" which can offer highly stable control over the delivery of therapeutics, and can be tuned for optimizing its role in biomedical applications. Physiological conditions in different tissues and organs exhibit unique biological environments, therefore engineering drug carriers with specific stimuli responsive properties that can exploit biological differences in organs and tissues can be highly beneficial for facilitating cell-specific targeting [12, 14, 15].

Thermo-responsive polymers undergo a reversible volume phase change from a swollen hydrated state (hydrophilic) to a shrunken dehydrated state (hydrophobic), also known as a coil-to-globule transition [16]. This behaviour is governed by the lower critical solution temperature (LCST) of the polymer solution, and is defined by a critical temperature threshold in which the components are miscible and undergo a coil-to-globule transition below this temperature, for example, polymeric solutions of N-isopropylacrylamide (NIPAM), N,N-diethylacrylamide (DEAM) and di(ethylene glycol) methyl ethyl methacrylate (DEGMA) (Figure 1-4) [17, 18].

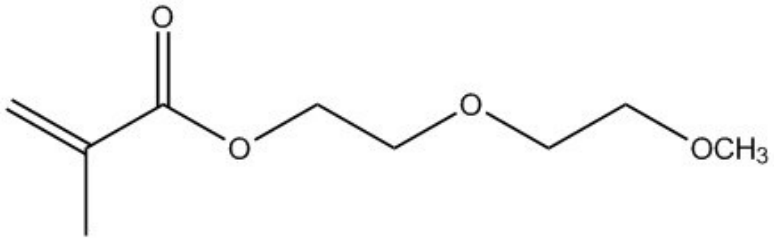

Figure 1-4. Structure of di(ethylene glycol)methylethylmethacrylate

Alternatively, the phase change behaviour can also be defined by the upper critical solution temperature (UCST), in which the polymer solution is completely miscible and undergoes a coil-to-globule transition above the critical temperature threshold of the system, for example, polymeric solutions of 2-hydroxyl methacrylate (HEMA) and 3-dimethyl(methacryloyloxyethyl) ammonium propane sulfonate (DMAPS) [15, 19, 20]. This phenomenon happens because it is energetically more favorable to assume a hydrophobic or hydrophilic state based on the energy of the system, governed by Gibbs free energy equation:

$$\Delta G = \Delta H - T\Delta S$$

where G = Gibbs free energy, H = enthalpy and S = entropy [21-23]. A key factor in driving the LCST of the solution is the thermodynamic mixture behaviour that is governed by the dominating unfavorable entropy of mixing; where the solution is completely miscible and forms strong hydrogen bonds below the LCST [24]. In essence, the hydrogen bonding properties of the polymer dictate the system, depending on whether intramolecular hydrogen bonding between polymers or intermolecular hydrogen bonding with water molecules is favored (Figure 1-5) [25].

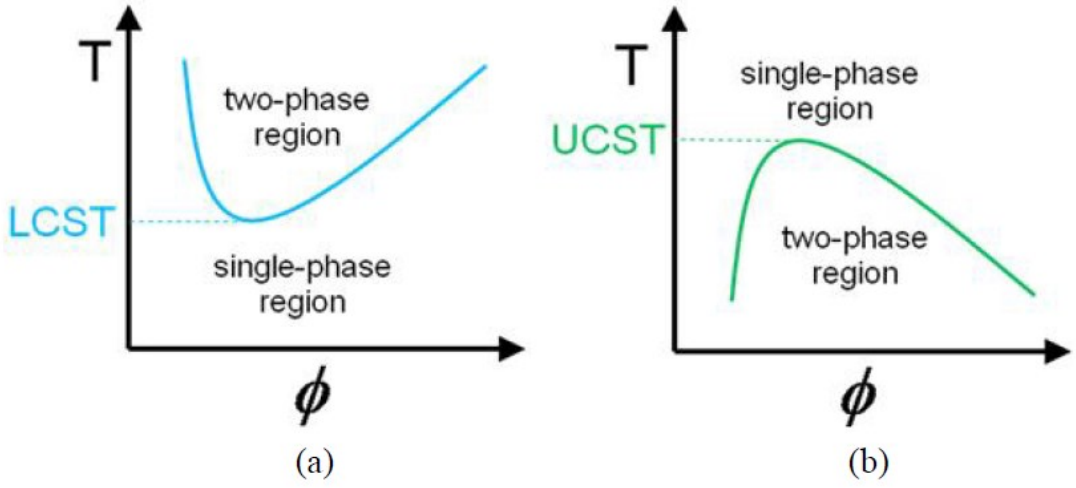

Figure 1-5. Schematic illustration of temperature vs polymer volume fraction for polymer solutions displaying lower critical solution temperature (LCST) and upper critical solution temperature (UCST) behaviour [25].

1.4 Stimuli-Responsive Nanogels for Drug Delivery

Nanogels are swollen cross-linked networks composed of hydrophilic or amphiphlic polymers, which offer many highly tunable characteristics, such as particle size, cationic/anionic nature, multivalent surface modification and biodegradability that can facilitate the encapsulation and delivery of various macromolecules [26-28]. Due to the high degree of control over these particles, the behaviour can be precisely engineered for the development of stimuli-responsive "smart drug delivery" systems. The sizes of nanogels are highly dependent on the length of the polymer chains and the cross-linker used within the core. Previous studies have demonstrated that the hydrodynamic size of nanogels increases as a function of increasing cross-linker percentage [29]. Interestingly, while the size of the particle directly affects the loading capacity of the nanogel, other parameters such as swelling/collapse ratio, pore size and functionalization with charged moieties (cationic/anionic) also impact the encapsulation ratio of macromolecules [19, 30]. The control of macromolecule encapsulation efficiency and drug release mechanisms is crucial when dealing with nanogels. With nanogel drug delivery systems, the encapsulation efficiency of the macromolecule should be relatively abundant with a highly controlled mechanism of release of the drug from the core [27]. Depending on the constituent monomers involved in the synthesis of the nanogel, the mechanism of release can be one of the following:

1) Simple Diffusion – The drug is released from the core of the nanogel through the pores/network in a slow, passive manner [31].
2) Nanogel Degradation – The drug is released via mechanisms of degradation of either the cross-linker or dissolution of the nanogel complex. This mechanism of release is dependent on the cross-linker hydrolysis and rate of polymer degradation [32].

3) Swelling and Collapsing – The drug is released via the LCST/UCST phenomenon of nanogel through increased or decreased pore sizes at different biological temperatures [30].
4) External Stimuli – The drug is released in a controlled fashion where an external stimulus is applied, such as light, pH change, magnetic or sound, which causes the nanogel to degrade or undergo conformational changes [33, 34].

In this study, galactose-based nanogels with thermosensitive monomer DEGMA in the cross-linked core have been synthesized via RAFT polymerization methods. The thermo-sensitive nanogel was used to encapsulate drug molecules, and the release profile of the drug from core was assessed via swelling and collapsing methods based on the LCST.

1.5 Hepatocellular Carcinoma and Asialoglycoprotein Receptor

The asialoglycoprotein receptor (ASGPR) is a 46-kDa transmembrane endocytotic cell surface receptor which is predominantly expressed in hepatocytes, and facilitates the uptake of macromolecules triggered by triantennary binding of terminally exposed galactose residues [31, 35]. The ability to transport macromolecules across the hepatocyte cellular membrane has made this receptor an intriguing tool for developing galactosylated drug delivery systems and use them in receptor-mediated delivery of therapeutics to hepatocytes [31, 35]. Previous studies have shown HepG2 cells express a high binding affinity (K_d = 7 x 10^{-9} M) of up to 500,000 ASGPRs per cell compared to fewer cell surface receptors binding sites per cell, such as insulin receptors in adipocytes which express only 10,000 per cell [35]. Other studies have shown that HepG2 cells have approximately 88% unoccupied receptors, and the rate of uptake and degradation of the native binding ligand, asialo-orosomucoid, is based on ligand concentration with maximum receptor saturation at 10ug/mL [38]. ASGPR is known as an endocytic cell surface receptor to internalize ligands for degradation in the lysosome compartment, however the exact mechanism and biochemical pathway of bound ligands to get internalized is still unknown [39-41]. By exploiting the overexpression of ASGPR-mediated uptake in hepatocytes, galactosylated delivery vesicles such as liposomes, micelles, nanogels and dendrimers have been extensively studied for their capability to deliver therapeutic genes and drug macromolecules to target hepatocytes [42-45]. Carbohydrate-based monomers have been the subject of intense evaluation due to their unique properties in cell surface receptor-ligand-mediated interaction, high biocompatibility and low cytotoxicity. In particular, 2-lactobionoamidoethyl methacrylate (LAEMA) is a galactose-based glycomonomer which can be synthesized by reacting 2-aminoethyl methacrylate (AEMA) with lactobionolactone under basic conditions [46]. Lately,

LAEMA and galactosylated polymers have been under intense evaluation for their potential in targeting ASGPR via carbohydrate-protein recognition interactions for drugs and gene delivery [46-48].

1.6 Tissue Hypoxia, Nitroimidazole-based Drugs and Hypoxia Imaging

Decreased tissue oxygen tension, clinically referred to as hypoxia, is a physiological condition in which the affected cells demonstrate lower oxygen levels in comparison to healthy cells. Hypoxic cells are inadequately oxygenated due to poor vasculature, insufficient blood supply (ischemia) or lower levels of oxygen in the blood [49, 50], which is typically observed due to the constraints of blood supply and vascular tissue formation that are inadequate to meet oxygen demands [51]. In cancer, hypoxia induces a more aggressive and metastatic phenotype causing the activation of uncontrolled cellular signalling pathways which affect angiogenesis, proliferation and apoptosis [49, 52]. Generally, solid hypoxic tumors are highly associated with poor patient prognosis and their cells have been shown to be 2-3x more resistant to the killing effects of radio- and chemotherapy as compared to normally oxygenated cells [53]. The presence of hypoxic regions within a tumor results in a higher probability of tumor recurrence, ultimately leading to therapy failure and poor survival of the patient. Therefore, there is an unprecedented need for the accurate evaluation and management of hypoxic tumors to develop innovative alternate treatments for cancer management and to improve patients' outcome.

A class of bioreductively-activated compounds, known as nitroimidazoles, has been observed to undergo enzymatic intracellular reduction depending on the concentration of oxygen available in

the tissue [51]. These compounds act as “oxygen mimetics”, which enhances the sensitivity of hypoxic cells to chemo- and radio-therapeutic treatments. Under the bioreductive microenvironment in hypoxic tissue, nitroimidazoles undergo a process called single electron transfer, where the nitro group is step-wise reduced by a total of six electrons to produce hydroxyl, hydroxylamino and amine radical intermediate products that form covalent macromolecular adducts with DNA and proteins within the hypoxic cell (Figure 1-6) [54]. This forms the basis of theranostic intervention of hypoxic tumors using nitroimidazole-based molecules. The first electron reduction is a reversible process, ensuring that the bioreductive activation of drug molecules does not take place in oxygenated (healthy) cells. Under hypoxic conditions, the reductive activation continues down the bioreductive cascade, resulting in the formation of cytotoxic drug adducts that bind to cytoplasmic macromolecules, thus providing a basis for the accumulation of nitroimidazole based cytotoxins within hypoxic tissue and leading to hypoxia-selective theranostic effects [51, 55]. Normally, molecular oxygen is considered the ultimate electron acceptor in the electron transport chain, however, other molecules can accept electrons and be reduced in the absence of oxygen. Under hypoxic conditions, the formation of the chemically reactive molecular adduct is metabolically activated by functional reductases such as Flavin-dependent cytochrome P450 reductase, xanthine oxidase, aldehyde oxidase and quinone oxidase [56].

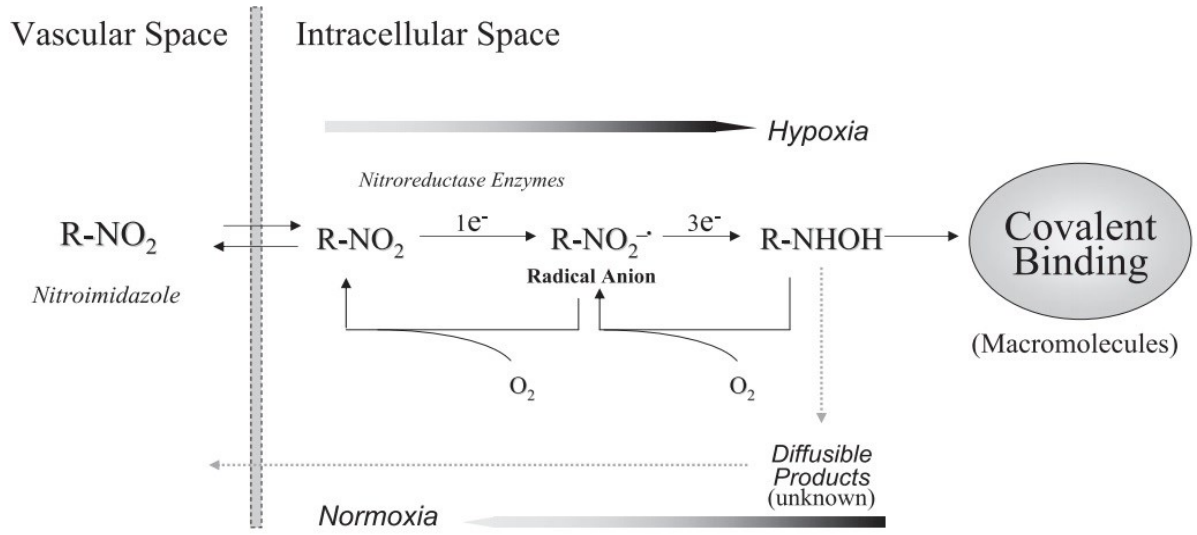

Figure 1-6. Mechanism of action for nitroimidazole single electron reduction in an hypoxic environment [57].

Nitroimidazole agents can advantageously function as radiosensitization agents in hypoxic cells, thus providing an innovative and alternative opportunity for oxygen mimetic radiotherapeutic management. Using low linear-energy transfer (LET) radiation therapy, the accumulation of nitroimidazoles in hypoxic cells can generate high concentrations of molecular free radicals, hydrated electrons, hydrogen radicals and hydroxy radicals which bind covalently within cells to form macromolecular adducts with DNA and intracellular proteins [49]. Generally, molecular adduct formation with DNA results in DNA damage which is irreparable by normal DNA repair pathways, leading to necrosis and apoptosis of the cell. Although many compounds possess radiosensitizing properties, single-electron reduction potentials and partition coefficient of nitroimidazoles have shown to be the most important physiochemical properties that affects their permeability into hypoxic cells and the ability to form reactive intermediate products therein (Figure 1-7)[58-60]. Typically, oxygen is the ultimate electron acceptor, however, in the absence of oxygen, other molecules can accept electrons and be reduced [55]. The single electron

reduction is crucial because it reflects the ability of the compound to accept electrons from cytochromes; the partition coefficient reflects the ability of the drug to diffuse into the target (hypoxic) cell. Early studies with various hypoxia selective compounds have shown that nitroimidazole derivatives with single electron potentials between -380 and -400 mV and partition coefficients between 0.1 - 10 demonstrated the greatest efficacy and lowest cytotoxicity [61]. Therefore, the precise modification to nitroimidazole derivatives is of clinical importance to modulate the therapeutic efficacy of these compounds. The extensive research and rational drug design have led to the development of several potentially useful nitroimidazole-based drugs, such as fluorine-18 labeled fluoroazomycin arabinofuranoside ([^{18}F]FAZA), fluoromisonidazole ([^{18}F]FMISO) and radioiodinated Iodoazomycin Arabinofuranoside [^{123}I]IAZA. FAZA and IAZA have demonstrated serious potential in offering multimodal applications in therapeutic management and diagnostic imaging of tumor hypoxia [62].

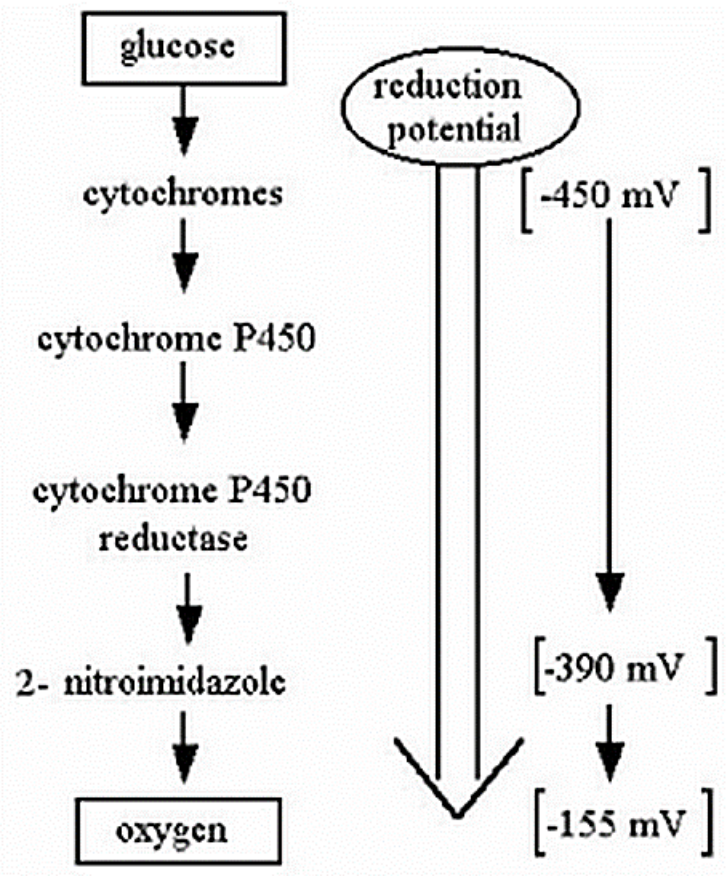

Figure 1-7. Electron flow from glucose to O_2 along the flavin-cytochrome system in metabolically viable tissue [61].

1.7 Iodoazomycin Arabinofuranoside

The synthesis of IAZA, chemically known as 1-α-D-(5-iodo-5-deoxyarabinofuranosyl)-2-nitroimidazole, was first reported in 1991 as a novel *in vivo* scintigraphic marker for tissue hypoxia by Mannan and colleagues (Figure 1-8) [63]. The formation of non-diffusible tissue adducts with reductive IAZA intermediates showed linear correlation to a wide range of oxygen concentrations, with the most rapid binding occurring at the lowest oxygen concentrations [64]. Using pivalic acid 'melt' and radioiodide exchange-based radiolabeling, IAZA can be easily labelled with different iodine radioisotopes for diagnostic and therapeutic applications [36]. With radiolabelled IAZA, the formation of adducts in hypoxic cells presents the opportunity for diagnostic imaging applications using modern nuclear medicine techniques and *in situ* low dose isotope molecular radiation therapy (MRT). Previous clinical studies with ^{123}I-IAZA in cancer patients established it as an imaging agent for diagnosing a variety of therapy-resistant hypoxic tumors and their therapy planning. Tissue hypoxia is a condition that is prevalent in several other peripheral vascular diseases [65-66]. 'Beyond cancer' explorations with IAZA in diabetes, rheumatoid arthritis and stroke-induced brain trauma demonstrated its usefulness in diagnosing the related hypoxia disorders [65-68]. Besides hypoxia selectivity of IAZA, highly unique radioactive emissions from various isotopes of radioiodine make IAZA medically very useful is **multimodal** theranosis of hypoxic tumors. Thus, IAZA, when synthesized with the appropriate iodine isotope ($^{123/124/131}$I), will allow the single photon emission (^{123}I) or positron emission (^{124}I)-based imaging of hypoxic tumors, the monitoring of disease status and hypoxia-selective molecular events and concurrently provide targeted radiotherapy (RT) options using X-ray beam radisensitization (XRT; using ^{127}I) or MRT (^{131}I) [67-69]. However ^{123}Iodine is more widely used for diagnostic imaging purposes due to it shorter decay time (half life 13.22 hours) [69].

Alternatively, ^{131}Iodine can also be used for diagnostic purposes, however, due to its dominant beta radiation character (10% gamma and 90% beta decay), its applications are more suited towards low-dose isotope radiation therapy and *in situ* MRT [36, 70].

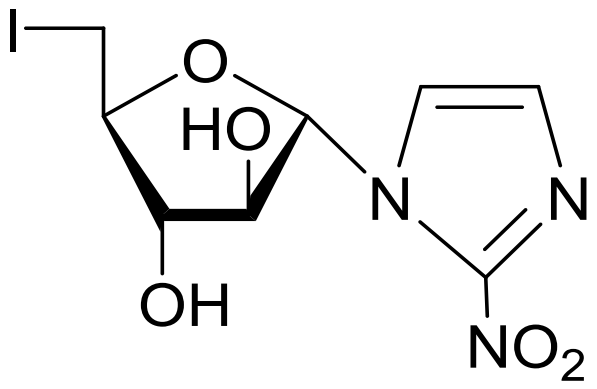

Figure 1-8. Structure of 1- α-D-(5-deoxy-5-iodoarabinofuranosyl)-2-nitroimidazole.

In preliminary studies, ^{123}I-IAZA demonstrated a binding rate which was three times higher compared to the reference compound ^{18}F-misonidazole (FMISO) with an initial binding rate of 284 pmole/10^6 cells/h and 89 pmole/10^6 cells/h, respectively [58]. In addition, the lipophilicity of ^{125}IAZA (logP = 0.46) also demonstrated an optimal feature to diffuse through poorly vascularized (ischaemic) tissue in comparison to ^{3}H-FMISO (logP = 0.40) and ^{3}H-misonidazole (logP = 0.37) [61]. Profoundly, the increased efficacy of IAZA as a radiosensitizing agent was also accompanied by an elevated *in vitro* cytotoxicity (30-40 times greater) compared to misonidazole [63, 73]. However systemic toxicity is discernable at low concentrations and the pharmacokinetics/radiation dosimetry of $^{123/131}$I-IAZA has been extensively studied in small animals, healthy volunteers and patients with various diseases [61, 73-75]. In photodynamic therapy (PDT) of Dunning 3327 prostate tumor models in Fisher x Copenhagen rat, ^{123}I-IAZA localized specifically in PDT-induced tumor hypoxia [61].

One of the most important factors with radiopharmaceutical compounds is maintaining the structural integrity of the active molecule. Previous studies have demonstrated ready-to-inject solutions of ^{131}I-IAZA can be stored in 15% ethanolic saline (pH 5.5) for up to 15 days with minimal radiochemical (2%) and chemical (6%) decomposition [36]. Although *in vitro* studies have shown IAZA resistance to phosphorolytic cleavage of the N-glycosidic bond between the nitroimidazole and arabinofuranose group by thymidine phosphorylase, *in vivo* enzymatic cleavage of the compound may compromise the structural integrity resulting in nonspecific uptake and high background noise [76]. Strong non-specific binding of radiolabelled IAZA metabolites with proteins in the blood plasma may result in longer body clearance times, poor tumor-to-background contrast and poor imaging. Other studies have shown that deiodination of the compound may lead to high uptake within the thyroid causing low-dose radiation damage, thus requiring standard thyroid blocking techniques prior to administration of radiolabelled IAZA [33]. Therefore maintaining the structure integrity of IAZA is of clinical relevance to maximize its therapeutic efficacy, hypoxia-targeted specificity, reduce non-specific interactions and increase tumour-to-background ratio as a theranostic agent.

1.8 References

[1] Nair, L., Cato L., *Prog. Poly. Sci.* **2007**, *32*, 762-798.

[2] Hubbell, J., *Nature Biotech.* **1995***, 13,* 565-576.

[3] Courtney, J. *Biomaterials*. **1994**, *15*, 737-744.

[4] Chiefari J., Chong Y., Ercole F., Krystina J., Jeffery J., Le T., *Macromolecules*. **1998**, *31*, 5559-62.

[5] Hawker J., *J. Amer. Chem. Soc.* **1994**, *116*, 11185-6.

[6] Mishra V., Kumar R., *J. Sci. Res.* **2012**, *56*, 141-76.

[7] Moad G., Chiefari J., Krstina J., Mayadunne R., Postma A., Rizzardo E., *Poly. Int.* **2000**, *49*, 993-1001.

[8] Chiefari, J., *Macromolecules.* **1998***, 31,* 5559-5562.

[9] Semsarilar M., Perrier S., *Nature Chem.* **2010,** *2*, 811-20.

[10] Mayadunne R., Rizzardo E., Chiefari J., Chong Y., Moad G., Thang S., *Macromolecules*. **1999**, *32*, 6977-80.

[11] Rapoport N., *Prog. Poly. Sci.* **2007**, *32*, 962-90.

[12] Gil E., Hudson S.*, Prog. Poly. Sci*. **2004**, *29***,** 1173-222.

[13] Qiu Y., Park K., Adv. Drug Del. Rev. **2012**, *64*, 49-60.

[14] Ganta S., Devalapally H., Shahiwala A., Amiji M., *J. Cont. Rel.* **2008**, *126*, 187-204.

[15] Bajpai A., Shukla S., Bhanu S., Kankane S., *Prog. Poly. Sci.* **2008**, *33*, 1088-118.

[16] Wang X., Qiu X., Wu C., *Macromolecules*. **1998**, *31*, 2972-6.

[17] Liu S., Liu M., *J. App. Poly. Sci.* **2003**, *90*, 3563-8.

[18] Nitschke M., Gramm S., Götze T., Valtink M., Drichel J., Voit B., *J. Biom. Mat. Res. Part A.* **2007**, *80*, 1003-10.

[19] Chacko R., Ventura J., Zhuang J., Thayumanavan S., *Adv. Drug Del. Rev*. **2012**, *64*, 836-51.

[20] Seuring J., Agarwal S., *Macromol. Rapid Comms*. **2012**, *33*, 898-920.

[21] Ward MA., Georgiou TK., *Polymers.* **2011**, *3*, 1215-42.

[22] Ougizawa T., Inoue T., Kammer HW., *Macromolecules*. **1985,** *18*, 2089-92.

[23] Ougizawa T., Inoue T., *J. Poly.* **1986,** *18*, 521-7.

[24] Sanchez I., Stone M., *Poly. Blends*. **2000,** *1*, 15-53.

[25] Schmaljohann D., *Adv. Drug Del. Rev*. **2006**, *58*, 1655-70.

[26] Oh J., Drumright R., Siegwart DJ., Matyjaszewski K., *Prog. Poly. Sci.* **2008**, *33*, 448-77.

[27] Raemdonck K., Demeester J., De Smedt S., *Soft Matter.* **2009**, *5*, 707-15.

[28] Oh J., Lee D., Park J., *Prog. Poly. Sci*. **2009**, *34*, 1261-82.

[29] Bhuchar N., Sunasee R., Ishihara K., Thundat T., Narain R., *Bioconj. Chem.* **2011**, *23*, 75-83.

[30] He J., Yan B., Tremblay L., Zhao Y., *Langmuir*. **2010**, *27*, 436-44.

[31] Kabanov AV., Vinogradov S., *Ange. Chem. Int. Ed.* **2009**, *48*, 5418-29.

[32] Shi L., Khondee S., Linz T., Berkland C., *Macromolecules.* **2008**, *41*, 6546-54.

[33] Lou S., Gao S., Wang W., Zhang M., Zhang J., Wang C., *Nanoscale*. **2015**.

[34] Klinger D., Landfester K., *J. Poly. Sci. Part A*: *Poly. Chem.* **2012**, *50*, 1062-75.

[35] Schwartz A., Fridovich S., Knowles B., Lodish H., *J. Bio. Chem.* **1981**, *256*, 8878-81.

[36] Kumar P., McQuarrie S., Zhou A., McEwan A., Wiebe L., *Nuc.Med. Bio.* **2005**, *32*, 647-53.

[37] Creixell M., Peppas N., *Nano Today*. **2012,** *7*, 367-79.

[38] Schwartz A., Fridovich S., Lodish H., *J. Bio. Chem.* **1982,** *257*, 4230-7.

[39] Stoorvogel W., Geuze H., Griffith J., Schwartz A., Strous G., *J. Cell Bio.* **1989**, *108*, 2137-48.

[40] Volz B., Orberger G., Porwoll S., Hauri H., Tauber R., *J. Cell Bio*. **1995,** *130*, 537-51.

[41] Strous G., Du Maine A., Zijderhand-Bleekemolen J., Slot J., Schwartz A., *J. Cell Bio*. **1985**, *101*, 531-9.

[42] Tao Y., He J., Zhang M., Hao Y., Liu J., Ni P., *Poly. Chem.* **2014**, *5*, 3443-52.

[43] Jiang H-L., Kim Y-K., Lee S., Park M., Kim E., Jin Y., *Arch. Pharm. Res.* **2010**, *33*, 551-6.

[44] Hu J., Liu J., Yang D., Lu M., Yin J., *Prot. Pep. Letters.* **2014**, *21*, 1025-30.

[45] Zhou X., Zhang M., Bryant Yung L., Zhou C., Lee L., Lee R.. *J. Int. Nanomed.* **2012**, *7*, 5465.

[46] Ahmed M., Narain R., *Biomaterials.* **2012,** *33*, 3990-4001.

[47] Li Y., Huang G., Diakur J., Wiebe L., *Curr. Drug Del.* **2008**, *5*, 299-302.

[48] KyungáKim S., MináPark K., JongáKim W., *Chem. Comm.* **2010**, *46*, 692-4.

[49] Harris AL., *Nature Rev. Can.* **2002**, *2*, 38-47.

[50] Welsh R., Jensen F., Cooper N., Oldstone M., Banapour B., Sernatiriger J., *Nature*. **1996,** *3*, 79-84.

[51] Nunn A., Linder K., Strauss HW., *J. Euro. Nuc. Med.* **1995**, *22*, 265-80.

[52] Höckel M., Vaupel P., *J. Nat. Can. Institute*. **2001**, *93*, 266-76.

[53] Dewey D., *Nature*. **1960**, *186*, 780-2.

[54] Fleming I., Manavaki R., Blower P., West C., Williams K., Harris A., *J. Brit. Can.* **2014**.

[55] Edwards D., *J. Antimicro. Chemo.* **1993**, *31*, 9-20.

[56] Biaglow J., Varnes M., Roizen-Towle L., Clark E., Epp E., Astor M. *Biochem. Pharm.* **1986**, *35*, 77-90.

[57] Takasawa M., Moustafa R., Baron J., *Stroke*. **2008**, *39*, 1629-37.

[58] Fowler J., *J. Int. Rad. Onc.* **1985**, 11, 665-74.

[59] Monney H., Parrick J., Wallace R., *Pharm. Thera.* **1981**, *14*, 197-216.

[60] Wardman P., *Clin. Onc.* **2007**, *19*, 397-417.

[61] Wiebe L., McEwan A., *Braz. Arch. Bio.Tech.* **2002**, *45*, 69-81.

[62] Kumar P., Bacchu V., Wiebe L., *Sem. Nuc. Med.* **2015,** 122-35.

[63] Mannan R., Somayaji V., Lee J., Mercer J., Chapman J., Wiebe L. *J. Nuc. Med.* **1991**, *32,* 1764-70.

[64] Urtasun R., Parliament M., McEwan A., Mercer J., Mannan R., Wiebe L., *J. Brit. Can. Supp.* **1996**, *27*, S209.

[65] Ye, J., *J. Int. Obesity.* **2009***, 33,* 54-66.

[66] Hajer, G., Timon W., Visseren F., *J. Euro. Heart.* **2008***, 29,* 2959-2971.

[67] Mannan R., Mercer J., Wiebe L., Kumar P., Somayaji V., Chapman J., *J. Nuc. Bio. Med.* **1991**, *36*, 60-7.

[68] Parliament M., Chapman J., Urtasun R., McEwan A., Golberg L., Mercer J., *J. Brit. Can.* **1992**, *65*, 90.

[69] Groshar D., McEwan A., Parliament M., Urtasun R., Golberg L., Hoskinson M., *J. Nuc. Med.* **1993**, *34*, 885.

[70] Vinjamuri S., O'Driscoll K., Maltby P., McEwan A., Wiebe L., Critchley M., *Clin. Nuc. Med*. **1999**, *24*, 891.

[71] Koehler L., Gagnon K., McQuarrie S., Wuest F., *Molecules*. **2010,** *15*, 2686-718.

[72] Mercer J., McEwan A., Wiebe L. *Curr. Radiopharm.* **2013**, *6*, 87-91.

[73] Reischl G., Dorow D., Cullinane C., Katsifis A., Roselt P., Binns D., *J. Pharm.Sci.* **2007,** *10*, 203-11.

[74] Al-Arafaj A., Ryan E., Hutchison K., Mannan R., Mercer J., Wiebe L., *J. Euro. Nuc. Med.* **1994**, *21*, 1338-42.

[75] Wiebe L. *Noujaim Inst. Pharm. Onc. Res.* **1997**. 189-94.

[76] Mercer J., Mannan R., Somayaji V., Wiebe L., Lee J., Chapman J., *Adv. Radiopharm.* **1990**.

2 Instrumentations and Techniques

2.1 Gel Permeation Chromatography

Gel permeation chromatography (GPC) is a type of size exclusion chromatography (SEC) that determines the molecular weight (M_n) and molecular weight distribution (M_w/M_n) of polymers and proteins based on hydrodynamic volume or radius of gyration (R_h) of the sample [1]. The analytes are separated through a packed column which contains porous material, such as polystyrene gels, silica beads or cross-linked acrylamide with meticulously controlled pore sizes. Based on the R_h properties of the analyte, larger molecules that are unable to penetrate the porous column material are eluted faster in the interstitial volume (V_i), thus separating analytes based on molecular size. In contrast, smaller molecules which are retarded in the pores are eluted more slowly with the solvent passing through the pores ($V_p + V_i$). The total volume of solvent eluting the particles through the column pores (V_e) is shown in equation:

$$V_e = V_i + K_{sec} \times V_p$$

Where, K_{sec} represents SEC equilibrium coefficient for retention time that is dependent on size of solvated molecule relative to packing pore size [2]. When characterizing molecules, a sample is injected manually or automatically, and a degassed continuous mobile phase flows through the system carrying the sample through the packed porous column where it is separated by hydrodynamic size (Figure 2-1) [3].

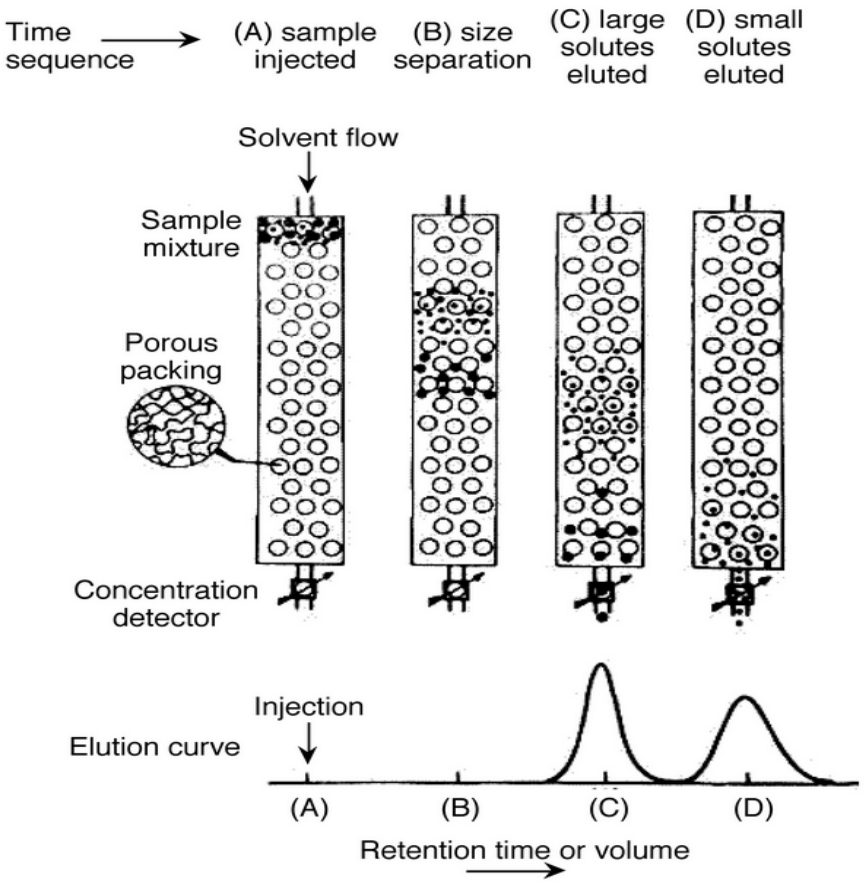

Figure 2-1. Schematic illustration of GPC separating a sample mixture [4].

Detectors that are connected to the GPC analyze the eluting solvent and generate a plot of analyte signal to time of elution. In general, the most commonly used GPC detectors are Refractive Index (RI), Ultraviolet/Visible (UV/VIS) and Light Scattering detectors.

1) Refractive Index (RI) Detectors: Measure the change in refractive index of the effluent passing through the flow-cell and calculate concentration of solute in solvent and molar mass, which is dependent on temperature and wavelength applied.
2) Ultraviolet/Visible (UV/VIS) Detectors: Measure the UV/VIS absorbance of a compound from the ground state to the excited state when UV or near infrared light radiation is applied at a fixed wavelength. Different compounds contain π-electrons that absorb

different wavelengths of light. Typically, this method can determine concentration of solute in solvent and molecular mass.

3) Light Scattering Detectors: This method measures the light scattering intensity at one or multiple scattering angles to determine molecular mass. Different types of light scattering detection methods, including Low Angle Laser Light Scattering (LALLS), Right Angle Laser Light Scattering (RALLS) and Multi Angle Laser Light Scattering (MALLS), can be used.

When equipped with different detectors, such as RI, UV/VIS, Viscometer and Light Scattering detectors, the sample can be analyzed by different calibration methods such as Conventional calibration, Universal calibration and Triple detection.

2.1.1 Conventional Calibration

Conventional calibration is the most common type of technique for the analysis of molecular weight usually using a RI or UV/VIS detector. Typically, standards of a known molecular weight are used to generate a calibration curve (log molecular weight (M_w) vs retention volume) which provide the estimation of the molecular weight of a sample (Figure 2-2). The calibration curve is created to fit into a simple polynomial equation:

$$Log\ M_w = A_0 + A_1V_1 + A_2V_2 + \ldots\ldots + A_nV_n$$

Conventional calibration is a simple and fast method for determining molecular weight for a sample, however there are some limitations to this technique. For example, the calculation of molecular weight is dependent on the assumption that the density and structural conformation of

the sample and standard are same. For this case, the calibration curve is typically generated with mono-disperse polymer standards having similar structural conformations as the sample [5].

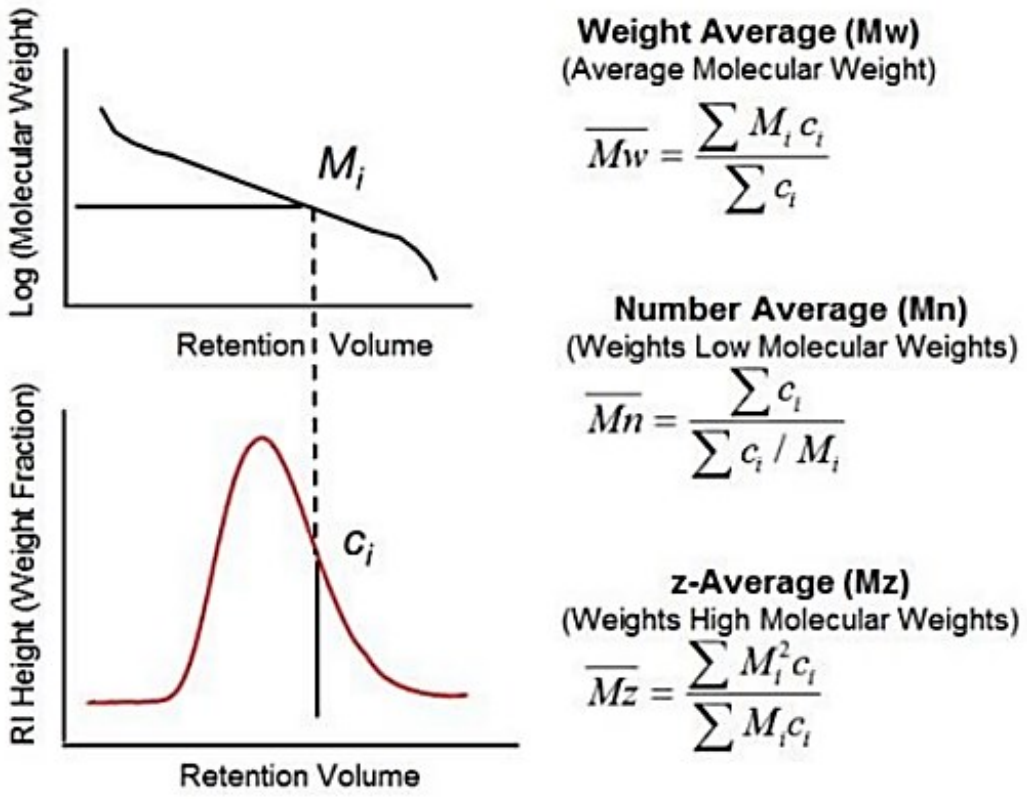

Figure 2-2. Calculation of molecular weight fraction by conventional calibration [6].

2.1.2 Universal Calibration

Universal calibration method overcomes the limitations of conventional calibration of assuming the density of the sample and standards are similar with the use of an additional detector, the viscometer detector. When combining viscometer detection with RI or UV/VIS detector, a calibration curve can be generated between log (M_w x IV) vs retention volume instead of M*w* vs retention volume (Figure 2-3). This allows for reducing the difference between the analytes and standards which can work with low and high molecular weight samples. By this method, the M_n

and M_w of a sample can be calculated with relatively high accuracy and additional structural property information such as hyperbanching with the analysis of polydispersity index (PDI). This method can determine the intrinsic viscosity (IV), hydrodynamic radius (V_h) and molecular weight (M_w) of the sample using this equation:

$$M_w \, x \, IV = \frac{5}{2} x \, N_a \, X \, V_h$$

where N_a is Avogadros constant.

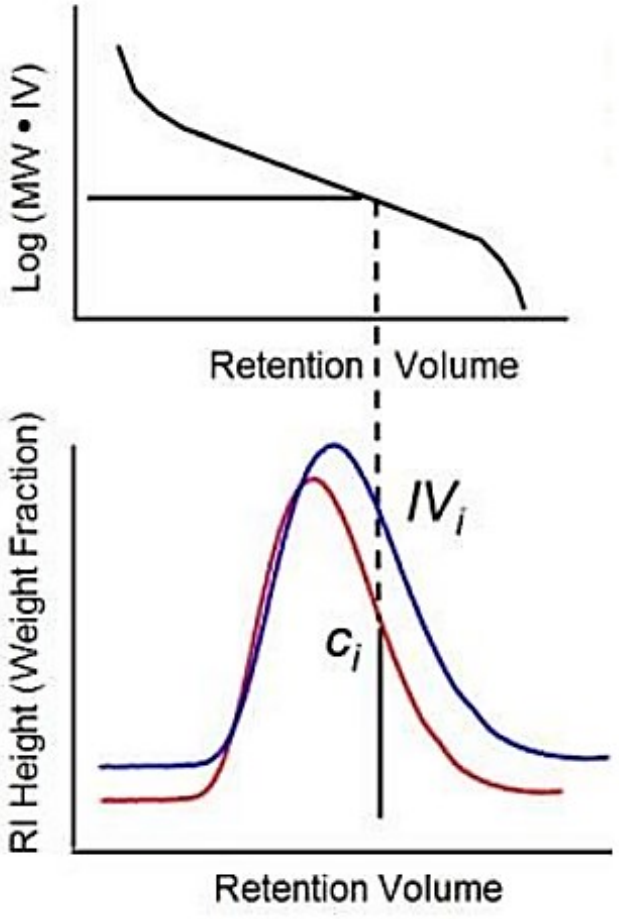

Figure 2-3. Calculation of molecular weight fraction by universal calibration [6].

2.1.3 Triple Detection Calibration

Triple detection calibration is the most accurate method available, which can calculate the absolute molecular weight of a sample with the use of three detectors (RI or UV-VIS, viscometer and light scattering) working together to provide synergistic data. The RI or UV-VIS detectors measures the polymer concentration, the viscometer directly measures the intrinsic viscosity or molecular density and the light scattering detector determines the absolute molecular weight. As a result, only a single narrow standard for calibration is needed. In order to determine the absolute molecular weight with the light scattering detector, Raleigh's light scattering equation is used:

$$R(\theta)\big|_{\theta \to 0} \cong KCM$$

where R is intensity, θ is the scattered light angle, K is optical constant, C is polymer concentration and M is the molecular weight [6]. However Raleigh's Equation assumes that the scattered light is measured at a zero angle which is not possible. Therefore, alternative methods are used to determine the intensity such as:

1) Measure the scattering using LALS at angles 10^{o} or less
2) Measure the scattering using MALS at multiple angle and extrapolate to 0^{o} angle

2.2 Nuclear Magnetic Resonance

Nuclear magnetic resonance (NMR) is a powerful analytical technique used by organic chemists to determine the structure of a compound at molecular level in a non-destructive manner. The application of NMR structure determination is dependent on isotopes that contain an odd number of protons or neutrons, such as ^{1}H or ^{13}C, which contain an intrinsic quantum mechanical magnetic moment. In the absence of an external magnetic field (B_0), the nuclear spins of the atomic isotopes are randomly oriented. However, in the presence of an external magnetic field, the nuclear spins align with or against the magnetic field. At a specific frequency, termed the resonance frequency, the magnetic pulse's energy is absorbed by those molecules aligned against the magnetic field and the nuclei is promoted to a higher energy state called A* state; conversely, the molecules aligned with the external magnetic field are in a lower energy state called A state (Figure 2-4) [7]. The difference in energy (ΔE) between these two states is a linear function of the magnetic field strength (B_0), and can be defined by:

$$\Delta E = h\nu$$

where h is Planck`s constant and ν is the resonance frequency.

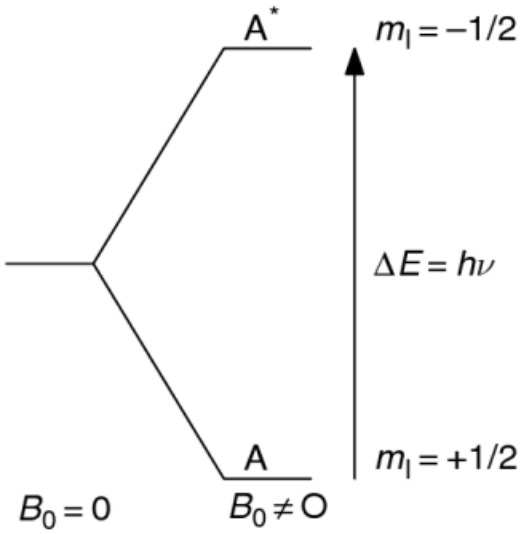

Figure 2-4. Energy levels of spin ½ states in the presence of an external magnetic field [7].

After the magnetization of nuclei by a pulse, the nuclei slowly return back to its original equilibrium ground state along the ZXY axis (longitudinal and transverse relaxation) giving the free induction decay (FID), which can be converted by Fourier transformation to provide an NMR spectrum. Depending on the difference in longitudinal (T1) and transverse (T2) relaxation times, the chemical shift of different functional groups within the molecule are different, and can be determined. The polymers can be accurately characterized using this technique with accurate details in terms of the polymerization conversion efficiency, end group analysis, molecular weight distributions and stereotacticity [8].

2.3 Dynamic Light Scattering

Dynamic light scattering (DLS), also known as Photon Correlation Spectroscopy and Quasi-Elastic Light Scattering, is an analytical technique that is used to characterize the size distribution of nanoparticles, polymers and colloids suspended in a solution. When using a monochromatic light source, such as a laser, particles in Brownian motion cause the light striking particle to undergo a Doppler shift and change the wavelength of the refracted light (Raleigh Light Scattering) (Figure 2-5). In essence, the larger the particle in solution the slower is its Brownian motion, and vice versa. Thus the change in light wavelength are measured as a function of time to determine the size of particles [9]. However the concept of DLS is based on the assumptions with 1) particles in solution are constantly in Brownian motion and 2) the particles under analysis are spherical. Since Brownian motion is vital, assumption in calculating the particle size, fluctuations in the temperature cause higher particle random movements in solution and affect the size interpretations [9]. Using Stokes-Einstein equation, the velocity of the particle can be related to its hydrodynamic radius:

$$D = kT/6\pi\eta a$$

Where, D is the diffusion velocity of the particle, k is Boltzmann constant, T is temperature**,** η is viscosity of the solution and a is the hydrodynamic radius. The concept of DLS for a solution with suspended particles is that small particles should diffuse faster than large ones based on Stokes-Einstein Equation [10]. When a broad dispersity of particle sizes exists, the effective diameter is measured using the average diameter of all particle scattered light intensities.

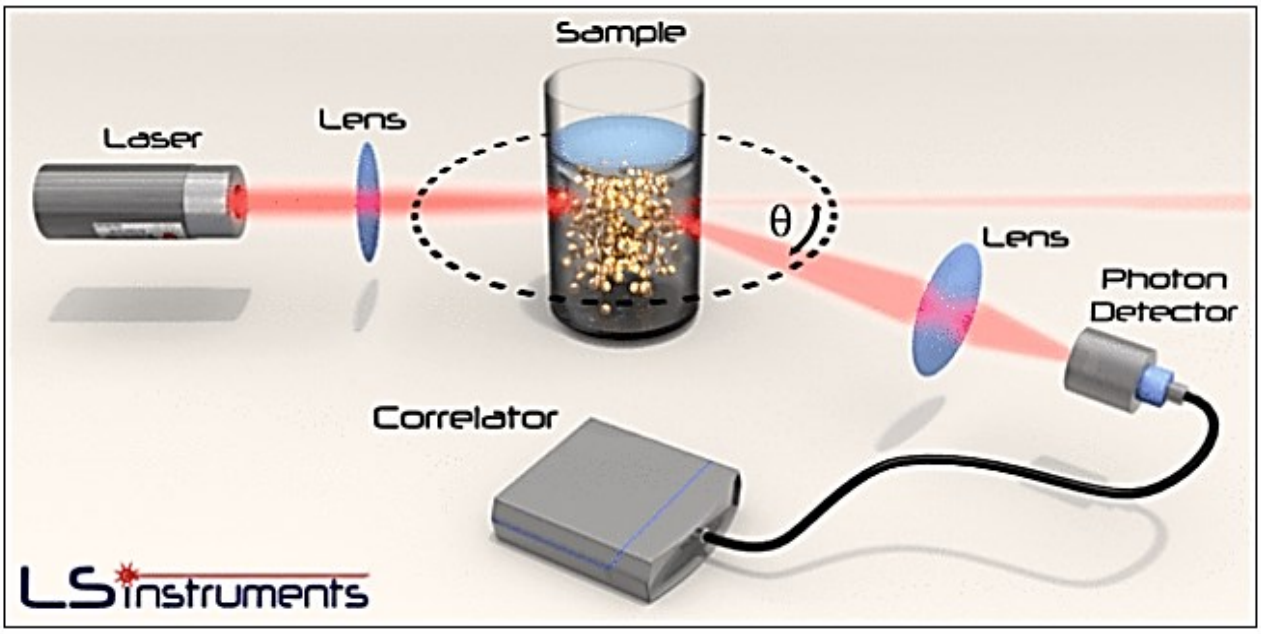

Figure 2-5. Schematic illustration for dynamic light scattering measuring a sample [9].

2.4 Flow Cytometry

Flow cytometry allows for the physical and chemical characterization of single particles, usually cells, in a fluid suspension as they pass through a laser-based detection apparatus. The use of flow cytometry can be applied to a multitude of biophysical detections such as cell counting, cell sorting, biomarker detection and protein engineering. Some properties that can be measured include the cell size, internal complexity, granularity and relative fluorescence intensity. In particular, flow cytometry has the capacity to sort the cells based on cellular fluorescent compartments that can be analyzed by excitation of laser-based optics and measuring the emitted wavelength [12]. This allows for easy separation of fluorescent positive and fluorescent negative sub-populations in experimental design. Every flow cytometer is composed of three basic main systems (Figure 2-6):

1. The fluidic system which allows for constant flow and detection of particles in suspension to pass through the laser detection apparatus

2. The optic systems which consist of lasers with different wavelengths of excitation for the application in fluorescence with various chromophores
3. The electronic systems that detect the excitations emitted from the chromophores, which can be analysed or further processed for alternatively equipped instrumentation, such as fluorescence-activated cell sorting (FACS) capabilities.

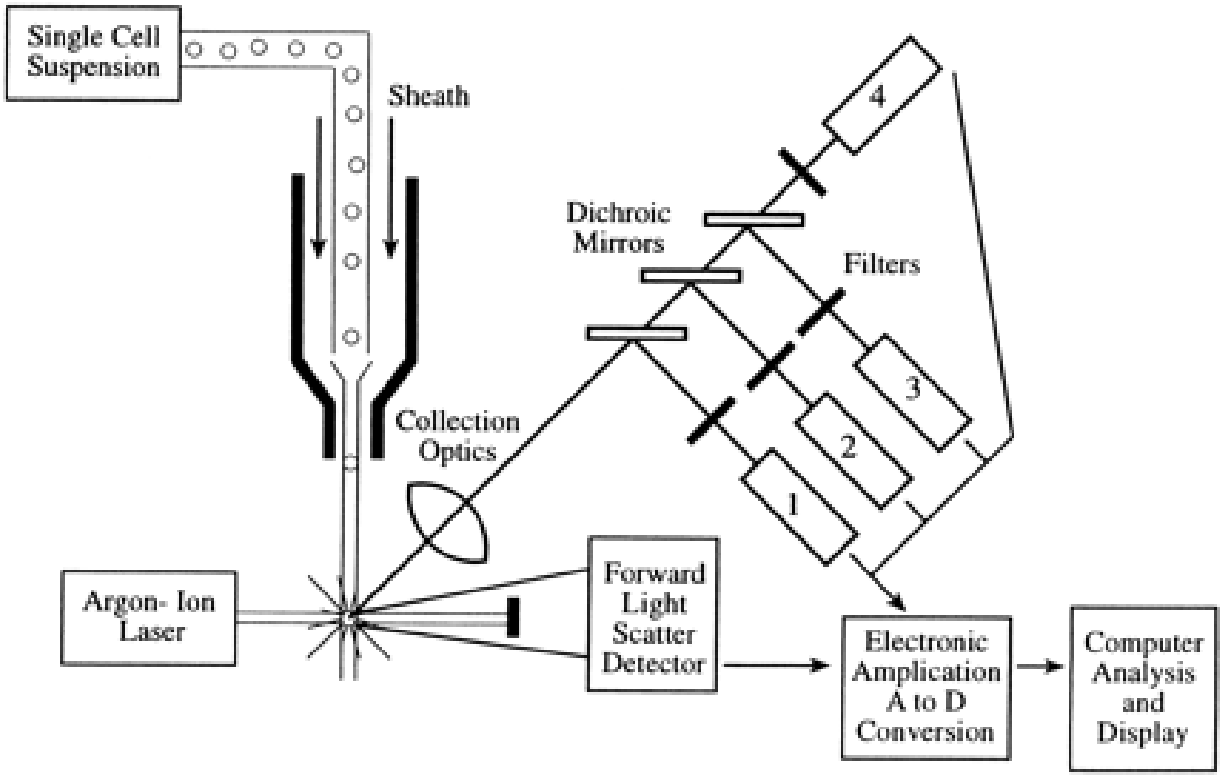

Figure 2-6. Schematic illustration for flow cytometer setup [11].

Flow cytometry can detect physical properties, such as internal complexity and cell size, based on the forward and side light scattering potential (Figure 2-7). Forward light scattering can detect the cell size and surface area by the diffracted light and incident laser beam in the forward direction towards the optics detector. Side light scattering detects the cell granularity and internal

complexity by the reflected light and changes in the refractive index. With these parameters, a suspension of a mixed population of cells, such as live, dead and irregular cells, can be analysed for a specific sub-population that would provide a more accurate analysis of data [12].

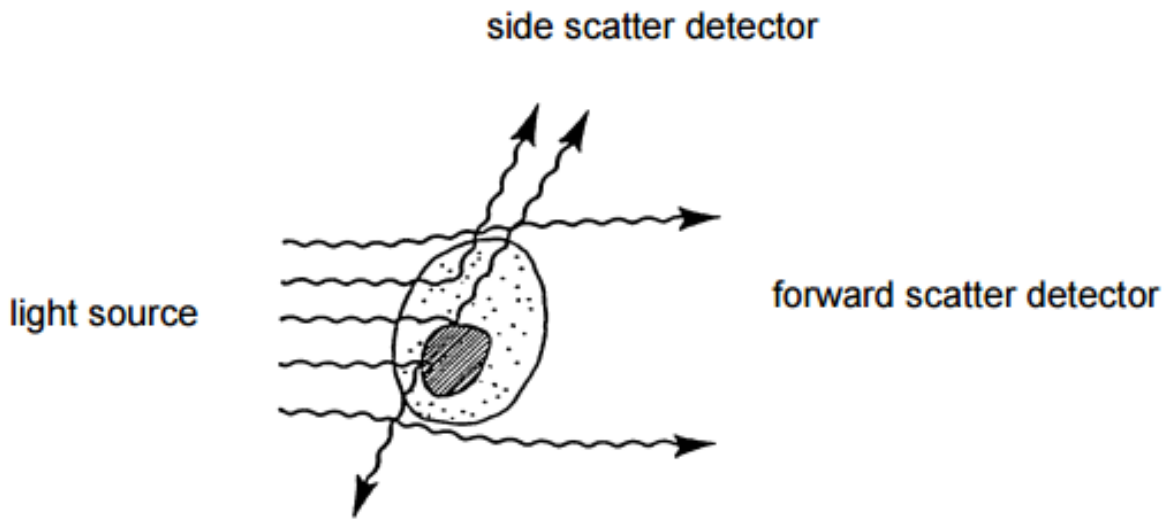

Figure 2-7. Schematic illustration for light scattering properties of single cells [13].

2.5 Gel Electrophoresis

Gel electrophoresis is a common bioanalytical technique used to separate DNA/RNA strands or proteins based on size and charge by applying an electric potential through the gel matrix. Typically, polyacrylamide or agarose are cross-linked to form the gel matrix, and DNA/RNA strands can be retarded through the porous gel network when an electric field is applied. Since DNA and RNA contain native positive charges from the phosphate groups on the ribose, the voltage applied from the electric field causes electrostatic repulsion with the DNA/RNA strands and facilitates their migration through the gel matrix (Figure 2-8). In some cases, with complex tertiary and quaternary proteins, the use of denaturing agents such as sodium dodecyl sulfate are used to assay proteins in their primary, linear conformation. Typically, by employing the use of

an intercalating agent, such as Ethidium bromide or SYBR Green, the migration rate of DNA, RNA and protein can be visualized when illuminated under ultraviolet exposure [13].

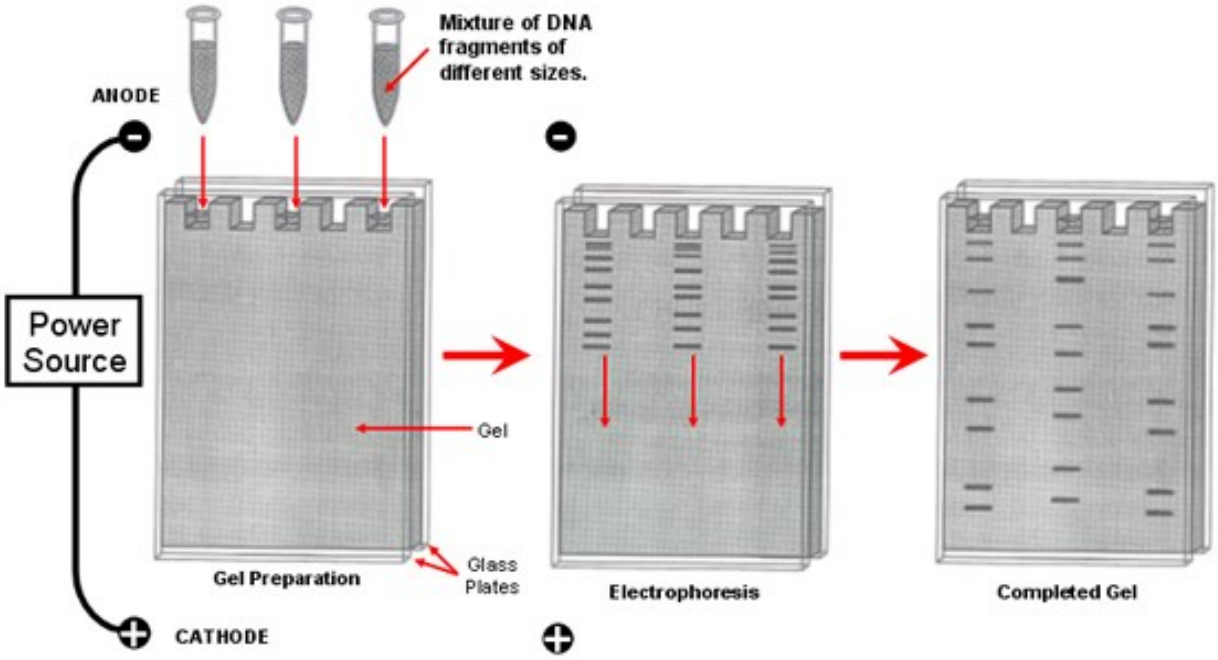

Figure 2-8. Schematic illustration of gel electrophoresis separation of a mixture of DNA [13].

2.6 MTT Cytotoxicity Assay

The MTT cytotoxicity assay is a colorimetric assay based on intracellular metabolic function that relies on mitochondrial oxidoreductase enzymatic activity. The reagent (3-(4,5-dimethylthiazol-2-yl)-2,5-diphenyltetrazolum bromide)) (MTT) is a yellow tetrazolium salt that is reduced to insoluble purple formazan product within live cells either enzymatically by dehydrogenases and reductases, or by direct reaction with NADH and NADPH (Figure 2-9) [14]. Typically, a solubilisation agent such as sodium dodecyl sulfate (SDS), dimethyl sulfoxide (DMSO) or hydrochloric acid (HCl) is required to lyse the cell and solvate the purple formazan ring precipitate that can be detected by a spectrophotometer at 570nm.

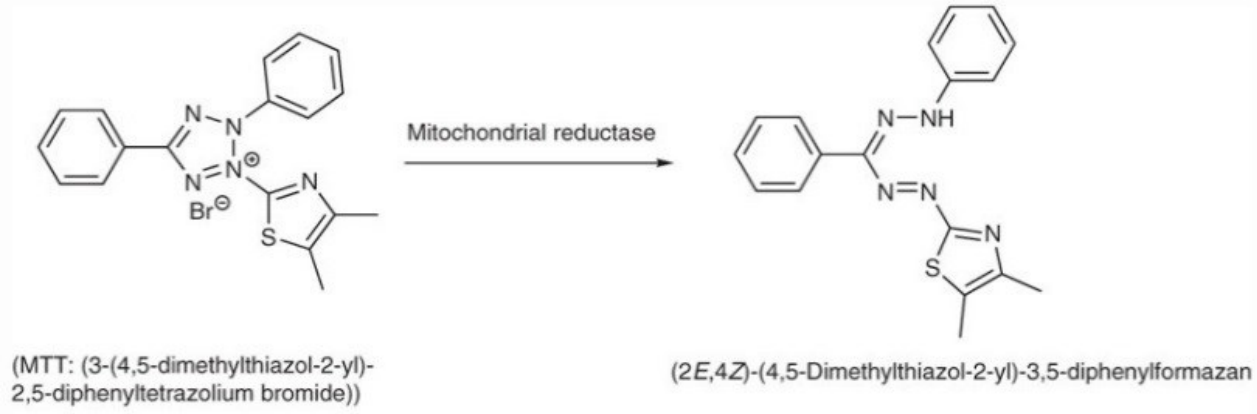

Figure 2-9. Mechanism of MTT cytotoxicity assay [14].

2.7 Enzyme-Linked Immunosorbent Assay

Enzyme-linked immunosorbent assay (ELISA) is a highly sensitive ligand binding assay that can detect the presence of antigens with the application of high-affinity epitope-specific antibodies conjugated with an enzyme. The use of monoclonal antibodies are used to reduce non-specific binding and enhance specificity for the target antigen. Typically, the antigen is immobilized on a solid surface and the primary detection antibody enzyme is used to detect the antigen and form a complex. In different variations of ELISA, the primary antibody can be conjugated with an enzyme (Direct) or the primary antibody can be detected with a secondary antibody that is conjugated to an enzyme (Indirect) (Figure 2-10) [15]. In the final step, the enzyme-conjugated antibody can be stimulated by the addition of substrate which can produce a colorimetric or fluorescent signal to give a direct measurement of antigen present in the sample. The intensity of color change or fluorescence gives a quantitative evaluation of the amount of target antigen in the sample.

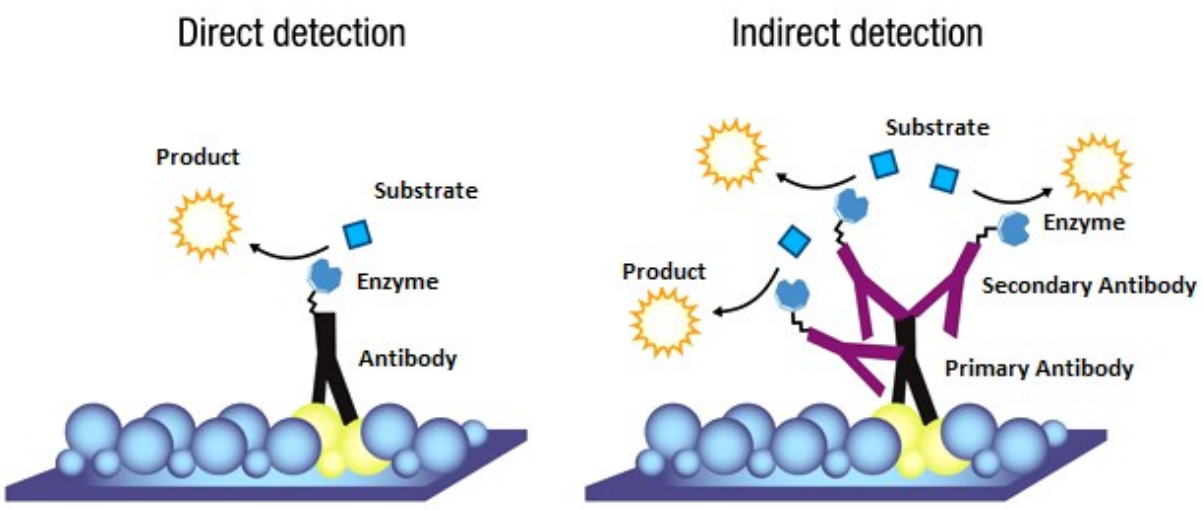

Figure 2-10.Schematic illustration of direct and indirect methods of enzyme linked immunosorbent assay [15].

2.9 References

[1] Moore, J., *J. Poly. Sci. Part A.* **1964**, *2*, 835-843.

[2] Gulrez I., Syed K., Glyn O., Phillips S., Saphwan A., *Intech Open Acc. Pub.* **2011**.

[3] Viscotek Setting the Standard for GPC. Complete Guide for GPC/SEC/GFC Instrumentation and Detection Technologies, 2006. Retrieved from: http://s3.amazonaws.com/zanran_storage/md-scientific.dk/ContentPages/993457484.pdf

[4] Lin Y., Barron, Rm *Size Exc. Chroma. App. Poly. Sci.* **2015**.

[5] Agilent Technologies. A Guide to Multi-Detector Gel Permeating Chromatography. 2006, Retrieved from: https://www.chem.agilent.com/Library/primers/Public/5990-7196EN.pdf

[6] Malvern. GPC/SEC Theory: Universal Calibration. 2013, Retrieved from: http://www.malvernkorea.co.kr/labeng/technology/gel_permeation_chromatography_theory/universal_calibration_gpc_theory.htm

[7] Holzgrabe, U., Wawer, I., Diehl, B., *Elsevier*, **2011**.

[8] O'Reilly, R. NMR spectroscopy for polymer chemists. 2014, Retrieved from: http://www2.warwick.ac.uk/fac/sci/chemistry/masters/courses/polymchem/polyintra/ch968/nmr_spectroscopy2.pdf

[9] Sartor, M. Dynamic light scattering to determine the radius of small beads in Brownian motion in a solution. Retrieved from: http://216.92.172.113/courses/phys39/light%20scattering/DLS%20LabView%20UCSD.pdf

[10] LS Instruments. Dynamic Light Scattering: Measuring the Particle Size Distribution. 2015, Retrieved from: http://www.lsinstruments.ch/technology/dynamic_light_scattering_dls/

[11] Brown M., Wittwer C. *Clin*. *Chem.* **2011,** *46*, 1221-1229.

[12] BD Biosciences. Introduction to Flow Cytometry: A Learning Guide. 2000, Retrieved from: http://www.d.umn.edu/~biomed/flowcytometry/introflowcytometry.pdf

[13] PCMB. Retrieved from: http://www.biosci.ohio-state.edu/~plantbio/osu_pcmb/pcmb_lab_resources/pcmb102_activities/biotech/biotech_gels.htm

[14] Ebada S.,Edrada R., Lin, W., Proksch, P., *Nature Proto.* **2008**, *3*, 1820-1831.

[15] Life Technologies. Secondary Antibodies as Probes. 2015, Retrieved from: https://www.lifetechnologies.com/ca/en/home/life-science/protein-biology/protein-biology-learning-center/protein-biology-resource-library/pierce-protein-methods/secondary-antibodies-probes.htm

A VERSION OF THIS CHAPTER HAS BEEN PUBLISHED: STEPHEN QUAN, YINAN WANG, AIHUA ZHOU, PIYUSH KUMAR AND RAVIN NARAIN, BIOMACROMOLECULES., **2015, 16, 1978-1986.

3 Galactose-based Thermosensitive Nanogels for Targeted Delivery of Iodoazomycin Arabinofuranoside (IAZA) for Theranostic Management of Hypoxic Hepatocellular Carcinoma

3.1 Introduction

Hepatocellular carcinoma (HCC) is currently the third leading cause of all cancer deaths worldwide, with more than half a million new patients being diagnosed each year [1]. While earlier stages of the disease can be managed by modern surgical excision, more advanced stage of the disease leads to the development of poorly vascularized hypoxic regions and metastases that are therapy-resistant. This generally results in poor prognosis and high mortality [2]. Hypoxia occurs in various debilitating vascular diseases and within certain cancerous tumors that proliferate to an abnormally large size and contain regions with poor intratumor blood flow [3]. Hypoxic microenvironment within tumors promotes the progression of a more metastatic phenotype and increases the resistance to conventional therapeutic approaches 2-3 fold [4], which presents a huge challenge to researchers. Therefore an innovative approach to diagnose and manage these hypoxic tumors to facilitate and maximize the delivery of clinical drugs in effective form and dosage is of significant therapeutic benefit to the patients and the clinical communities. Interestingly, several studies have shown that hepatocytes display an overexpression of the endocytic cell surface receptor called the asialoglycoprotein receptor (ASGPR), which facilitates receptor-mediated binding [5, 6], clathrin-coated vesicle internalization and trafficking via the lysosome for degradation of asialoglycoproteins and glycoproteins containing terminal galactose and N-acetyl-glucosamine moieties [7]. This

approach can be exploited to design and synthesize galactose-decorated delivery systems for a facile delivery and transport of macromolecule drugs, such as doxorubicin [8], oridonin [9], acyclovir [10] and paclitaxel [11] in HCCs.

Nanogels are swollen nanosized cross-linked polymer chains composed of hydrophilic or amphiphilic polymer chains, which offer many unique properties for an efficient drug delivery [12]. The advantages of these drug delivery vehicles are 'multifaceted', including high biocompatibility, tunability of size from micro to nanometers, a large surface area for functionalization of cell targeting biomolecules and incorporating stimuli sensitive monomers for controlling macromolecule delivery [13, 14]. Interestingly, the individual property of the polymer chains also offers a high degree of control over the functional properties of nanogels. For example, di(ethylene glycol) methyl ethyl methacrylate (DEGMA) is a thermoresponsive monomer that undergoes a reversible lower critical solution temperature (LCST) phase transition from a swollen hydrated state (hydrophilic) to a shrunken dehydrated state (hydrophobic) around 32 °C in aqueous solution [15]. By combining different types of functional monomers into statistical or copolymer scaffolds, the symbiosis of complementary properties can lead to versatile smart drug delivery vehicles.

Over the past decade, a number of hypoxia-selective imaging agents have been developed and evaluated in a clinical setting. Nitroimidazoles in particular have been extensively studied due to their ability to bind to subcellular compartments within viable hypoxic tissues with a linear relationship to decreased oxygen concentration. Interestingly, nitroimidazole derivatives, when radiolabelled with positron/single photon-emitting radionuclides, (such as F-18 and I-123/124) as in ^{18}FAZA, ^{18}FMISO and $^{123/124}$IAZA, have demonstrated proven clinical usefulness

in scintigraphic imaging for the identification and treatment planning of radiotherapy-resistant hypoxic tumor cells [18]. In particular, IAZA is a Theranostic (Therapy+Diagnostic) molecule that has multimodal applications in modern nuclear medicine therapy depending on the type of the radionuclide, is proposed to have its potential in imaging (^{123}I and ^{124}I), radiosensitization (^{127}I), MRT (^{131}I) and in chemotherapy [19]. An important physiochemical property of IAZA is the water-lipid partition coefficient, which governs the molecules permeability. In comparison to other hypoxic selective radiosensitizers, ^{125}IAZA (logP = 0.46) demonstrates an optimal feature to diffuse through poorly vascularized (ischaemic) tissue in comparison to ^{3}H-FMISO (logP = 0.40) and ^{3}H-misonidazole (logP = 0.37). However, the carbon-iodine bond, being primary in nature experiences some deiodination under physiological conditions and non-specific interactions with circulating blood proteins that need to be overcome to maximize its therapeutic benefits. By exploiting the physiological role of ASGPR in hepatocytes, the development of thermosensitive galactose-decorated nanogels for the targeted delivery of IAZA to hypoxic HCC that may potentially maximize its theranostic effects.

Carbohydrate-based nanogels utilized as ‘smart’ drug delivery systems have been explored to enhance the therapeutic efficacy and decrease the toxic side-effects, usually associated with these compounds [13]. Stimuli responsive polymeric nanogels have gained huge attention due to their highly sensitive properties, such as biocompatibility, biodegradability, cationic/anionic functionalization, pH responsiveness and temperature sensitivity [14, 20, 21], which aid in their application and make them highly useful as novel drug delivery vehicles. Recently, nanogels have been recognized in the biomedical community as highly versatile macromolecule carriers contributing to gene, protein and drug delivery systems specifically in

cancer therapy [20-22]. Glycopolymers also possess a desirable capacity for mediating cellular interactions with lectins displayed on the extracellular surface, such as Concavalin A and ASGPR targeting [22-24]. In this study, the synthesized of statistical glycopolymers using 2-lactobionamidoethyl methacrylamide (LAEMA) with 2-aminoethylmethacrylamide hydrochloride (AEMA) decorated as the outer shell component with thermosensitive di(ethylene glycol) methyl ethyl methacrylate (DEGMA) and crosslinker (N,N'-Methylenebisacrylamide, MBAm) as the inner core component of the nanogel (Figure 3-1).

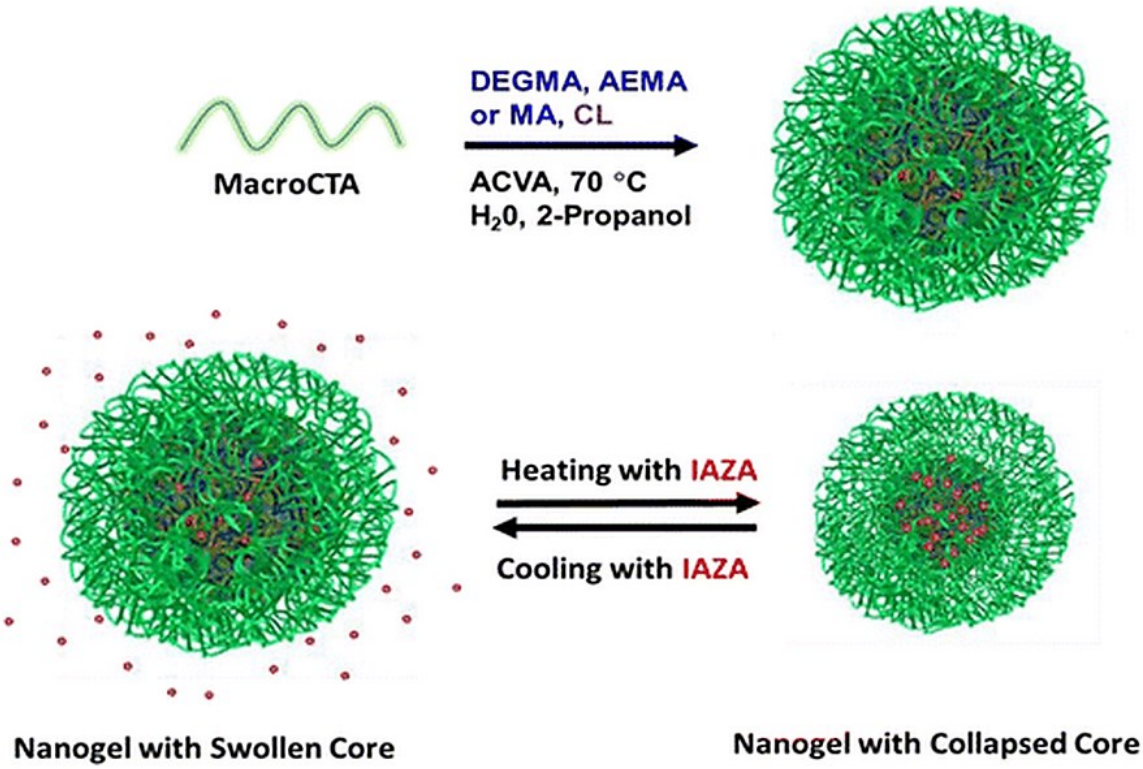

Figure 3-1. Synthesis of galactose-decorated nanogel and the encapsulation of IAZA within the thermosensitive nanogel core

3.2 Experimental

3.2.1 Materials

LAEMA, AEMA and the chain transfer agent (CTA) cyanopentanoic acid dithiobenzoate (CTP) were synthesized in the laboratory according to reported protocols [25-27]. 4,4′-Azobis-(cyanovaleric acid) (ACVA), methacrylic acid (MA). DEGMA and the crosslinker N,N'-Methylenebisacrylamide (MBAm) were purchased from Sigma-Aldrich (Oakville, Canada) (Figure 3-2). IAZA was generously gifted by Novolytics Inc., Edmonton, which was re-analyzed and certified for its chemical authenticity and purity through the Chemistry Analytical Services, University of Alberta. The organic solvents were purchased from Caledon Laboratories Ltd (Georgetown, Canada).

A VERSION OF THIS CHAPTER HAS BEEN PUBLISHED: STEPHEN QUAN, YINAN WANG, AIHUA ZHOU, PIYUSH KUMAR AND RAVIN NARAIN, BIOMACROMOLECULES., **2015, 16, 1978-1986.

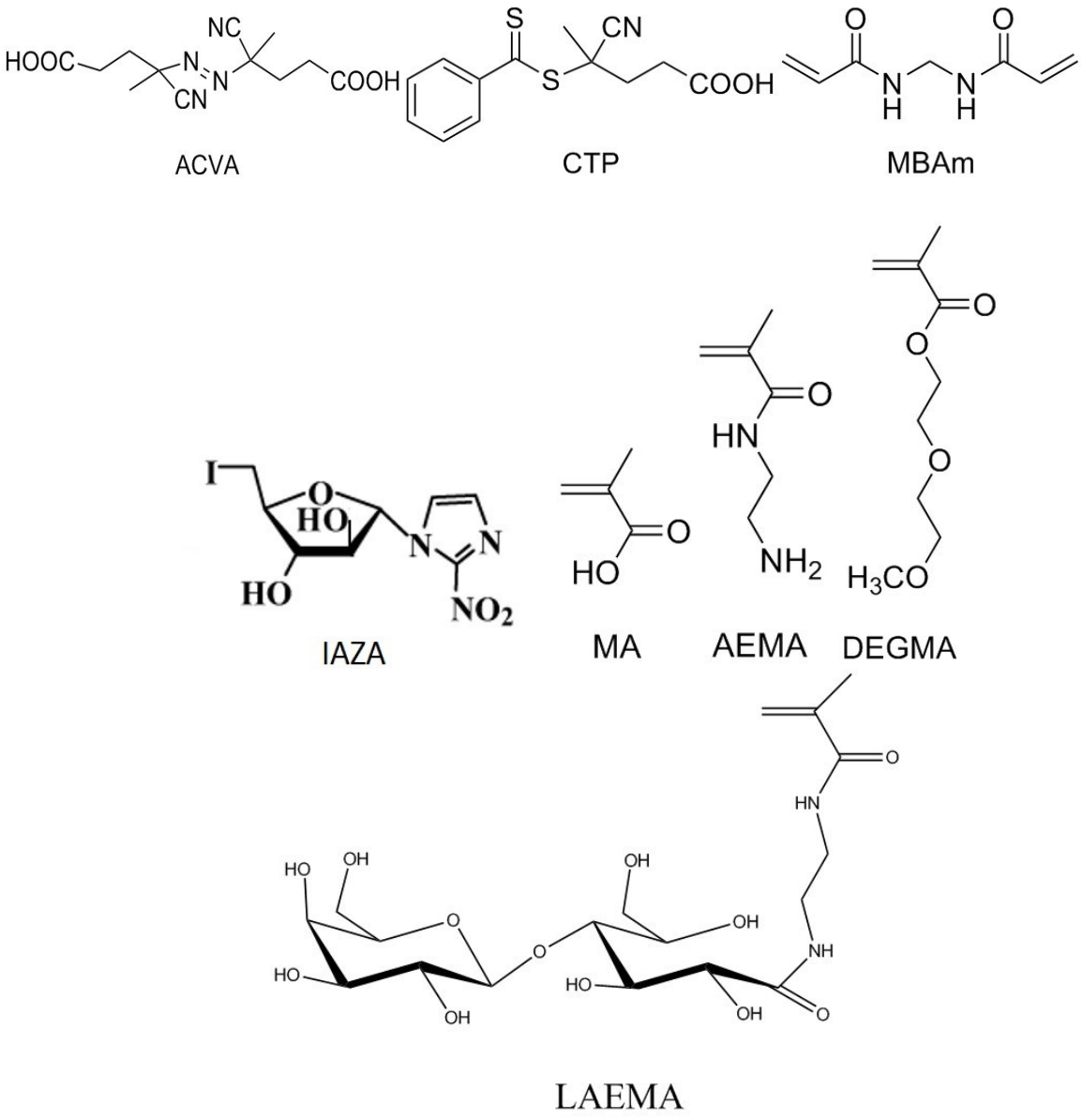

Figure 3-2. Chemical structure of monomers 2-lactobionamidoethyl methacrylamide (LAEMA), 2-aminoethylmethacrylamide hydrochloride (AEMA), methacrylic acid (MA), di(ethylene glycol) methyl ethyl methacrylate (DEGMA), crosslinker (N,N'-Methylenebisacrylamide, MBAm), chain transfer agent (4-cyanopentanoic acid dithiobenzoate, CTP) and polymerization initiator (4′-azobis(4-cyanovaleric acid, ACVA).

3.2.2 Methods of Polymer Characterization

^{1}H NMR spectra of the monomers and polymers were recorded using a Varian spectrometer (500 MHz) to confirm and determine the chemical structures of the synthesized polymers using D_2O as the solvent. Molecular weight and molecular weight distributions were determined by conventional Viscotek gel permeation chromatography (GPC) system using aqueous eluents, two Waters WAT011545 columns at room temperature (22 °C) and a flow rate of 1.0 mL/min using a 0.5 M sodium acetate / 0.5 M acetic acid buffer as eluent. The polymers were characterized based on seven near-monodisperse Pullulan standards (M_w) 5900-404000 g mol^{-1}.

3.2.3 Dynamic Light Scattering (DLS) and Zeta Potential Analysis

The hydrodynamic diameter and charge on nanogels surfaces were determined at 15 and 37 °C using Zeta Plus-Zeta Potential Analyzer (Brookhaven Instruments Corporation) at a scattering angle $\theta = 90°$ with Jasco ETC-505T temperature controller. The nanogels were filtered through Millipore membranes (0.45 μm pore size). The data was recorded with Omnisize Software.

3.2.4 Transmission Electron Microscopy (TEM)

Size and morphology of nanogels at 23 °C were also analyzed by TEM on a Philips transmission electron microscope operated at 80 kV and fitted with a CCD camera. To do this, a droplet of a nanogel aqueous solution (0.1 mg/mL) was placed on the TEM carbon coated copper grid and allowed to air-dry overnight prior to observation.

3.2.5 UV-Visible Spectroscopy

UV-Visible adsorption spectra (320 nm) were recorded on Jasco V-630 UV-Visible spectrometer from aqueous solutions of IAZA in 95% EtOH at 23 °C.

3.2.6 Synthesis of LAEMA Macro-CTA with Cationic or Anionic Components

Macro-CTAs carrying different charges [Poly(LAEMA) (neutral), poly(LAEMA-*st*-AEMA) (positive charges), or poly(LAEMA-*st*-MA) (negative charges)] were synthesized in a similar way as previously reported [28-30]. In a typical protocol for poly(LAEMA-st-AEMA) synthesis, LAEMA (0.79 g, 1.7 mmol) and AEMA (0.28 g, 1.7 mmol) were dissolved in 5 mL of DI water with 1 mL of CTP (10 mg, 36 μmol) and ACVA (5 mg, 18 μmol) DMF stock solution in a 25 mL reactor. The solution was degassed by purging nitrogen for 30 min and placed in an oil bath at 70 °C for 5 h. The reaction was then quenched in liquid nitrogen, and the polymer obtained was precipitated in acetone and washed with methanol to remove the residual monomers and RAFT agents (Table 1-1).

Table 3-1. Molecular weight (M_n) and PDI (M_w/M_n) of macro-CTAs synthesized by RAFT process.

Polymer	**Charges**	M_n **(GPC, g/mol)**	M_w/M_n
P($LAEMA_{25}$)	Neutral	11,700	1.23
P($LAEMA_{19}$-*st*-$AEMA_{19}$)	Cationic	12,300	1.22
P($LAEMA_{19}$-*st*-MA_{24})	Anionic	11,100	1.25

3.2.7 Synthesis of Nanogel Complexes with Cross-linked Core

The syntheses of the nanogels were conducted at 70 °C, employing ACVA as the initiator and poly(LAEMA), poly(LAEMA-*st*-AEMA), or poly(LAEMA-*st*-MA) as macro-CTA. A typical procedure for the synthesis of poly[(LAEMA-*st*-AEMA)-*b*-(DEGMA-*st*-MBAm-*st*-LAEMA)] nanogel is provided. In a 25 mL reactor, poly($LAEMA_{19}$-*st*-$AEMA_{19}$) macroCTA (200 mg, 0.016 mmol) and LAEMA (248 mg, 0.53 mmol) were first dissolved in 8 mL DI water. Then DEGMA (400 mg, 2.13 mmol), MBAm as cross-linker (41 mg, 0.27 mmol) (10 mol% with respect to total moles of DEGMA and LAEMA) and ACVA (2.3 mg, 0.008 mmol) were dissolved in 2 mL of 2-propanol and added to the above solution. The solution was purged with nitrogen for 30 min and the reaction was carried out at 70 °C for 24 h (Figure 3-3). The reaction was then quenched in liquid nitrogen and the product was purified by dialysis against DI water for three days using dialysis membrane with a molecular weight cut-off of 6,000. The nanogel was obtained as a white powder after freeze–drying overnight and was stored in a refrigerator (4 °C) [29, 30].

A VERSION OF THIS CHAPTER HAS BEEN PUBLISHED: STEPHEN QUAN, YINAN WANG, AIHUA ZHOU, PIYUSH KUMAR AND RAVIN NARAIN, BIOMACROMOLECULES., **2015, 16, 1978-1986.

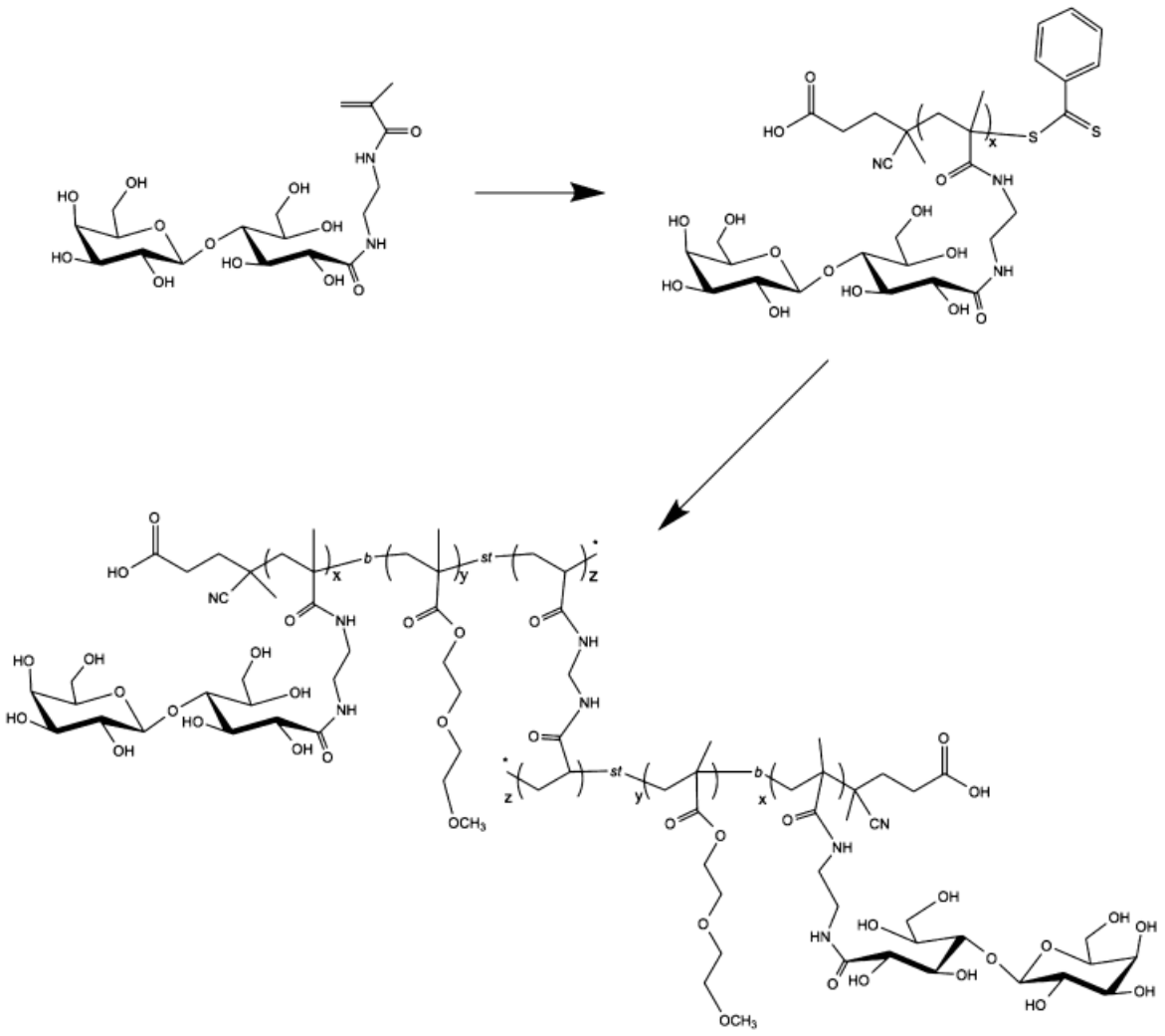

Figure 3-3. Synthesis of galactose decorated nanogel with crosslinked core p(LAEMA-*b*-DEGMA-*st*-MBAm) via RAFT polymerization.

3.2.8 IAZA Encapsulation

IAZA was 'loaded' using the incubation method. Aqueous solutions of nanogels were prepared in 5mg/mL concentrations in PBS. The nanogel solution was mixed with 50 μL of 1 mM IAZA pre-dissolved in 95% ethanol at 10:1 feed ratio with nanogel in excess and incubated for 24 h at 4 °C. The samples were centrifuged at 40 °C in Beckman Coulter Centrifuge (Microfuge 22R) at 14,000 rpm for 30 min. The solution was separated into a gelatinous white pellet and supernatant. The amount of drug encapsulated in the nanogel was determined by sampling the supernatant using UV-Visible Spectroscopy at 320 nm (UVmax for IAZA). The spectroscopic sample reader was pre-calibrated using varying concentrations of IAZA in ethanol. The amount of drug encapsulated (%) was calculated as follows:

$$\%\ Drug\ Encapsulated = \frac{Total\ Drug - Free\ Drug}{Total\ Drug}$$

with free drug being the amount of drug in the supernatant.

3.2.9 Release Profile of Encapsulated Drug from Nanogels

In order to study the release profile of the encapsulated drug, the nanogel was precipitated by centrifuging the sample at 40 °C at 14,000 rpm for 30 min. The supernatant was removed and the gelatinous white pellet was divided into 8 aliquots and re-suspended in 40 °C preheated PBS. The samples were incubated at 23, 30 and 37 °C and, at regular intervals, the nanogel aliquots were re-precipitated and total drug content in the supernatant (released drug) was determined by Jasco V-630 UV-Visible Spectrometer at 320 nm.

3.2.10 Cell Culture

HepG2 hepatocellular carcinoma, MCF-7 breast cancer, MRC-5 human lung fibroblasts and HeLa cervical cancer cell lines were incubated in low-glucose (0.1 W/V %) DMEM media supplemented with 10% fetal bovine serum (FBS), 2 mM glutamine and 1% antibiotic-antimycotic (100 units of penicillin, 100 μg streptomycin and 0.0085% fungizone) in a humidified atmosphere at 37 °C and 5% CO_2. At about 80% confluency, the cells were subcultured by dissociating with 0.25% trypsin in versene, and were cultured twice per week. All tissue culture reagents were purchased from Gibco.

3.2.11 Cytotoxicity of Nanogels and IAZA

HepG2, MCF-7, HeLa and MRC-5 Fibroblasts (10,000 cells/well) were seeded into 96 well tissue culture plates in triplicates and were allowed to adhere overnight. The medium was removed and replaced with fresh DMEM medium containing 10% FBS with varying concentrations (1 to 10 mg/mL) of nanogel and cells were incubated for 24 h with nanogel under evaluation. The cell viability was determined by MTT assay. Briefly, 15 μL of 5 mg/mL MTT solution was added to each well and cells were incubated for 4 h, followed by the addition of 50% DMSO, 50% isopropanol lysis solution. The 96 well tissue culture microplates were shaken for 15 minutes and the absorbance was read at 570 nm using TECAN microplate reader. The IC_{50} values were calculated by sigmoidal curve fitting on Boltzmann distribution function using Origin 9.1 Pro graphing software.

3.2.12 Dynamic Light Scattering and Lower Critical Solution Temperature Characterization of Nanogel

Nanogel solution was analyzed at 1 mg/mL in PBS and the measurements were made at 2 min intervals to allow solution to adjust to temperature fluctuations. The lower critical solution temperature was characterized based on turbidity of solution and measured using Jasco ETC-505T temperature controller. The size of the particle was analyzed by Dynamic Light Scattering (DLS) using ZetaPlus-Zeta Potential Analyzer (Brookhaven Instruments Corporation) at a scattering angle $\theta = 90°$. The solution was filtered through Millipore membrane (0.45 μm pore size) and the data were recorded using Omni size software.

3.2.13 Fluorescent Labelling of Nanogel and Asialofetuin

Nanogels are labeled fluorescently with FITC by activating hydroxyl groups on carbohydrate moieties, and asialofetuin is labelled fluorescently with RITC by covalent coupling through lysine ε-amino groups as previously reported [30, 31]. Briefly, nanogels/asialofetuin are dispersed in 4% $NaHCO_3$ in deionized water and calibrated to pH = 8.5 to make 5 mg/mL solution. FITC and RITC were dissolved in DMSO to make 1 mg/mL solution. FITC/RITC-DMSO was added to the aqueous nanogel/asialofetuin solution in a drop-wise manner (100μL/mL of nanogel/asialofetuin) and stirred for 5 days in the dark conditions. The FITC/RITC-labeled nanogel/asialofetuin solution was dialyzed to remove free FITC/RITC. The fluorescent nanogel and asialofetuin were freeze-dried and obtained as a yellow (FITC) and bright orange powder (RITC), respectively (Appendix A Figure S1).

3.2.14 Cellular Uptake of Fluorescently Labelled Nanogel and Asialofetuin

HepG2 and MCF7 cells ($1x10^6$ cells/well) were seeded onto a glass coverslip slide in 6-well tissue culture plates and allowed to adhere overnight. The media was removed and replaced with 1 mg/mL of FITC-labelled nanogel or RITC-labelled asialofetuin in 5 mM glucose serum-free DMEM media. The cells were incubated for 3 h, followed by 3 washes with PBS and fixed with 3.7% formalin in PBS for 15 min at 23 °C. The formalin was removed and washed 3 times with PBS. The glass coverslip was fixed on microscope slide with nitrocellulose (30% in isopropyl alcohol) dissolved in ethyl acetate and the cells were imaged using Olympus Fluoview FV10i Confocal Microscope at 490 nm and 570 nm emission spectra for FITC and RITC, respectively.

3.2.15 Hypoxia-selective Radiosensitization

Cell radiosensitization potential for IAZA was determined used a ^{60}Co X-ray source together with a clonogenic survival assay [32]. Briefly, HepG2 cells (1×10^5 cells/dish) were seeded into 6 cm tissue culture dishes and allowed to adhere overnight. The media was removed and replaced with 2 mL of DMEM medium containing 0.3-1 mM IAZA (stock solution 54.6 mM in 95% ethanol) and incubated under 5% CO_2 in air at 37 °C for 2 h. The dishes were assigned to either the control (normoxic) or hypoxic groups. Those in the hypoxic group were de-gassed to hypoxia by six consecutive vacuum and nitrogen fill cycles in a vacuum chamber and left under hypoxia for 2 h. The cells were then irradiated in a ^{60}Co γ-irradiator at 0 (control), 4, 8, 12, 20 Gray (Gy) in N_2 (hypoxic sub-group) and oxygenated chambers (normoxic sub-group). The cells were recovered from each dish by two consecutive washes with PBS, followed by the addition of

trypsin. Cells were plated at densities of 400 and 1000 cells/5 mL medium. The cells were incubated for 10-14 days at 37 °C under 5% CO_2, then fixed with 3.7% formalin and stained with crystal violet 0.1% w/v dissolved in ethanol, clones counted and the surviving fractions were calculated using Origin Pro 9.1 graphing software. Tests were done in triplicates. The sensitization enhancement ratio (SER) was calculated by ratio of D_o in the radiation group alone over D_o in the radiation group with the drug treatment under hypoxic conditions.

3.3 Results and Discussion

3.3.1 Synthesis and Characterization of Nanogels

Macro-CTAs, homopolymers with active chain transfer agents, of neutral (pLAEMA), cationic (pLAEMA-*st*-AEMA) and anionic (pLAEMA-*st*-MA) charges were first synthesized by the RAFT method (Table 1). The polymer molecular weights and compositions have been characterized by GPC and ^{1}H NMR (Table 1 and Appendix A Figure S2, respectively). The macro-CTAs are used to copolymerize with thermosensitive DEGMA, cationic AEMA, anionic MA in the presence of cross-linker MBAm in a water/2-propanol solvent mixture (Scheme 3). After purification by dialysis and lyophilization, the nanogels are re-dispersed in water and characterized for their hydrodynamic sizes, size distributions and surface charges at 15 and 37 °C (Table 1-2).

The following nanogels, **NG1**, **NG2**, **NG5**, **NG6** and **NG7** show a net neutral charge at both 15 and 37 °C. **NG3** has a cationic charge of 24.63 ± 1.15 and 28.60 ± 0.63 while **NG4** has an anionic charge of -10.77 ± 0.47 and -10.93 ± 1.18 at 15 and 37 °C, respectively (Table 1-2).

Interestingly, **NG2** containing a cationic core revealed to have a net neutral charge as confirmed by zeta potential analysis, which suggests the inner core is completely shielded by the hydrophilic glycopolymers on the outer shell.

The core of the nanogels is composed essentially of cross-linked di(ethylene glycol) methyl ethyl methacrylate (DEGMA) polymer chains, and hence is thermo-responsive in nature and undergoes a reversible lower critical solution temperature (LCST) phase transition from a swollen globule hydrated state (hydrophilic) to a shrunken coil dehydrated state (hydrophobic) around 32 °C in aqueous solution (Appendix A Figure S3)[15, 23]. The synthesized nanogels ranged in hydrodynamic size from approximately 86 to 178 nm at 15 °C and 59 to 95 nm at 37 °C (Table 1-2, Appendix A Figure S4). Initially, the thermoresponsive properties of the nanogels measured at 1 mg/mL indicated an increase in size as the temperature increased, suggesting that the nanogels may be aggregating at higher temperatures. However, at 0.1mg/mL, all of the nanogel samples collapsed in size and precipitated out of solution as the temperature was raised to 37 °C, thus demonstrating the thermoresponsive properties of the DEGMA monomer crosslinked cores of each individual nanogel particle.

Table 3-2. Analysis and characterization of the composition, hydrodynamic size, particle charge and polydispersity of synthesized nanogels

Nanogel	Composition	Cross-linker %	Hydrodynamic Diameter (nm)		Zeta Potential		PDI
			15 °C	37 °C	15 °C	37 °C	
NG1	poly[(LAEMA$_{25}$)-*b*-(DEGMA-*st*-MBAm-*st*-LAEMA)$_{180}$]	10	86.1 ± 0.3	77.4 ± 0.2	0	0	0.183
NG2	poly[(LAEMA$_{25}$)-*b*-(DEGMA-*st*-MBAm-*st*-AEMA)$_{180}$]	10	111 ± 3.0	59.4 ± 1.8	0	0	0.333
NG3	poly[(LAEMA$_{19}$-*st*-AEMA$_{19}$)-*b*-(DEGMA-*st*-MBAm-*st*-LAEMA)$_{180}$]	10	110 ± 0.7	95.9 ± 0.7	24.63 ± 1.15	28.60 ± 0.63	0.017
NG4	poly[(LAEMA$_{19}$-*st*-MA$_{24}$)-*b*-(DEGMA-*st*-MBAm-*st*-LAEMA)$_{180}$]	10	86.5 ± 0.5	71.7 ± 0.4	-10.77 ± 0.47	-10.93 ± 1.18	0.27
NG5	Poly[(LAEMA$_{21}$)-*b*-(DEGMA-st-MBam)$_{300}$]	5	150.5 ± 11.1	68.0 ± 0.7	0	0	0.16
NG6	Poly[(LAEMA$_{21}$)-*b*-(DEGMA-st-MBam)$_{300}$]	7	178.2 ± 1.6	82.3 ± 0.9	0	0	0.18
NG7	Poly[(LAEMA$_{21}$)-*b*-(DEGMA-st-MBam)$_{180}$]	7	124.1 ± 2.5	91.3 ± 0.7	0	0	0.129

*The degree of polymerization values (DP) of the cores were calculated as [(DEGMA) + (MBAm) + (monomer)]/[Macro-CTA].

3.3.2 Efficiency of IAZA Encapsulation within Nanogel Core

An important feature of stimuli-responsive nanogels is the capability to encapsulate drug molecules in their core for delivery. Cross-linking the polymer core provides a stable nanogel structure, which can be optimized to encapsulate diverse sizes of molecules. The thermosensitive nature of the core plays a vital role in encapsulating and releasing drugs within the core as a function of temperature. At low temperatures (4 °C), the nanogel core is hydrophilic and swells in aqueous solution, however as the temperature rises (37 °C) the nanogel core becomes hydrophobic causing the core to collapse and allow the encapsulation of (macro)molecules [33]. Above the LCST, the polymer precipitates out of solution due to hydrophobic interactions with the aqueous solution, which allows for easy separation from the solution by maintaining a high temperature and simple centrifugation. The nanogels were collapsed to trap IAZA within the core and precipitated at 14,000 RPM and 40 °C for 30 min. The amount of encapsulated IAZA was estimated by calculating the difference between the total amount of IAZA added in solution and the amount of free IAZA in the aqueous supernatant after the nanogel was precipitated, following a procedure reported by Bhuchar et al [34].

The synthesized nanogels **NG1**, **NG2** and **NG3** displayed encapsulation efficiencies of 0.42± 0.01%, 48.57 ± 1.92% and 50.35 ± 2.62%, respectively (Figure 3-4 A). Interestingly, these nanogels did not precipitate out of solution under physiological conditions. The addition of LAEMA, a hydrophilic monomer, in the core of the nanogel has most likely increased the solubility of the nanogels above the LCST temperature. Furthermore, while **NG2** and **NG3** showed encapsulation rates of 48.57 ± 1.92% and 50.35 ± 2.62%, respectively, the IAZA was immediately released upon resuspension of the nanogels in buffer solution. The hydrophilic

LAEMA monomer in the core of **NG2** and **NG3** may have been affecting the release of IAZA, presumably by altering the physiological properties of the LCST in the core of the nanogel [35, 36].

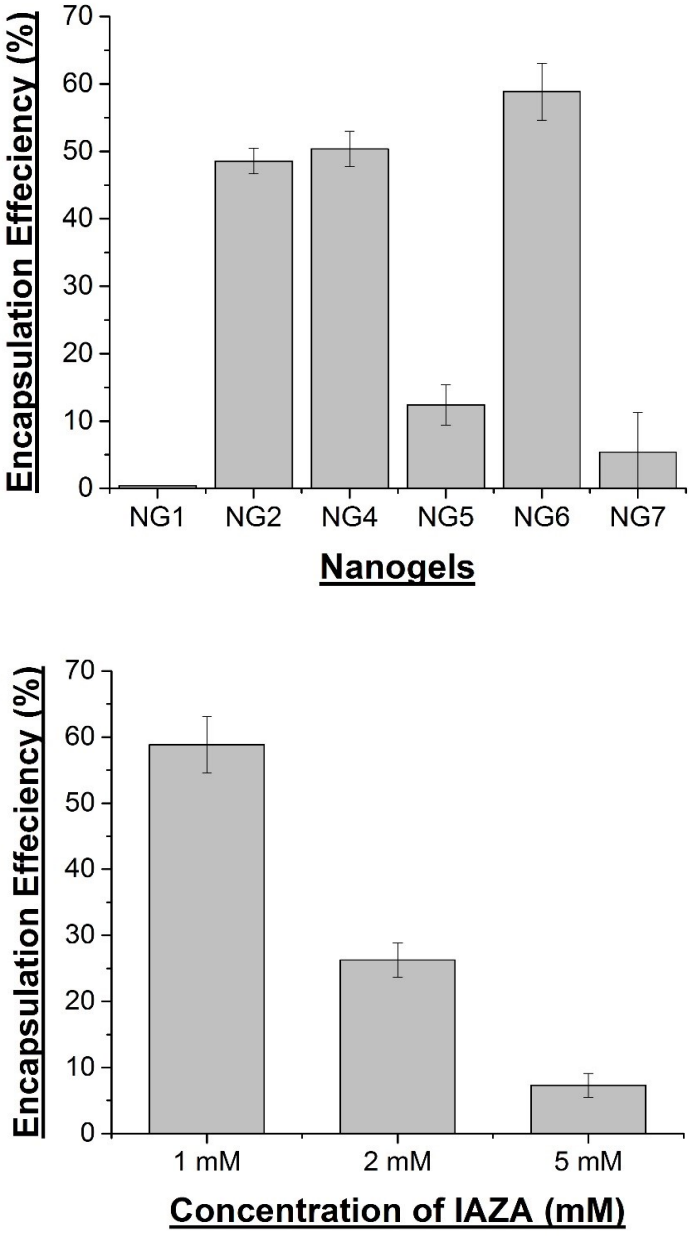

Figure 3-4. (A) Encapsulation efficiency of 1 mM IAZA within nanogel core and (B) maximum loading capacity of **NG6** with 1, 2 and 5 mM IAZA.

In an attempt to lower the LCST in the core, new nanogels (**NG5**, **NG6** and **NG7**) were prepared with exclusively DEMGA in the core of the nanogel structures (Table 1-2). Notably, two factors played an important role in enhancing the encapsulation capacity of IAZA within the nanogels without LAEMA within the core; firstly, the degree of cross-linking within the core with MBAm and secondly, the hydrodynamic size of the nanogel. Of these three nanogels, **NG5** was synthesized with the lowest mole percentage of cross-linker within the core of only 5%. Compared to **NG6**, the chemical compositions of the shell and core components are almost identical to **NG5**, however there was a notable difference between the LCST hydrodynamic size transition and encapsulation loading capacity. Interestingly, lowering the molar percentage of cross-linker to 5% in **NG5** allowed the core to collapse, protecting the hydrophobic core and decreasing overall in size (150.5 ± 11.1 nm at 15 °C to 68.0 ± 0.7 nm at 37 °C); increasing the molar percentage of cross-linker to 7% in **NG6** caused an overall increase in size at both the below and above the LCST (178.1 ± 1.6 nm at 15 °C to 82.3 ± 0.9 nm) (Table 1-2). Previous reports by Messanger *et al*. indicated that the degree of swelling of the nanogels was highly dependent on cross-linking density within the core, which affected its sensitivity towards external stimuli such as pH and the temperature [34]. Inversely, this also affected the encapsulation rates of nanogels with approximately 12.38 ± 2.96 mM and 58.86 ± 4.22 mM of **NG5** and **NG6**, respectively (Figure 3-4 A). These results suggest that having a higher degree of cross-linking in the core may contribute to a higher encapsulation efficiency of macromolecules due to stronger, more complex network of crosslinking. In contrast, **NG6** and **NG7** were synthesized with the same molar percentage of cross-linker of 7%, however the core component of **NG7** was significantly smaller compared to **NG6** (124.1 ± 2.5 at 15 °C and 91.3 ± 0.7 at 37 °C) (Table 1-2). In relation to the encapsulation efficiencies, **NG7** demonstrated the capacity to

encapsulate only 5.38 ± 5.88% of IAZA within the core, which suggests that the smaller hydrodynamic size of nanogels also play an important role in modulating the encapsulation efficiency. Of all the nanogels synthesized, **NG6** demonstrated the highest encapsulation efficiency with 58.86 ± 4.22% of 1 mM IAZA (Figure 3-4 A). In another experiment, **NG6** was able to encapsulate 26.25 ± 2.59% of 2 mM IAZA and 7.30 ± 1.8% of 5 mM IAZA (Figure 3-4 B). Overall, with respect to the average encapsulating efficiencies of 1, 2 and 5 mM IAZA, **NG6** demonstrated maximum loading capacity i.e., 0.49 ± 0.11 mM of IAZA within the core.

3.3.3 Release Profile of Encapsulated IAZA from Nanogel Core

The release profile of IAZA encapsulated in the core of **NG6** was studied at varying temperatures (Figure 3-5 A). With **NG6** at a concentration of 5 mg/mL, and in excess, IAZA (1 mM) was incubated at a 10:1 feed ratio for 24 h at 4 °C. The nanogels were precipitated at 40 °C and were stabilized to 37, 30 or 23 °C for 1 h before determining the amount of IAZA released by UV-VIS spectroscopy at regular intervals. Above the LCST at 37 °C, approximately 80% of IAZA was slowly released from the core over 10 h by passive diffusion in a non-burst release manner. The release of IAZA at 30 °C demonstrated an initial burst release profile, with approximately 50% of IAZA released within the first hour and approximately 80% of IAZA after 6 h. The initial release of approximately 50% of IAZA at 30 °C may be attributed to the large polydispersity of the nanogel complexes, as the particle size differential of the core may be causing some nanogels to have a slightly lower LCST. However, at 23 °C, a burst release profile of approximately 80-85% of encapsulated IAZA was observed within 1 h. The LCST phase change of **NG6** was characterized at 28 °C where the nanogel in aqueous solution rapidly

precipitated out of solution by analysis of turbidity (Figure 3-5 B). Below the LCST, the hydrodynamic meter of the nanogel is approximately 180 nm. However, as the temperature is increased to the initial threshold of the LCST at 25 °C, the hydrodynamic meter drastically decreases to approximately 80 nm. (Figure 3-5 B).

A VERSION OF THIS CHAPTER HAS BEEN PUBLISHED: STEPHEN QUAN, YINAN WANG, AIHUA ZHOU, PIYUSH KUMAR AND RAVIN NARAIN, BIOMACROMOLECULES., **2015, 16, 1978-1986.

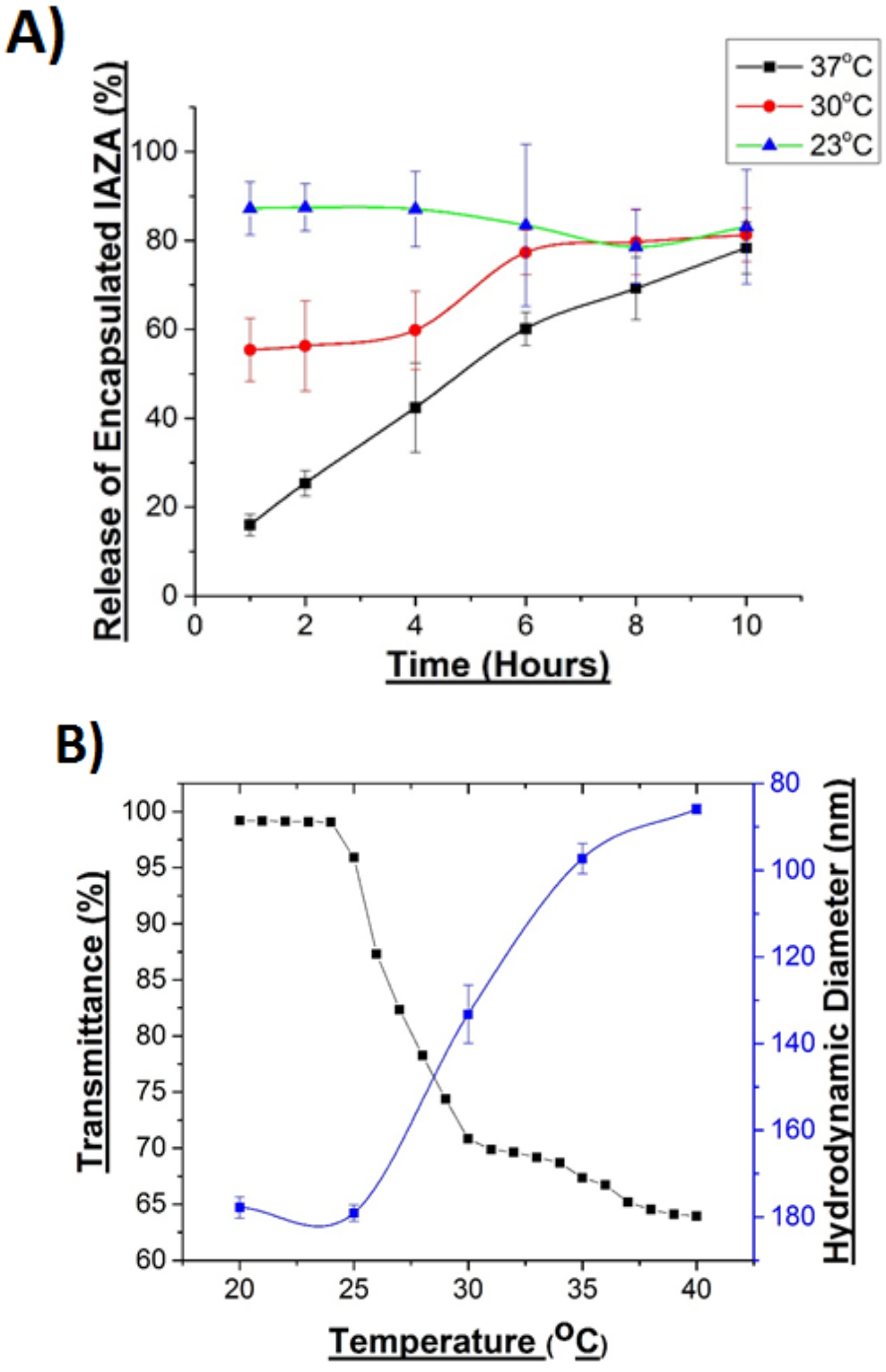

Figure 3-5. (A) Release profile of IAZA encapsulated in **NG6** at 23, 30 and 37 °C and (B) Lower critical solution temperature and dynamic light scattering of **NG6**

3.3.4 Cytotoxicity Studies of IAZA and Nanogels

Radioiodinated IAZA, a 2-nitroimidazole-based α-nucleoside, has demonstrated promising potential in clinical imaging of cancer patients diagnosed with solid hypoxic tumors [37-39]. Mechanistically, nitroimidazoles sensitize hypoxic tumors to the killing effects of ionization radiation by oxygen-mimicking within the cell, thus generating reactive oxygen species in hypoxic environments. HPLC analysis-based stability studies of ^{131}I-IAZA radiopharmaceutical in 15% ethanolic saline (vol/vol; stored at 4 °C) over an extended period of 15 days demonstrated it to be very stable as the radiochemical and chemically purities were found to be >98% and >94%, respectively [40]. IAZA was evaluated for its cytotoxic effects *in vitro* under oxygenated conditions in HepG2 hepatocellular carcinoma, MCF-7 mammalian breast cancer and MRC-5 fetal lung fibroblast cells lines at concentrations ranging from 0.25 – 1.5 mM (Figure 3-6 A). While the compound is relatively biocompatible, the cytotoxicity data indicated that IAZA was relatively non-toxic at concentrations below 0.5 mM, and the IC_{50} was established at approximately 1 mM after 72 h of incubation, except for MRC-5 cells which showed marked reduction in survival after 0.75 mM (Figure 3-6 A). The IC_{50} of IAZA at approximately 1 mM was consistent with previous toxicity results in EMT-6 murine mammary tumor cells [40]. Furthermore, the IC_{50} toxicity profile also showed a close correlation to the corresponding fluorinated nitroimidazole analogue, flouroazomycin arabinofuranoside (FAZA) [32, 39].

A VERSION OF THIS CHAPTER HAS BEEN PUBLISHED: STEPHEN QUAN, YINAN WANG, AIHUA ZHOU, PIYUSH KUMAR AND RAVIN NARAIN, BIOMACROMOLECULES., **2015, 16, 1978-1986.

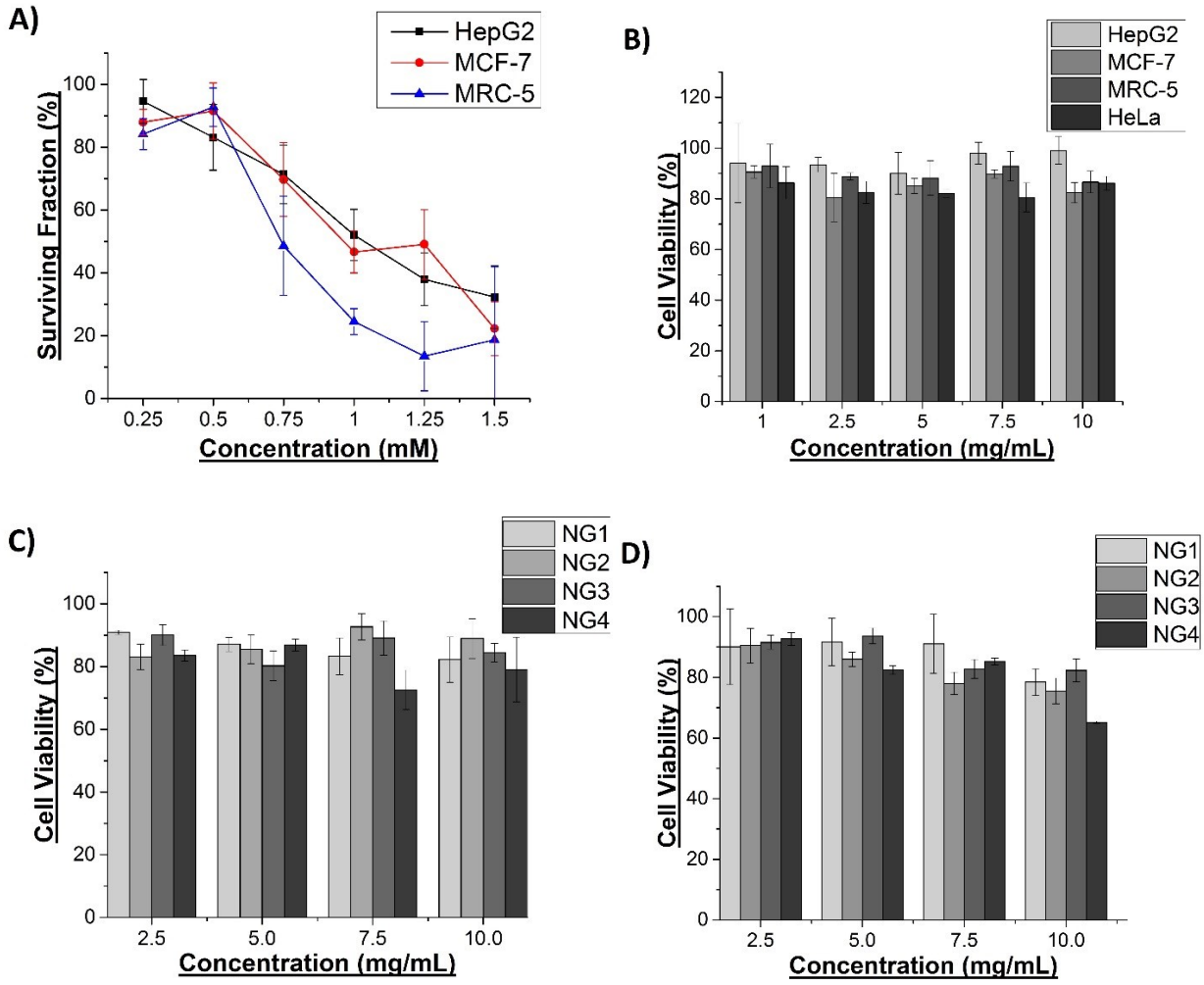

Figure 3-6. Cytotoxicity evaluation of (A) IAZA in HepG2, MCF-7 and MRC-5 cells (B) **NG6** in HepG2, MCF-7, MRC-5 and HeLa cells (C) **NG1-4** in HepG2 cells and (D) **NG1-4** in MCF-7 cells as determined by MTT cell viability assay.

The cytotoxicity of **NG6** polymers in HepG2 HCC, MCF-7 human breast cancer cells and MRC-5 fetal lung fibroblasts is analyzed using MTT assay (Figure 3-6 B). **NG6** demonstrated relatively low cytotoxicity and high biocompatibility up to a concentration of 10 mg/mL in all three cell lines. Interestingly, increasing the concentration of the **NG6** polymer complex in solution correlates with a slight increase in cell viability and proliferation of HepG2 cells

compared to MRC-5 and MCF-7 cells (Figure 3-6 B). The galactose moiety LAEMA, decorated on the shell of **NG6** complex interacting in a receptor-specific manner with the ASGPR, is highly uptaken via receptor-mediated endocytosis and metabolized as a substrate to enhance cellular processes and replication, a phenomenon previously reported by Ahmed *et al* [41-43]. Furthermore **NG1-NG4** were tested for cytotoxicity in HepG2 and MCF-7 cells up to a concentration of 10 mg/mL and showed relatively low toxicity and high biocompatibility in both cell lines. (Figure 3-6 C and 3-6 D, respectively).

3.3.5 *In Vitro* Uptake of Nanogels via ASGPR Overexpression on Cell Surface

The interaction and uptake of FITC-labeled-**NG6** with the ASGPR after 3 h of incubation is studied using confocal fluorescence microscopy in ASGPR expressing HepG2 and ASGPR-deficient HeLa cells (Figure 3-7). ASGPR is well known for receptor-mediated binding, clathrin-coated vesicle internalization, endosomal trafficking and metabolic lysosomal degradation of asialoglycoproteins and glycoproteins containing terminal galactose and N-acetyl-glucosamine moieties [38, 44]. Similar studies on hepatic-targeting with galactose-decorated polyplexes have demonstrated high uptake in HepG2 cells expressing ASGPR with promising efficacy for delivery of various macromolecular substances [11, 39, 45]. Confocal microscopic images show the higher uptake of FITC-labeled-**NG6** in ASGPR expressing HepG2 cells compared to ASGPR-deficient HeLa cells, due to the high affinity interaction between the receptor and galactose-decorated surface of **NG6**.

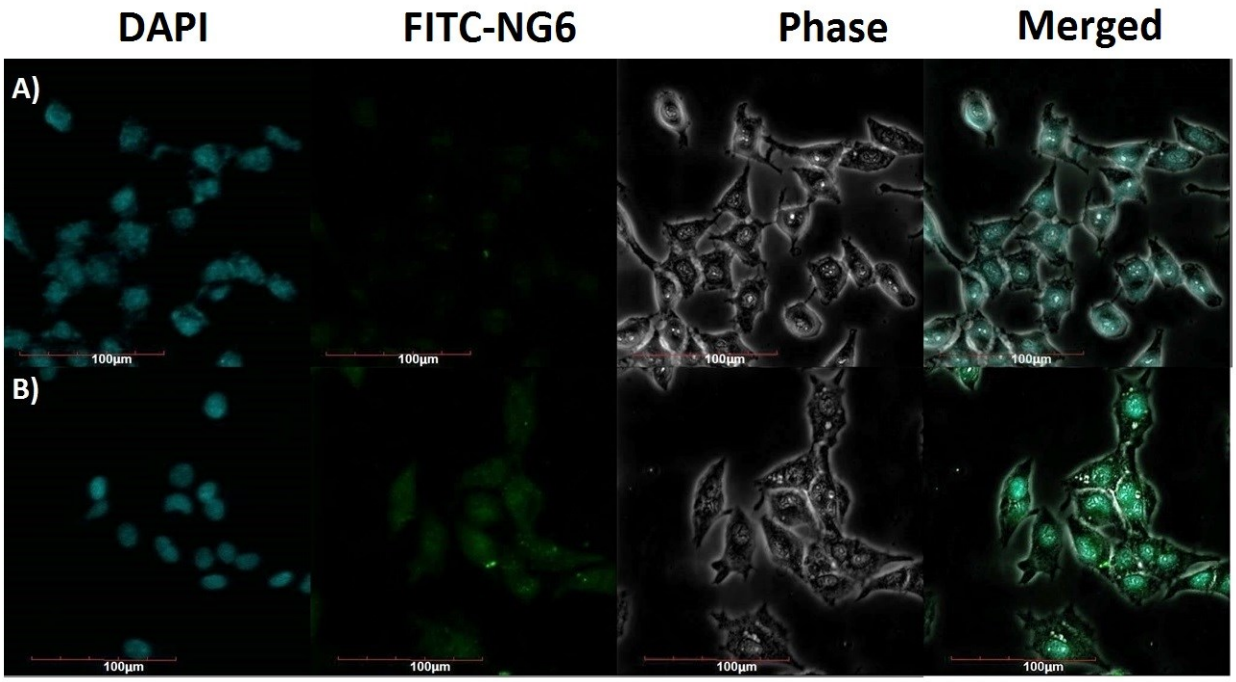

Figure 3-7.Uptake of FITC-labeled-**NG6** in (A) HeLa cells and (B) HepG2 cells after 3 h of incubation.

3.3.6 Competitive Binding of ASGPR with Asialofetuin

In this study, ASGPR expressing HepG2 cells were saturated with RITC-labelled-asialofetuin, a native glycoprotein binding substrate to the ASGPR, in order to determine the uptake of the FITC-labelled-**NG6** in the presence of ASGPR blocked cells (Figure 3-8). Previous studies by Li *et al*. demonstrated that competition by free galactose for ASGPR binding sites-inhibited the uptake of ^{125}I-asialoorosomucoid, a native binding ligand asialyated glycoprotein with a pendant of galactosyl residues [46]. RITC-labelled-asialofetuin in serum free media was incubated with HepG2 cells for 3 h before removal, followed by two subsequent washes with PBS, addition of FITC-labelled-**NG6**, and then further incubation for another 3 h. In this study, the blocking of the ASGPR in HepG2 cells was to implicate if mechanism of uptake of **NG6** was through the

ASGPR or by non-specific interaction through secondary receptors. Interestingly, the fluorescence intensity of FITC-labelled-**NG6** is similar to that of ASGPR-deficient HeLa cells (Figure 3-7), which suggests that the primary route of uptake of these nanogel complexes are through the ASGPR.

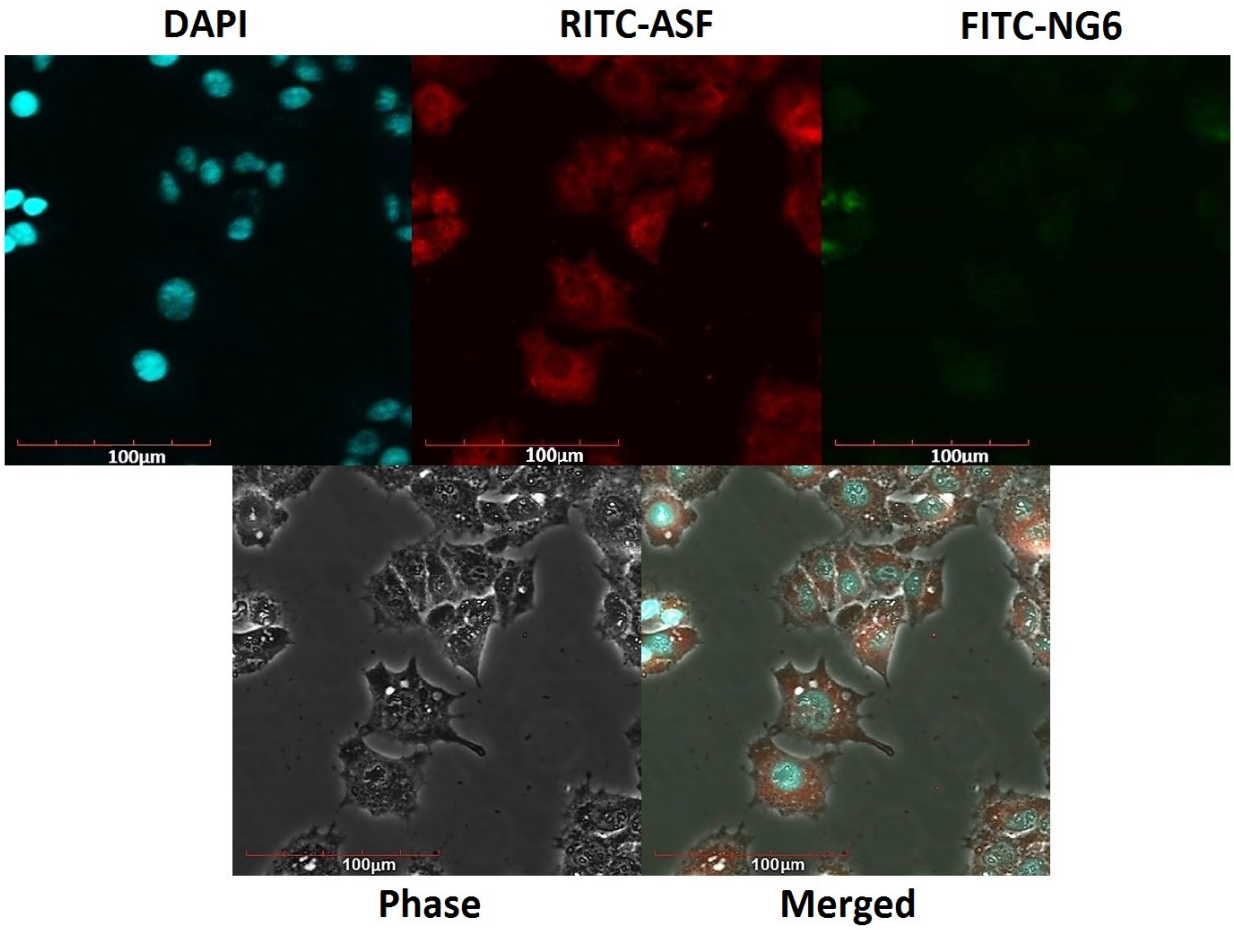

Figure 3-8. Competitive binding and uptake of FITC-labeled-**NG6** after RITC-labelled-asialofetuin blocked HepG2 cells.

3.3.7 Hypoxia-Selective Radiosensitization

The survival curves determined for IAZA under oxygen and nitrogen conditions by using a ^{60}Co X-ray source together with a clonogenic survival assay is a standard protocol for determining hypoxia-selective radiosensitization potential of an agent [13, 47, 48]. The cells were incubated with IAZA under hypoxic conditions for 2 h before exposure to ^{60}Co X-ray radiation, and the toxicity of IAZA to normoxic cells at this concentration is expected to be minimal. The data confirmed that the radiosensitization effects of IAZA increased linearly as a function of concentration from 0.3 to 1 mM (Figure 3-9). In another experiment, **NG6** was used to encapsulate approximately 0.6 mM of IAZA (Figure 3-4 B) to determine whether encapsulation modulates the radiosensitization potential of IAZA, which was evaluated by the clonogenic survival assay. While the data on the radiosensitizing effects up to 8 Gy single dose of radiation with 0.6 mM IAZA alone and IAZA encapsulated in **NG6** showed similar effects up until 10% surviving fractions, IAZA and **NG6** complex demonstrated a slightly superior sensitization enhancement ratio ($SER_{0.6mMIAZA}$ ~ 1.33 vs. $SER_{IAZA+NG6}$~ 1.62) in HepG2 cells. Furthermore, the radiosensitization effects of **NG6**+IAZA proved to be similar to the effects with dosages of 1mM of IAZA past 10% surviving fraction. This demonstrates **NG6** to be a potentially useful drug delivery system for targeting hypoxic cells using nitroimidazole-based radiosensitizers [14].

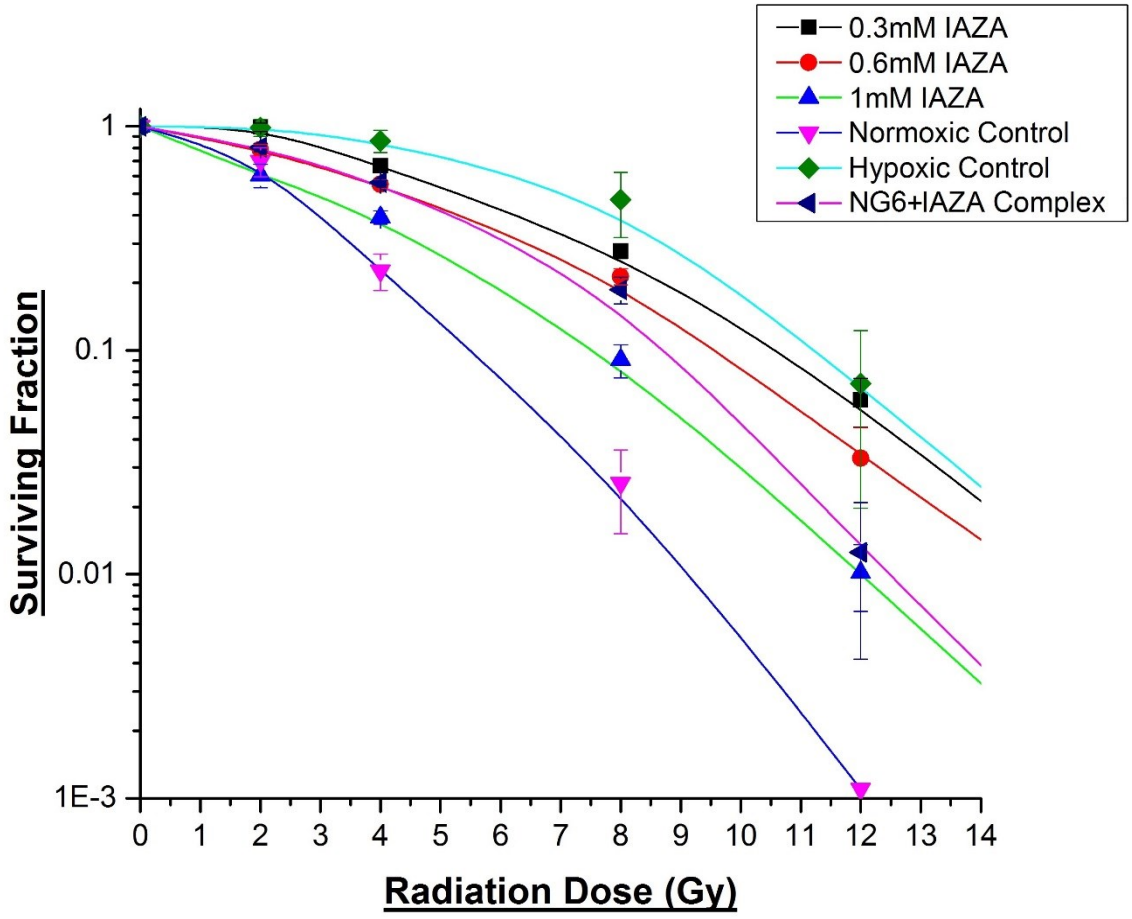

Figure 3-9. *In vitro* radiosensitization of HepG2 HCC cells by IAZA and IAZA encapsulated in **NG6** under hypoxic condition as demonstrated by their survival curves.

3.4 Conclusion

This study provides the detailed synthesis of carbohydrate-based nanogels of different sizes with cationic and ionic components for the encapsulation and delivery of IAZA to HepG2 cells. It is found that the encapsulation efficiency of the nanogels is dependent on the size and hydrophobic property of the core during LCST phase change. Interestingly, **NG6** showed a maximum loading capacity of 0.49 ± 0.11 mM of IAZA within the core and can be released by passive diffusion over 10 h. The biocompatible, nontoxic nanogels demonstrated high specificity towards ASGPR on HepG2 cells and demonstrated a slightly superior SER compared to IAZA alone ($SER_{0.6mM\ IAZA}$ ~ 1.33 vs. $SER_{IAZA+NG6}$ ~ 1.62). Alternatively, the nanogel-IAZA complex demonstrated a slightly lower oxygen enhancement ratio (OER) compared to 0.6mM of IAZA alone at 10% survivability, with an OER of 1.52 and 1.66, respectively. These preliminary studies offer encouraging support to the carbohydrate-based nanogels as superior drug delivery carriers of nitroimidazole-based hypoxia radiosensitizers and other drug compounds specifically towards hepatocellular carcinomas. Their role in delivering other classes of hypoxia-selective drugs is therefore legitimate and is highly warranted to maximize the therapeutic benefits.

3.5 References

[1] Dykxhoorn D., Palliser D., Lieberman J., *Gene Thera.* **2006**, *13*, 541-52.

[2] Li J., Zacharek S., Chen X., Wang J., Zhang W., Janczuk A., *Bioorg. Med. Chem.* **1999**, *7*, 1549-58.

[3] Chapman J., Engelhardt E., Stobbe C., Schneider R., Hanks G., *Radio. Onc.* **1998**, *46*, 229-37.

[4] Harris A., *Nature Rev. Can.* **2002**, *2*, 38-47.

[5] Lundquist J., Toone E., *Chem. Rev.* **2002**, *102*, 555-78.

[6] Mishra V., Kumar R., *J. Sci. Res.* **2012**, *56*, 141-76.

[7] Hrzenjak A., Frank S., Wo X., Zhou Y., Vanberkel T., Kostner G., *J. Biochem.* **2003**, *376*, 765-71.

[8] Yu J-M., Li W-D., Lu L., Zhou X., Wang D., Li H., *J. Mat. Sci.* **2014**, *25*, 691-701.

[9] Zheng D., Duan C., Zhang D., Jia L., Liu G., Liu Y., *J. Int. Pharm.* **2012**, *436*, 379-86.

[10] Jain D., Kumar A., J. *Biomed. Pharm. Res.* **2013**, *2*.

[11] Eichman J., Bielinska A., Kukowska-Latallo J., Baker J., *Pharm. Sci. Tech. Today.* **2000**, *3*, 232-45.

[12] Kabanov A., Vinogradov S., *Ange. Chemie Int. Ed.* **2009,** *48*, 5418-29.

[13] Hector A., Schmid B., Beierkuhnlein C., Caldeira M., Diemer M., Dimitrakopoulos P., *Science*. **1999**, *286*, 1123-7.

[14] Yoo H., Mok H., *Arch. Pharm. Res.* **2015**, *38*, 129-36.

[15] Ramos J., Imaz A., Forcada J., *Poly. Chem.* **2012**, *3*, 852-6.

[16] Semsarilar M., Perrier S., *Nature Chem.* **2010**, *2*, 811-20.

[17] Takasawa M., Moustafa R., Baron J., *Stroke*. **2008**, *39*, 1629-37.

[18] Nunn A., Linder K., Strauss H., *J. Euro. Nuc. Med.* **1995**, *22*, 265-80.

[19] Fleming I., Manavaki R., Blower P., West C., Williams K., Harris A., *J. Brit. Cancer*. **2014**.

[20] Baio J., Schach D., Fuchs A., Schmüser L., Billecke N., Bubeck C., *Chem. Comm.* **2015**, *51*, 273-5.

[21] Richardson S., Kolbe H., Duncan R., *J. Int. Pharm.* **1999**, *178*, 231-43.

[22] El-Sayed A., Futaki S., Harashima H., *J. Amer. Assoc. Pharm. Res.* **2009**, *11*, 13-22.

[23] Benns J., Choi J., Mahato R., Park J., Kim S., *Bioconj. Chem.* **2000**, *11*, 637-45.

[24] Wang F., Wang Y., Wang H., Shao N., Chen Y., Cheng Y., *Biomaterials*. **2014**, *35*, 9187-98.

[25] Benaglia M., Rizzardo E., Alberti A., Guerra M., *Macromolecules*. **2005,** *38,* 3129-40.

[26] Deng Z., Li S., Jiang X., Narain R., *Macromolecules*. **2009,** *42*, 6393-405.

[27] Deng Z., Bouchackif H., Babooram K., Housni A., Choytun N,. Narain R., *J. Poly. Sci. Part A.* **2008**, *46*, 4984-96.

[28] Deng Z., Ahmed M., Narain R., *J. Poly. Sci. Part A.* **2009**, *47*, 614-27.

[29] Sunasee R., Wattanaarsakit P., Ahmed M., Lollmahomed F., Narain R., *Bioconj. Chem.* **2012**, *23*, 1925-33.

[30] Ahmed M., Narain R., *Mole. Pharm.* **2012**, *9*, 3160-70.

[31] Detampel P., Witzigmann D., Krähenbühl S., Huwyler J., *J. Drug Targ.* **2013**, *22*, 232-41.

[32] Kumar P., Naimi E., McEwan A., Wiebe L., *Bioorg. Med. Chem.* **2010**, *18*, 2255-64.

[33] Lee J., Jung J., Kim Y., Lee E., Choi J., *J. Int. Pharm.* **2014**, *459*, 10-8.

[34] Yang Y., Yang Y., Xie X., Wang Z,. Gong W,. Zhang H., *Biomaterials*. **2015**, *48*, 84-96.

[35] Plummer, R., Hill D., Whittaker, A., *Macromolecules*. **2006**, *39*, 8379-8388.

[36] Wang Y., Kotsuchibashi Y., Liu Y., Narain R., *Langmuir*. **2014**, *30*, 2360-2368.

[37] Liu X., Liu C., Zhou J., Chen C., Qu F., Rossi J., *Nanoscale.* **2015**.

[38] Aujard I., Benbrahim C., Gouget M., Ruel O., Baudin J., Neveu P., *J. Euro. Chem. A.* **2006**, *12*, 6865-79.

[39] Pack D., Hoffman A., Pun S., Stayton P., *Nature Rev. Drug Disc.* **2005**, *4*, 581-93.

[40] Chacko R., Ventura J., Zhuang J., Thayumanavan S., *Adv. Drug Del. Rev.* **2012**, *64*, 836-51.

[41] Booth A., Coxon T., Gough J., Webb S. *Cambridge Univ Press*. **2014**. mrss14-1688-y05-14.

[42] Park I., Kim T., Kim Y., Choi Y., Nah J., Cho C., *Key Eng,. Mat.* **2007**, *342*, 437-40.

[43] Gonçalves C., Berchel M., Gosselin M., Malard V., Cheradame H., Jaffrès P., *J. Int. Pharm.* **2014**, *460*, 264-72.

[44] Rigopoulou E., Roggenbuck D., Smyk D., Liaskos C., Mytilinaiou M., Feist E., *Autoimm. Rev.* **2012**, *12*, 260-9.

[45] Striegel A., Yau W., Kirkland J., Bly D., *John Wiley & Sons.* **2009**.

[46] Trathnigg B., *Prog. Poly. Sci.* **1995**, *20*, 615-50.

[47] Cheng C., Saltzman W., *Biomaterials*. **2011**, *32*, 6194-203.

[48] Chen P., Jafari M., Xu W., Chen B., Pan R., Karunaratne N., *US Patent 20,140,350,082*, **2014**.

4 Cationic Galactose-Conjugated Copolymers for Epidermal Growth Factor (EGFR) siRNA Knockdown in Cervical Adenocarcinoma

4.1 Introduction

Over the past decade, the development of gene therapeutics for the systemic disruption of gene expression to treat various malignant and genetic diseases has been extensively pursued [1-3]. Small interfering RNA (siRNA) therapy has the capability to interfere with critical cellular pathways by knocking down and silencing gene expression of essential proteins, thus opening new pathways for alternative treatments of chemotherapy-resistant diseases [4, 5]. However the effectiveness of siRNA therapies *in vivo* has been compromised and limited since siRNA are prone to degradation by Ribonuclease (RNase) enzymes in the blood stream. This results in transient expression with low tissue selectively and relatively poor cellular uptake [6, 7]. Reports have reaffirmed that the design of effective non-viral gene carriers with lipids, carbohydrates, proteins and viral vectors can significantly improve the outcome of oligonucleotide therapies [8]. In this regard, much effort has been dedicated to the development of versatile nanocarriers that can improve the pharmacokinetics and potential applications of these innovative gene therapy tools.

Synthetic glycopolymers have recently drawn enormous attention due to their unique capabilities to imitate naturally occurring polysaccharides, increase blood biocompatibility of gene delivery vehicles, and promote carbohydrate-specific recognition in cell-cell communication [9-11]. It has been reported that the carbohydrate-protein interactions are significantly improved with multivalent display of carbohydrate ligands, referred to as the “glycosidic cluster effect” [12-14]. However the strength and affinity of these interactions are largely governed by their pendant

display, density and relative spatial arrangement [15, 16]. Many studies have demonstrated glycopolymers delivery vehicles to improve colloidal stability in physiological conditions, provide active modes of cellular targeting for delivery and minimize the degradation of plasmid DNA/siRNA and other non-specific interactions in the blood stream [4-6]. Recent, Narain *et al*. have validated the potential of pendant galactose moieties conjugated on glycopolymer delivery systems for targeting liver cancers that overexpress the ASGPR [17-19]. Thus, exploiting glycopolymer-conjugated gene delivery vehicles to improve the knockdown efficacy and the biocompatibility, typically associated with many toxic commercially available transfection agents, is a logical way to target liver cancers.

In a variety of cancers such as ovarian, lung and breast carcinomas, epidermal growth factor receptor (ErBb1/EGFR) is largely overexpressed, and is responsible for uncontrolled cell proliferation and evading apoptotic pathways [20-22]. Reports render the evidences that silencing the EGFR gene blocks EGFR-mediated cell proliferation pathways and inhibits downstream cell-signalling pathways between other ErBb family members, which can subsequently increase chemotherapeutic sensitivity and induce tumor kill [22, 23]. The research have shown that HeLa cells overexpressing EGFR on the cell surface can be knocked down effectively without compromising the cell viability [24, 25]. Herein, we report the RAFT synthesis of a family of statistical and block glycopolymers with LAEMA and AEMA for the complexation and delivery of EGFR siRNA in HeLa cells to examine the gene knockdown efficiency, cellular uptake and cytotoxicity are reported.

4.2 Experimental

4.2.1 Materials

2- LAEMA, 2- AEMA and the chain transfer agent (CTA), cyanopentanoic acid dithiobenzoate (CTP) were synthesized in the laboratory according to previously reported protocols [19, 24, 26]. 4,4′-Azobis-(cyanovaleric acid) (ACVA) was purchased from Sigma-Aldrich (Oakville, Canada). Branched PEI (M_w = 25 kDa) was purchased from Polysciences Inc. DMEM/F12 media, penicillin (10 000 U mL^{-1}), streptomycin (10 mg mL^{-1}), 0.25% trypsin–EDTA, Opti-MEM (OMEM) and Fetal Bovine Serum (FBS) were obtained from Gibco. Human EGFR-specific small interfering RNA (EGFR siRNA), control EGFR siRNA–FITC conjugate and primary antibody (rabbit polyclonal EGFR specific IgG) were purchased from Santa Cruz Biotechnology. Human EGFR–siRNA consists of 19–25 nucleotides specific for genetic chromosomal locus 7p11.2. Fluorescein-conjugated control siRNA is a non-specific scrambled siRNA of 19–25 nucleotides. Horseradish peroxidase (HRP)-conjugated secondary antibody (Anti-rabbit IgG) and HRP-stabilized (3,3′, 5,5′-tetramethylbenzidine) (TMB) substrate were purchased from Promega Corporation. SYBRSafe DNA gel stain was obtained from Fisher Scientific. The organic solvents were purchased from Caledon Laboratories Ltd (Georgetown, Canada), and were used without further purification.

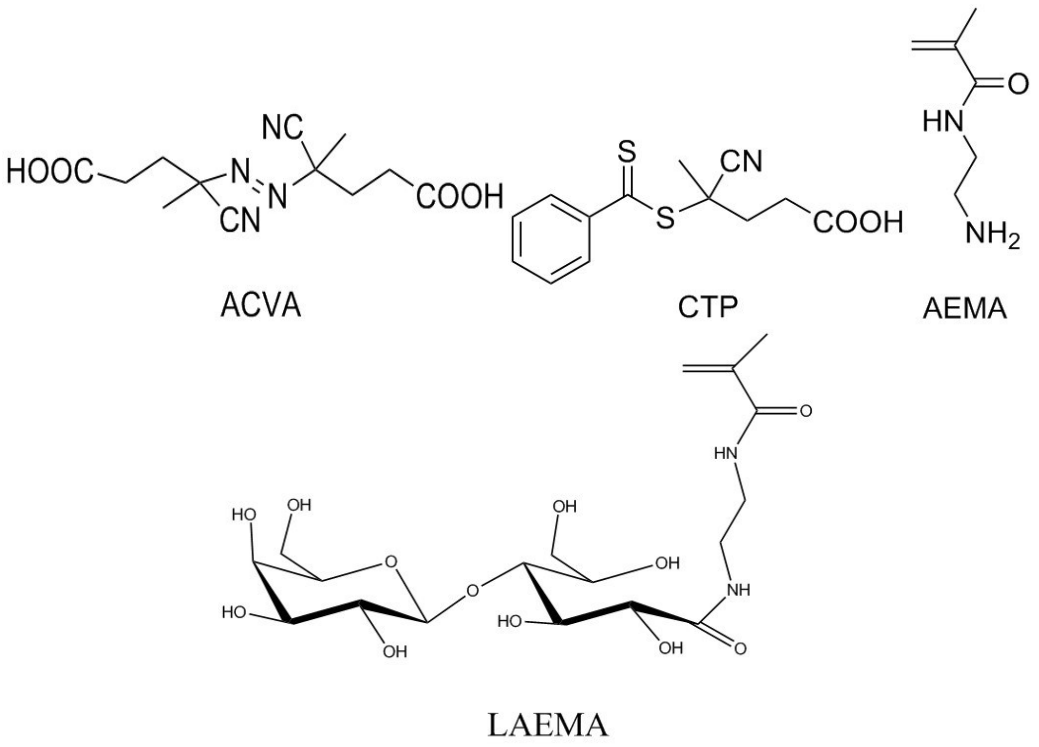

Figure 4-1. Chemical structure of monomers 2- LAEMA, 2- AEMA, chain transfer agent (4-cyanopentanoic acid dithiobenzoate (CTP) and polymerization initiator (4′-azobis(4-cyanovaleric acid (ACVA).

4.2.2 Synthesis of Cationic Glycopolymers by RAFT Polymerization

The cationic glycopolymers were synthesized according to a reported procedure [18]. In a typical synthesis of a block copolymer, the AEMA macroCTA is polymerized using CTP as the chain transfer agent (CTA) and ACVA as the initiator (Figure 4-1). In a 10 mL Schlenk flask, AEMA (591 mg or 3.5 mmol) was dissolved in double distilled water (4 mL) before the addition of 1 mL CTP (10 mg or 0.035 mmol, target DP_n = 50) and ACVA (2 mg or 0.0047 mmol) in N,N'-dimethylformamide (DMF) solution. The solution was degassed by purging with nitrogen for 30 min, and the reaction was carried out at 70 °C for 6 h. The polymerization was quenched in liquid nitrogen and the polymer was precipitated in acetone with residual monomer removed by 2-propanol washes. Subsequently, $P(AEMA_{58})$ was used as the macroCTA to synthesize

P(AEMA$_{58}$-*b*-LAEMA$_{56}$) diblock copolymer. The second monomer, LAEMA (1.22 g or 2.6 mmol) was added to p(AEMA$_{58}$) solution (0.5 g or 0.052 mmol) in double distilled water, followed by the addition of ACVA (2.9 mg) in DMF (1 ml). The reaction mixture was degassed by liquid nitrogen purge and the reaction was carried out at 70 °C for 24 h. The diblock copolymer p(AEMA$_{58}$-*b*-LAEMA$_{56}$) was precipitated in acetone and followed by three methanol washes to remove residual monomer.

4.2.3 Formulation of Cationic Glycopolymer-siRNA Complexes

EGFR-siRNA (250 ng) was combined with cationic glycopolymers (in water or OMEM media) at different weight/weight ratios and the mixture was incubated at 23 °C for 30 min.

4.2.4 Dynamic Light Scattering (DLS) and Zeta Potential Measurements

The hydrodynamic size and charge of the cationic glycopolymer-siRNA complexes were analyzed using ZetaPlus-Zeta Potential Analyzer (Brookhaven Instruments Corporation) at a scattering angle θ = 90 °C. The cationic glycopolymer-siRNA complexes were formulated at w/w ratio of 15 in water and OMEM media. The aggregation of glycopolymer-siRNA complexes was further studied by the addition of serum proteins in OMEM. The net charge of complexes was studied in deionized water.

4.2.5 Gel Permeation Chromatography

Molecular weight and molecular weight distributions were determined by conventional Viscotek gel permeation chromatography (GPC) system using aqueous eluents; two WAT011545 Waters columns at 23 °C and a solution of 0.5 M sodium acetate / 0.5 M acetic acid buffer as eluent at a flow rate of 1.0 mL/min were used in chromatography. The polymers were characterized based on seven near-monodisperse Pullulan standards (Mw) 5900-404000 g mol^{-1}.

4.2.6 Agarose Gel Electrophoresis

The polyplexes were formulated in water at varying weight/weight ratios as described above and were loaded in 1% agarose gel containing 1:10000 dilution SYBRsafe DNA gel stain in 1X TAE buffer. The gel was run for 45 min at 130 V and illuminated with UV light using UV transilluminator (Alpha Innotech; San Leandro, CA) to visualise the siRNA bands.

4.2.7 Cell Culture

HeLa cells were cultured in DMEM medium supplemented with 10% fetal bovine serum (FBS) and 1% antibiotic-antimycotic (100 units of penicillin, 100 μg streptomycin and 0.0085% fungizone) in a humidified atmosphere at 37 °C and 5% CO_2. At about 80% confluency, the cells were sub-cultured by dissociating with 0.25% trypsin-EDTA, and were cultured twice per week.

4.2.8 Fluorescent Labelling of Glycopolymers

The glycopolymers are fluorescently labelled with rhodamine isothiocyanate (RITC) by activating hydroxyl groups on carbohydrate moieties following a previous report [27]. Briefly, the glycopolymers are solubilized in 4% $NaHCO_3$ at pH 8.5 to make 5 mg/mL solution. RITC was dissolved in DMSO to prepare 1 mg/mL solution, added dropwise to aqueous glycopolymer solution (100μL/mL of glycopolymer), and stirred in the dark for 5 days. The solution was dialyzed to remove free RITC and lyophilized to obtain bright orange powder.

4.2.9 Flow Cytometry

HeLa cells were cultured as described above. The cells were trypsinized, seeded into 6 well plate at 500,000 cells per well and then allowed to adhere overnight. HeLa cells were treated for 4 h with cationic glycopolymer-FITC-labelled control EGFR siRNA complexes at w/w ratio of 100 in OMEM with 10% FBS. The media was removed, the cells were washed three times with 1xPBS (pH 7.4) and trypsinized. The cells were centrifuged at 300 rpm and the pellet was resuspended in FCS buffer (1 × PBS pH 7.4, 0.5% FBS, 2 mM EDTA, 0.05% w/v sodium azide). The cells were analyzed using a BD FACS dual laser (488 and 635 nm) caliber flow cytometer (Flow Cytometer Facility, Cross Cancer Institute).

4.2.10 Transfection of EGFR-siRNA

HeLa cells were trypsinized and seeded into 96 well tissue culture plates at the density of 10000 cells per well. The cells were then allowed to adhere overnight. The glycopolymer–siRNA complexes were formulated in OMEM (in the presence or absence of serum proteins) as

described above, 100 µL of a complexation mixture containing siRNA or control siRNA was added per well, and then incubated for 6 h. The medium was removed and replaced with 100 µL of DMEM medium supplemented with 10% FBS. The cells were allowed to grow for another 48 h, followed by their analysis for siRNA knockdown efficiency.

4.2.11 In-Cell Enzyme-Linked Immunosorbent Assay (ELISA)

All of the buffers were prepared in house using a reported protocol [25]. TBS pH 7.4 (0.1 M NaCl, 2 mM KCl, and 20 mM tris–base), permeabilization buffer (10% tritonX-100 in 1× TBS (1 : 99 dilution)), wash buffer (10% tween in 1× TBS (1 : 99 dilution)), blocking buffer (2% w/v BSA in 1× TBS), quenching solution (10% H_2O_2 in 1× TBS) and primary anti-body dilution buffer (1 : 1 v/v ratio of blocking buffer and wash buffer) were prepared. The cells were allowed to grow for 48 h post-transfection, the media was removed and the cells were fixed in well using 3.7% formalin in 1× TBS at 23 °C for 10 min. The cells were washed twice with 1× TBS and permeabilized for 15 min using permeabilization buffer. The cells were washed again twice with 1× TBS and quenched for 15 min using quenching solution. The cells were washed twice with TBS and then incubated with blocking solution for 30 min. The primary antibody rabbit polyclonal EGFR-IgG was diluted in dilution buffer (1 : 250 dilutions) and 50 µL of this solution was added to each well. The plate was incubated at 23 °C for 1 h. The primary antibody solution was removed and the wells were washed with 200 µL of wash buffer three times, followed by the addition of 100 µL of the HRP-conjugated secondary antibody solution (1 : 10 000 dilution in wash buffer). The plate was incubated at 23 °C for 1 h. The secondary antibody solution was removed and the wells were washed with 200 µL of wash buffer per well three times, followed by the addition of 100 µL of TMB substrate per well. The plate was incubated in the dark for 20 min, the blue precipitates were solubilized with 0.1 M phosphoric acid solution (100 µL per well)

and the yellow color formed (indicating the presence of EGFR receptors) was recorded using a TECAN microplate reader at λ = 420 nm. The percentage of EGFR receptors on cell surface are calculated:

$$\%\ EGFR\ = \frac{siRNA\ treated\ sample - negative\ control}{positive\ control - negative\ control}\ x\ 100$$

4.2.12 Janus Green Assay for Cell Viability

Janus green solution was prepared by dissolving 0.3% w/v Janus green dye in distilled deionized water. The plate content (after siRNA ELISA analysis) was removed. The plate was washed with 1xPBS pH 7.4 three times, and 100 µL of Janus green solution was added per well. The plate was incubated at 23 °C for 30 min. The Janus green solution was removed and the plate was washed five times with 1xPBS pH 7.4, followed by the addition of 0.5 M HCl solution for 10 min. The plate was read using a TECAN microplate reader at λ = 570 nm. The cell viability after transfection was determined by:

$$\%\ Cell\ Viability = \frac{siRNA\ treated\ cells - negative\ control}{positive\ control - negative\ control}$$

4.2.13 Confocal Fluorescence Microscopy

HeLa cells were cultured as mentioned above. The cells were trypsinized, seeded onto glass cover slips in 6 well plate at 100,000 cells per well and allowed to adhere overnight. The media was removed and replaced with RITC-labelled glycopolymer-FITC control EGFR siRNA complexes at w/w ratio of 100 in OMEM. The cells were incubated for 4 h in a humidified atmosphere at 37 °C and 5% CO_2. The media was removed, washed three times with 1xPBS and

treated with 1µg/mL of DAPI dissolved in PBS for 10 min. The solution was removed, washed three times with 1xPBS and the cells were fixed with 3.7% formalin in 1xPBS for 10 min. The formalin was removed, washed three times with 1xPBS and the glass coverslip was fixed on a microscope slide with nitrocellulose (30% isopropyl alcohol) dissolved in ethyl acetate. The cells were imaged using Olympus Fluoview FV10i Confocal Microscope at 490 and 570 nm emission spectra for FITC and RITC, respectively.

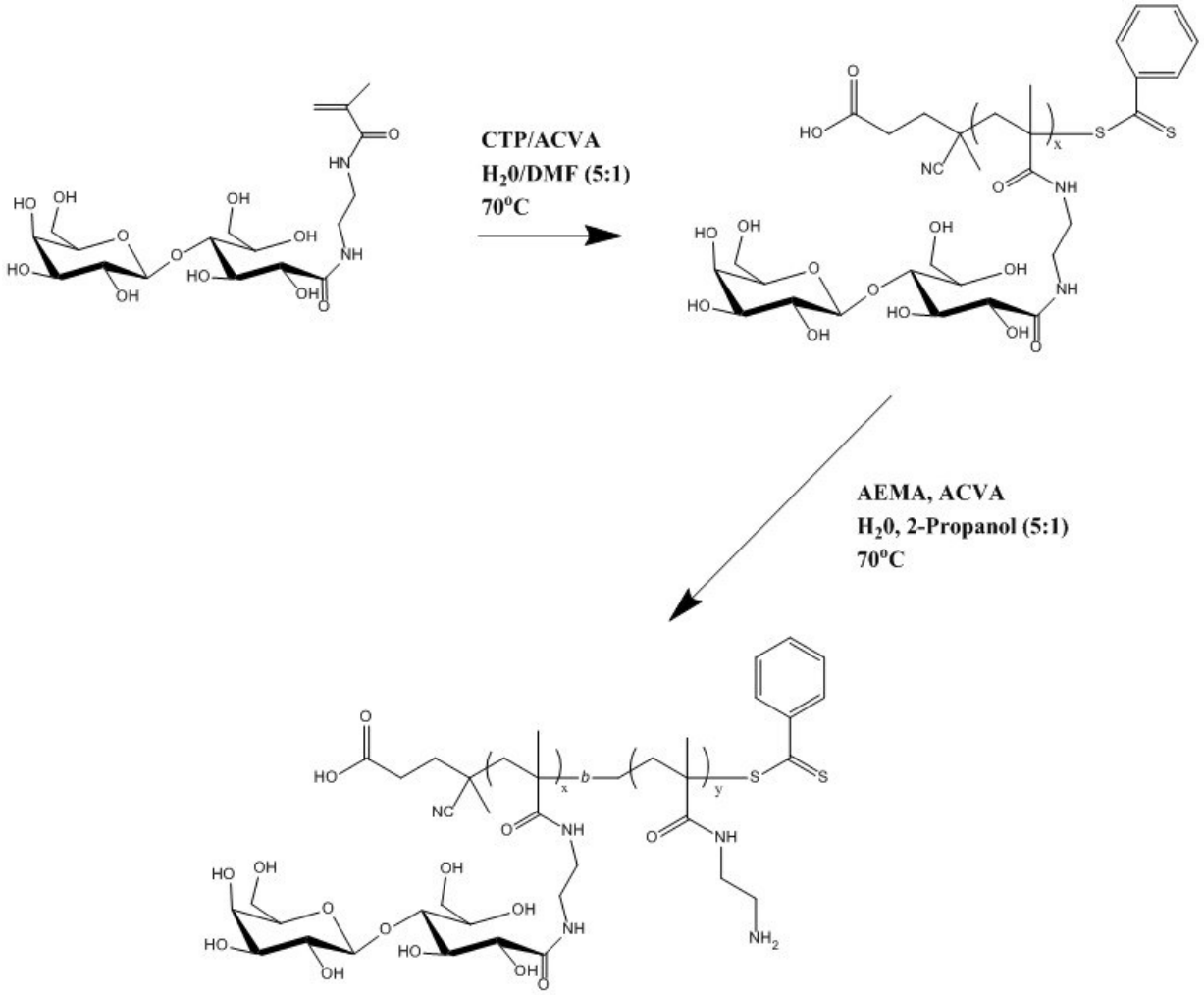

Figure 4-2. Synthesis of cationic block glycopolymer via RAFT polymerization

4.3 Results and Discussion

4.3.1 Synthesis and Characterization of Glycopolymers

Macro-CTAs that are homopolymers with active chain transfer agents, and statistical copolymers were first synthesized by the RAFT method and characterized by GPC (Appendix B Table s1). The macro-CTAs were used to copolymerize with LAEMA in a water/2-propanol solvent mixture (Figure 4-2). After purification by dialysis filtration and lyophilization, the polymer molecular weights and polydispersity index were characterized by GPC and ^{1}H NMR spectra (Appendix B Figure S1). Well-defined polymers of molecular weights ranging from 10-40 kDa with narrow polydispersity values were obtained (Table 4-1).

Table 4-1. Determination of molecular weight (*Mn*) and polydispersity (PDI) of diblock glycopolymers by gel permeation chromatography (GPC)

Polymer Composition	M_n (kDa)	PDI (M_n/M_w)
$AEMA_{40}$	6.52	1.39
P($AEMA_{17}$-*b*-$LAEMA_{17}$)	10.23	1.22
P($AEMA_{22}$-*st*-$LAEMA_{22}$)	14.55	1.33
P($AEMA_{58}$-*b*-$LAEMA_{56}$)	38.53	1.30
P($AEMA_{50}$-*st*-$LAEMA_{45}$)	35.84	1.15

4.3.2 Cationic Glycopolymer-siRNA Polyplex Complexation

The efficiency of glycopolymer binding with EGFR control siRNA has been evaluated at different weight to weight (w/w) ratios by agarose gel electrophoresis (Figure 4-3). All glycopolymer-siRNA plasmids were able to form stable polyplexes at a w/w ratio greater than 1. However P($AEMA_{17}$-*b*-$LAEMA_{17}$) was able to fully condense with siRNA plasmids at w/w ratio lower than 1 indicating that the cationic glycopolymers demonstrated a very high capacity for binding with the negatively charged EGFR siRNA plasmid. In addition, branched PEI (25kDa) and linear homopolymer $AEMA_{40}$ were able to form stable complexes at w/w ratio of 5. Analysis by dynamic light scattering (DLS) confirmed that P($AEMA_{17}$-*b*-$LAEMA_{17}$) formed the smallest stable polyplexes with EGFR siRNA plasmids that were approximately 300 nm, compared to P($AEMA_{22}$-*st*-$LAEMA_{22}$) which formed complexes of approximately 500 nm size at a w/w ratio of 15 in deionized water (Figure 4-4). As expected, the low molecular weight copolymers formed smaller polyplexes with EGFR siRNA plasmids in water, whereas the higher molecular weight copolymers P($AEMA_{58}$-*b*-$LAEMA_{56}$) and P($AEMA_{50}$-s-$LAEMA_{45}$) formed complexes that were approximately 800 and 600 nm, respectively (Figure 4-4). Interestingly, the addition of 10% FBS to the solution created much smaller glycopolymer complexes which were 150-200 nm in size presumably by serum proteins helping compact the particle size, a phenomenon earlier reported [24]. The addition of serum also affected the zeta potential of the glycopolymer complexes with the most dramatic decrease from 13 to 2 mV with the P($AEMA_{50}$-*st*-$LAEMA_{45}$)-siRNA complexes (Figure 4-4 and Appendix B Figure S2). Similar studies by Reineke *et al*. showed that diblock AEMA copolymers when complexed with siRNA in serum-containing media formed substantial aggregation products [28]. This may be due to the binding of serum proteins

neutralizing the cationic charge of the complexes and creating smaller and more robust, compact nanoparticles.

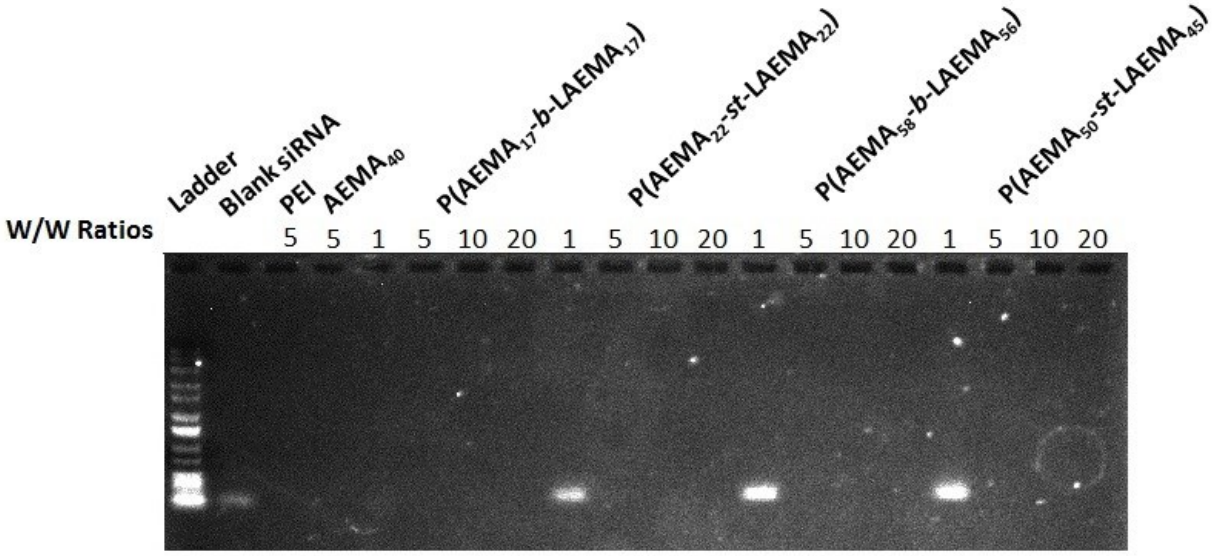

Figure 4-3. Agarose gel electrophoresis showing the polyplex formation at various weight/weight ratios of cationic glycopolymers with EGFR siRNA plasmid (250 ng).

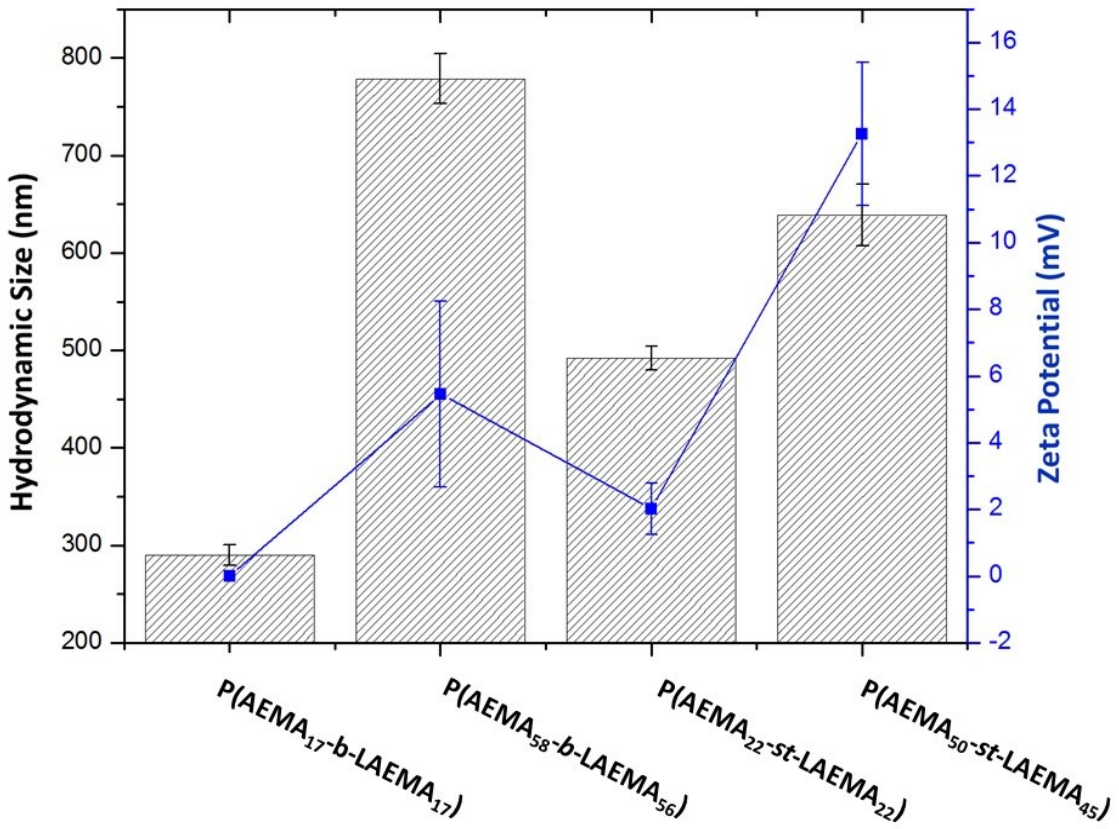

Figure 4-4. Hydrodynamic size and charges of glycopolymer-siRNA complexes in deionized water determined by DLS and zeta potential instrumentation

4.3.3 *In Vitro* Uptake of Glycopolymer-siRNA Complexes

The binding interaction and uptake of RITC-labelled-P(AEMA$_{17}$-*b*-LAEMA$_{17}$) complex with FITC-control EGFR siRNA in HeLa cells was studied by confocal fluorescence microscopy 4 h post-transfection (Figure 4-5). The fluorescence images showed that the RITC-glycopolymer and FITC-control siRNA have a strong binding affinity and form stable complexes at w/w ratio of 100. Interestingly, the polyplexes localized towards the outer wall of the cell nucleus in the HeLa cells, thus demonstrating the capacity for endosomal escape and exogenous macromolecule trafficking towards cell nucleus for siRNA gene silencing without dissociation or

degradation of the glycopolymer delivery vesicle. These results are consistent with previously published data showing FDNT biopolymers complexes with pEGFR-GFP trafficked towards the nuclear membrane actively in less than 80 min visualized by real-time live cell particle tracking [29]. This may be a suitable method for *in vivo* delivery of siRNA to protect the plasmid from RNase degradation while being transported in the blood stream to the tumor site; further *in vivo* studies should be conducted.

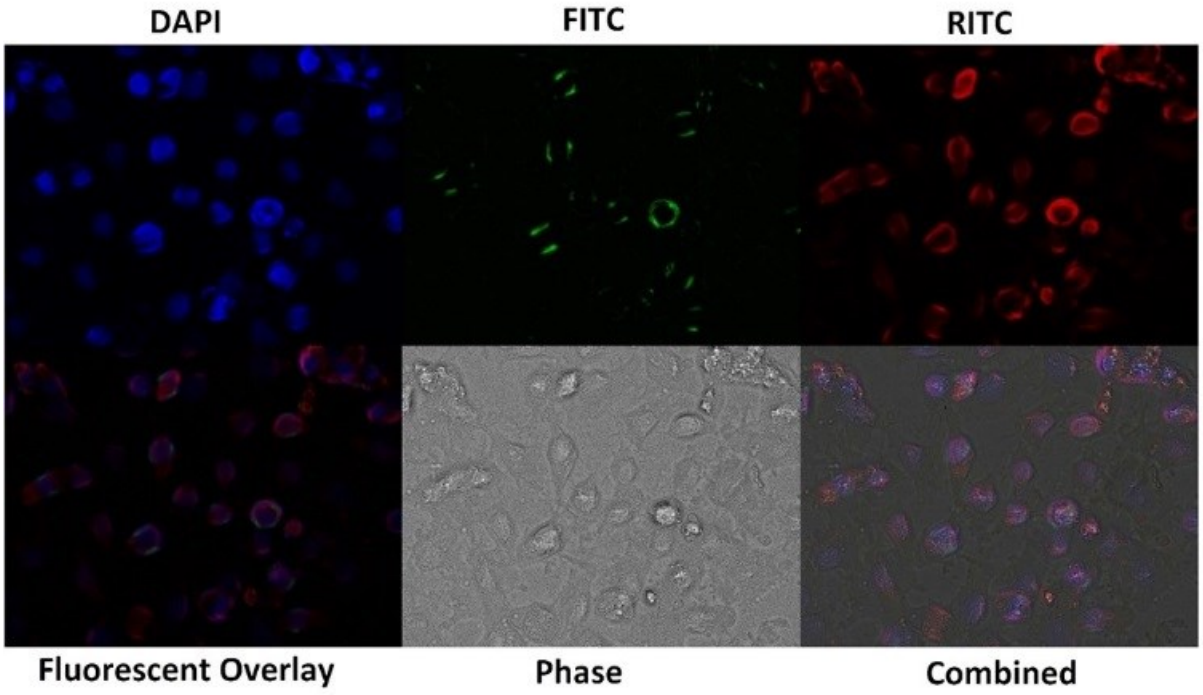

Figure 4-5. Cellular uptake of RITC-labelled-P($AEMA_{17}$-*b*-$LAEMA_{17}$) complexed with FITC-control EGFR siRNA at w/w ratio of 100 after 4 h incubation; imaged using confocal fluorescence microscopy

4.3.4 Flow Cytometry Uptake of Fluorescently Labelled Glycopolymers

The cellular uptake of control FITC-EGFR siRNA glycopolymer complexes in HeLa cells is studied in the presence of serum proteins (Figure 4-6). The untreated HeLa cells are used as a

negative control and the gated cells are evaluated for the mean fluorescence intensity (MFI) as compared to the negative control group defined by marker M1. The analysis of FITC fluorescence intensity indicates that P($AEMA_{17}$-*b*-$LAEMA_{17}$) complexes demonstrated the highest uptake ability with and MFI of 6.39 and 20.51% positive fluorescent cells within the gated region (Figure 4). Both low molecular weight glycopolymers displayed higher uptake compared to the high molecular weight counterparts, with P($AEMA_{22}$-*st*-$LAEMA_{22}$) reported 6.2% positive fluorescent cells within the gated region and MFI of 3.67. The highest molecular weight glycopolymer-FITC siRNA complexes demonstrated poor uptake compared to the low molecular weight copolymers.

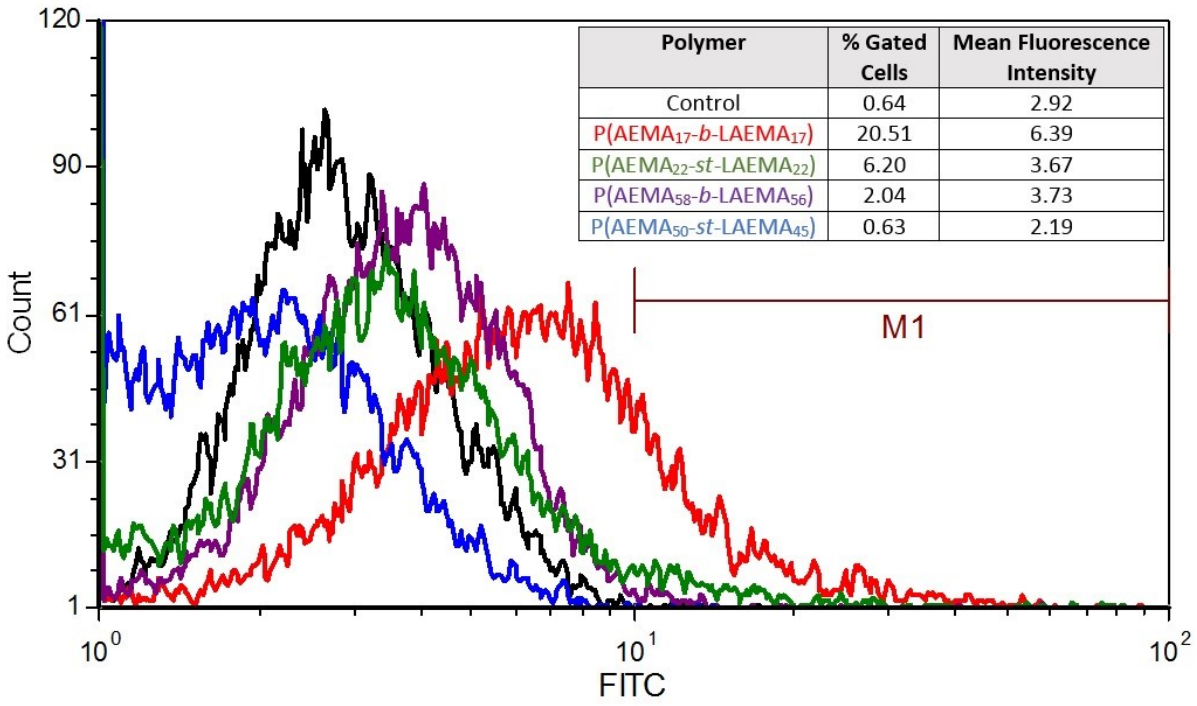

Figure 4-6. Flow cytometry analysis of cellular uptake of control FITC-EGFR siRNA-glycopolymer complexes at a w/w ratio of 100 in HeLa cells. Percent of gated cells and fluorescence intensities for all treated samples in the gated region defined by the negative control marker (M1)

4.3.5 Knockdown of EGFR in HeLa cells

The overexpression of EGFR in cancer leads to constant ligand binding and activation of downstream genetic events, such as angiogenesis, metastasis and uncontrolled cellular proliferation [30, 31]. HeLa cells have been used in this study due to the prevalence and overexpression of EGFR on the cell surface, which can be knocked down effectively without compromising the cell viability [24, 25]. Previous studies by Lyon *et al*. demonstrate clear improvement in chemotherapeutics sensitivity from EGFR knockdown in HeLa cells [32, 33]. The gene knockdown efficacies of the cationic glycopolymer-EGFR siRNA complexes were studied by enzyme linked immunosorbent assay (ELISA) at different w/w ratios in the presence and absence of serums, at a dose of 0.2 nmol or 250 ng of EGFR siRNA per treatment (Figure 4-7). Branched 25kDa PEI-siRNA complexes formulated at w/w of 5 showed approximately 18-20% knockdown efficiency as compared to the siRNA control. The increase in w/w ratio above 5 with branched PEI increased the overall cytotoxicity of the system, which is in agreement with previous reports [34-36]. The low molecular weight diblock glycopolymer P($AEMA_{17}$-*b*-$LAEMA_{17}$) showed efficient EGFR knockdown of approximately 20-22% at a w/w ratio of 15 with relatively high cell viability as compared to the control siRNA treatment. However the toxicity of the system drastically increased with increase in the w/w ratios since the results indicated less than 50% cell viability 72 h post-transfection at a w/w of 100. The transfection efficiency and cell viability were assessed for the high molecular weight glycopolymer complexes and results indicated minimal knockdown efficacy, but relatively high cell viability at a w/w ratio of 60 (Appendix B Figure S3). These findings are consistent with the results obtained by Reineke *et al*. that found the toxicity and cell viability of the system decreased as the AEMA block lengths for glycopolymer increased [10]. On the contrary, P($AEMA_{22}$-*st*-$LAEMA_{22}$)

demonstrated relatively low gene transfection efficiency of approximately 5-7% and 10-12% at w/w ratios of 15 and 200, respectively (Figure 4-7). Interestingly, even at w/w ratios up to 200, the toxicity of the system demonstrated higher biocompatibility as compared to the low molecular weight diblock conformation. It is hypothesized that the higher cell viability may be associated with charge distribution along the polymer chain; with a high local charge distribution in a diblock polymer compared to a dispersed charge distribution in a statistical conformation.

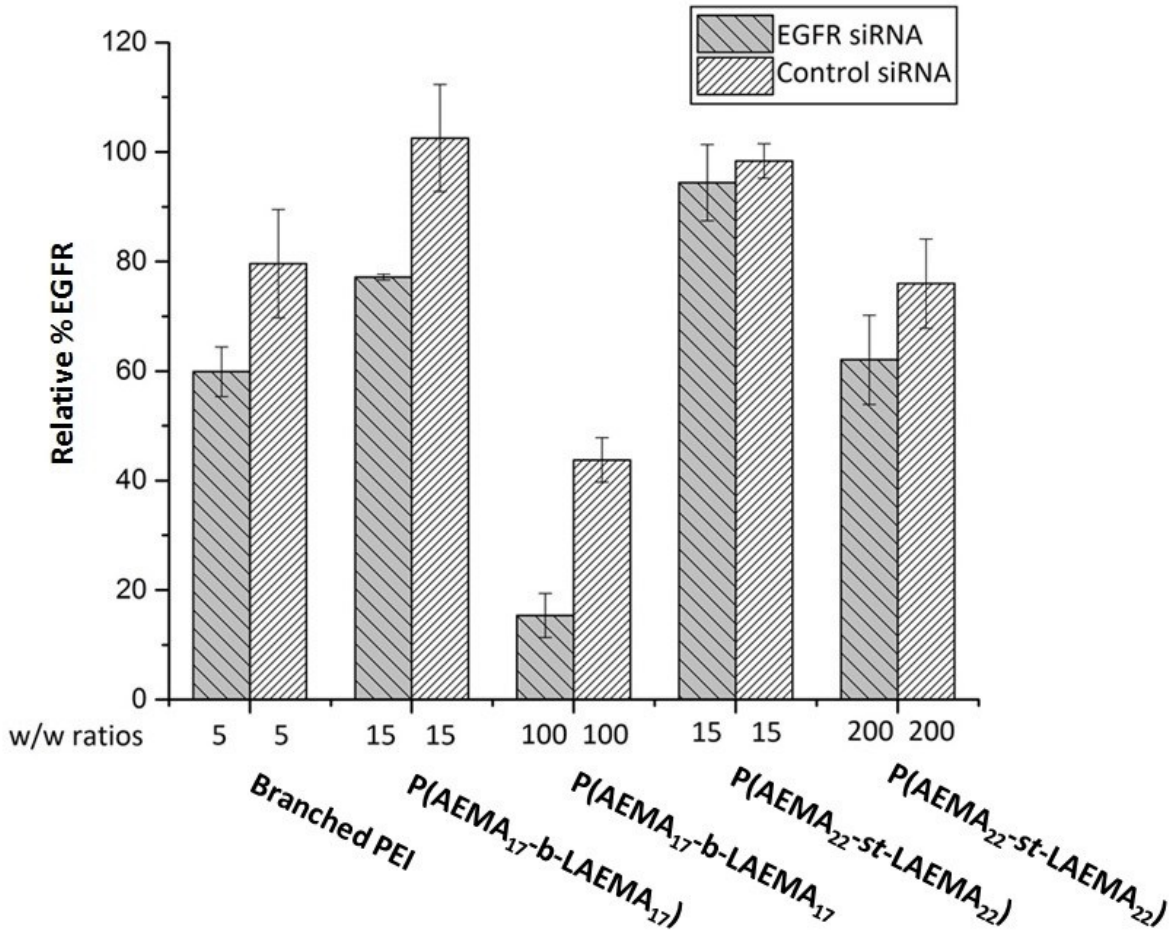

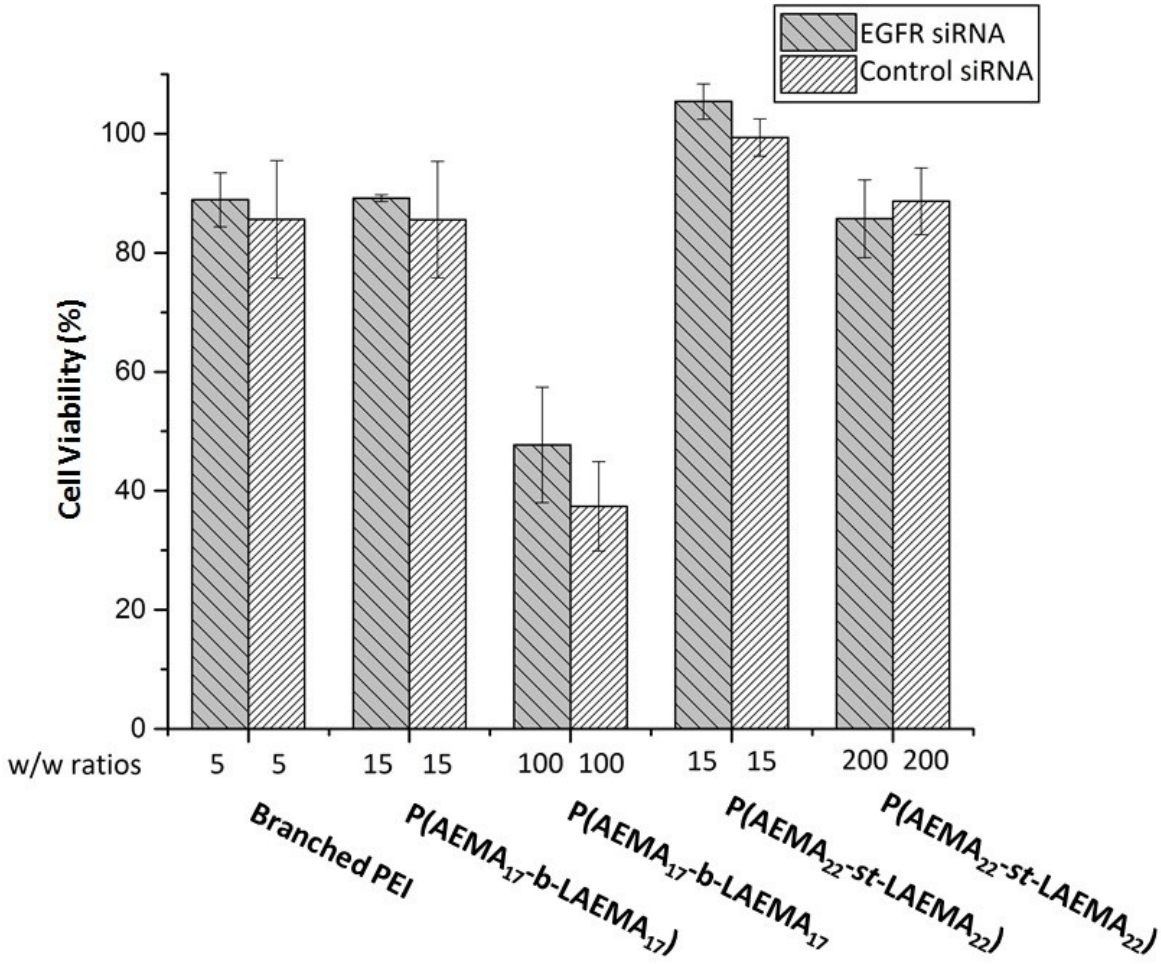

Figure 4-7. Relative percent of EGFR expression on cell surface of HeLa cells 48 h post transfection with EGFR or control siRNA (250 ng or 0.2 nmol) and cell viability of HeLa cells 48 h post-treatment with siRNA of control polyplexes, as determined by Janus green assay.

4.4 Conclusion

The synthesis and preparation of cationic glycopolymer siRNA delivery vectors have been evaluated. AEMA based copolymers demonstrated the capability to form stable nanoparticles with EGFR siRNA in the presence and absence of serum. The polyplexes demonstrated efficient gene knockdown in HeLa cells, however diblock polymers contributed to a higher cellular toxicity at high w/w ratios as compared to statistical conformations. Furthermore, the incorporation of carbohydrate residues on the polymer chain increased biocompatibility of the delivery system, presumably by enhancing the stability of complexes under physiological conditions. Further studies are being focussed on synthesizing different architectures of the copolymer and evaluate the biological response of siRNA delivery *in vivo*.

4.5 References

[1] Soutschek J., Akinc A., Bramlage B., Charisse K., Constien R., Donoghue M., Elbashir S., Geick A., Hadwiger P. Harborth, J., *Nature.* **2004**, *432*, 173-178.

[2] de Fougerolles A., Vornlocher H., Maraganore J., Lieberman J., *Nature Rev. Drug Disc.* **2007**, *6*, 443-453.

[3] Dykxhoorn D., Palliser D., Lieberman J. *Gene Ther.* **2006**, *13*, 541-552.

[4] Creixell M., Peppas N., *Nano Today.* **2012**, *7*, 367-379.

[5] Schiffelers R., Ansari A., Xu J., Zhou Q., Tang Q., Storm G., Molema G., Lu P., Scaria P., Woodle M., *Nucl. Acids Res.* **2004**, *32*, e149-e149.

[6] Kim S., Garg H., Joshi A., Manjunath N., *Trends Mole. Med.* **2009**, *15*, 491-500.

[7] Chen S., Zhaori G., *J. Euro. Clin. Invest.* **2011**, *41*, 221-232.

[8] Mintzer M., Simanek, E., *Chem. Rev.* **2008**, *109*, 259-302.

[9] Li J. Zacharek S., Chen X., Wang J., Zhang W., Janczuk A., Wang P., *Bioorg. Med. Chem.* **1999**, *7*, 1549-1558.

[10] Smith E., Sizovs A., Grandinetti G., Xue L. Reineke T., *Biomacromolecules.* **2011**, *12*, 3015-3022.

[11] Christian D., Cai S., Bowen D., Kim Y., Pajerowski J., Discher D., *J. Euro. Pharm. Biopharm.* **2009**, *71*, 463-474.

[12] Lundquist J., Toone E., *Chem. Rev.* **2002**, *102*, 555-578.

[13] Narla S., Nie H., Li Y., Sun X., *J. Carb. Chem.* **2012**, *31*, 67-92.

[14] Deng Z., Li S., Jiang X., Narain R., *Macromolecules.* **2009**, *42*, 6393-6405.

[15] Ahmed M., Jawanda M., Ishihara K., Narain R., *Biomaterials.* **2012**, *33*, 7858-7870.

[16] Ahmed M., Narain R., *Eng. Carb. Mat. Biomed. App. Wiley, Hoboken.* **2011**, 167-188.

[17] Chen J., Ahmed M., Liu Q., Narain, R., *J. Biomed. Mat. Res. Part A.* **2012**, *100*, 2342-2347.

[18] Adokoh C., Quan, S., Hitt M., Darkwa J., Kumar P., Narain R., *Biomacromolcules.* **2014**, *15*, 3802-3810.

[19] Quan S., Wang Y., Zhou A., Kumar P., Narain R., *Biomacromolecules.* **2015**.

[20] Steichen S., Caldorera-Moore M., Peppas N., *J. Euro. Pharm. Sci.* **2013**, *48*, 416-427.

[21] Diaz-Padilla I., Monk B., Mackay H., Oaknin A., *Crit. Rev. Onc. Hema.* **2013**, *85*, 303-314.

[22] Garofalo M., Romano G., Di Leva G., Nuovo G., Jeon Y., Ngankeu A., Sun J., Lovat F. Alder H., Condorelli G., *Nature Med.* **2012**, *18*, 74-82.

[23] MacEwan S., Chilkoti A., *Wiley Interdisc. Rev. Nanomed. Nanobio.* **2013**, *5*, 31-48.

[24] Kigawa, J., *Yonago acta medica.* **2013**, *56*, 43.

[25] Ahmed M., Wattanaarsakit P., Narain R., *Poly. Chem.* **2013**, *4*, 3829-3836.

[26] Ahmed M., Ishihara K., Narain R., *Chem. Commun.* **2014**, *50*, 2943-2946.

[27] Bhuchar N., Sunasee R., Ishihara K., Thundat T., Narain R., *Bioconj. Chem.* **2011**, *23*, 75-83.

[28] Ahmed M., Narain R., *Mole. Pharm.* **2012**, *9*, 3160-3170.

[29] Sizovs A., Xue L., Tolstyka Z.,Ingle N., Wu Y., Cortez M., Reineke, T., *J. Amer. Chem. Soc.* **2013**, *135*, 15417-15424.

[30] Canine B., Wang Y., Ouyang W., Hatefi A., *J. Cont. Rel.* **2011**, *151*, 95-101.

[31] Kobayashi S., Boggon T., Dayaram T., Jänne P., Kocher O., Meyerson M., Johnson B., Eck M., Tenen D., Halmos B., *New Eng. J. Med.* **2005**, *352*, 786-792.

[32] Sebastian S., Settleman J., Reshkin S., Azzariti A., Bellizzi A., Paradiso A., *Biochem. Biophy. Acta. Rev. Can.* **2006**, *1766*, 120-139.

[33] Dickerson E., Blackburn W., Smith M., Kapa L., Lyon L., McDonald J., *Bmc. Can.* **2010**, *10*, 10.

[34] Smith M., Lyon L, *Acc. Chem. Res.* **2011**, *45*, 985-993.

[35] Beyerle A., Irmler M., Beckers J., Kissel T., Stoeger T., *Mole. Pharm.* **2010**, *7*, 727-737.

[36] Zintchenko A., Philipp A., Dehshahri A., Wagner E., *Bioconj. Chem.* **2008**, *19*, 1448-1455.

[37] Lemkine G., Demeneix B., *Curr. Opin. Mole. Thera.* **2001**, *3*, 178-182.

5 Conclusions and Future Directions

This thesis focuses on the synthesis of galactose-decorated polymers and nanogels using RAFT polymerization, and their biological evaluation to purse the biomedical applications in tumor-targeted delivery of small drug molecules and gene plasmids were evaluated. The glycopolymers developed here offer many biocompatible properties such as reduced cytotoxicity of materials, protein-carbohydrate specific recognition and mediating uptake via the ``glycosidic cluster effect``, which can be advantageously exploited for multiple uses in biomedical research. By combining the properties of biocompatible glycopolymer monomers with stimuli-responsive molecules, the enhanced polymeric carriers have exponential value as novel nanotechnology vehicles for their applications in *in vitro* drug and gene delivery.

5.1 Thermosensitive Galactose-Based Nanogels for the Encapsulation and Delivery of IAZA in Hypoxic Liver Cancer

This study component pursued a detailed exploration of the synthesis and applications of thermosensitive galactose-decorated nanogels for the encapsulation and delivery of IAZA in hypoxic liver cancer cells. The nanogels were synthesized via RAFT polymerization with varying percentages of cross-linker and temperature sensitive monomer DEGMA in the core. The thermosensitive properties of all nanogels demonstrated a marked increase in size below the LCST (approximately 86-178 nm) and below the LCST, all nanogels collapsed forming smaller, more discrete particles sizes (approximately 59-95 nm). Of the synthesized library of nanogels, NG6 in particular demonstrated a stable, non-burst release of encapsulated IAZA over 10 h with a maximum loading capacity of 0.6 mM. The toxicity studies of the nanogels demonstrated high biocompatibility in multiple cell lines. Confocal fluorescence microscopy studies showed

superior uptake of the nanogel complexes due to the interactions of galactose-decorated shell with the ASGPR in HepG2 cells compared to non-ASGPR expressing HeLa cells. Additional fluorescence microscopy studies also demonstrated the reduced uptake of the fluorescently labelled nanogels when the ASGPR is saturated with a native binding ligand, thus provided further evidence of ASGPR-mediated uptake of the nanogel complexes. The radiosensitization studies indicated that IAZA in encapsulated form offers a superior radiosensitization potential as compared to parent IAZA drug in hypoxic HepG2 cells (sensitization enhancement ratio (SER) was 1.33 and 1.62 for IAZA alone and core encapsulated IAZA, respectively). These preliminary studies indicated galactose-based nanogels may serve as versatile drug delivery systems for IAZA and other hypoxia-selective nitroimidazole-based radiosensitizers. Future studies in our lab with the nanogel drug delivery system will focus on the *in vivo* evaluation of IAZA as a *multimodal* theranostic (therapy+diagnostic) agent i.e., as a radiosensitizer, in molecular imaging and as an *in situ* molecular radiotherapy agent for the management of hypoxic liver cancer. Current studies demonstrate an enhanced delivery payload of IAZA, which will translate into much superior theranostic effects.

5.2 Cationic Glycopolymers for Delivery of EGFR-siRNA in Cervical Cancer

The second study component of the thesis presents the detailed study of cationic glycopolymers for the complexation of EGFR small interfering RNA (siRNA) in the presence and absence of serum for knockdown of cell surface EGFR n HeLa cells. The stability of the polyplexes analyzed by gel electrophoresis demonstrated excellent binding capacity in the presence and absence of serum proteins above w/w ratio of 1. Dynamic light scattering of the glycopolymer

complexed with siRNA formed discrete nanoparticles approximately 300-750 nm in deionized water, while nanoparticles ranged in size between 130-200 nm in the presence of serum proteins in OMEM media. With the library of synthesized statistical and block glycopolymers, the shortest AEMA glycopolymer P($AEMA_{17}$-*b*-$LAEMA_{17}$) was the most effective at silencing EGFR expression in HeLa cells, however it was evidently more toxic as compared to its statistical counterpart at higher w/w ratios. Confocal fluorescent images of RITC-labelled-P($AEMA_{17}$-*b*-$LAEMA_{17}$) complexed with FITC-control siRNA displayed excellent uptake and subcellular localization towards the nucleus in HeLa cells. Flow cytometry studies indicated that P($AEMA_{17}$-*b*-$LAEMA_{17}$) – siRNA complexes were the most abundantly uptaken within the cell compared to other glycopolymer complexes. The siRNA-glycopolymer complexes demonstrated EGFR knockdown capacity both in the presence and absence of serum proteins. Follow up work in our lab focuses on exploring the *in vivo* applications of cationic glycopolymers for gene delivery in tumor models.

Bibliography

Chapter 1

[1] Nair, L., Cato L., *Prog. Poly. Sci.* **2007**, *32*, 762-798.

[2] Hubbell, J., *Nature Biotech.* **1995***, 13,* 565-576.

[3] Courtney, J. *Biomaterials.* **1994**, *15*, 737-744.

[4] Chiefari J., Chong Y., Ercole F., Krystina J., Jeffery J., Le T., *Macromolecules*. **1998**, *31*, 5559-62.

[5] Hawker J., *J. Amer. Chem. Soc.* **1994**, *116*, 11185-6.

[6] Mishra V., Kumar R., *J. Sci. Res.* **2012**, *56*, 141-76.

[7] Moad G., Chiefari J., Krstina J., Mayadunne R., Postma A., Rizzardo E., *Poly. Int.* **2000**, *49*, 993-1001.

[8] Chiefari, J., *Macromolecules.* **1998***, 31,* 5559-5562.

[9] Semsarilar M., Perrier S., *Nature Chem.* **2010,** *2*, 811-20.

[10] Mayadunne R., Rizzardo E., Chiefari J., Chong Y., Moad G., Thang S., *Macromolecules*. **1999**, *32*, 6977-80.

[11] Rapoport N., *Prog. Poly. Sci.* **2007**, *32*, 962-90.

[12] Gil E., Hudson S.*, Prog. Poly. Sci*. **2004**, *29***,** 1173-222.

[13] Qiu Y., Park K., Adv. Drug Del. Rev. **2012**, *64*, 49-60.

[14] Ganta S., Devalapally H., Shahiwala A., Amiji M., *J. Cont. Rel.* **2008**, *126*, 187-204.

[15] Bajpai A., Shukla S., Bhanu S., Kankane S., *Prog. Poly. Sci.* **2008**, *33*, 1088-118.

[16] Wang X., Qiu X., Wu C., *Macromolecules*. **1998**, *31*, 2972-6.

[17] Liu S., Liu M., *J. App. Poly. Sci.* **2003**, *90*, 3563-8.

[18] Nitschke M., Gramm S., Götze T., Valtink M., Drichel J., Voit B., *J. Biom. Mat. Res. Part A.* **2007**, *80*, 1003-10.

[19] Chacko R., Ventura J., Zhuang J., Thayumanavan S., *Adv. Drug Del. Rev*. **2012**, *64*, 836-51.

[20] Seuring J., Agarwal S., *Macromol. Rapid Comms*. **2012**, *33*, 898-920.

[21] Ward MA., Georgiou TK., *Polymers.* **2011**, *3*, 1215-42.

[22] Ougizawa T., Inoue T., Kammer HW., *Macromolecules*. **1985,** *18*, 2089-92.

[23] Ougizawa T., Inoue T., *J. Poly.* **1986,** *18*, 521-7.

[24] Sanchez I., Stone M., *Poly. Blends*. **2000,** *1*, 15-53.

[25] Schmaljohann D., *Adv. Drug Del. Rev*. **2006**, *58*, 1655-70.

[26] Oh J., Drumright R., Siegwart DJ., Matyjaszewski K., *Prog. Poly. Sci.* **2008**, *33*, 448-77.

[27] Raemdonck K., Demeester J., De Smedt S., *Soft Matter.* **2009**, *5*, 707-15.

[28] Oh J., Lee D., Park J., *Prog. Poly. Sci*. **2009**, *34*, 1261-82.

[29] Bhuchar N., Sunasee R., Ishihara K., Thundat T., Narain R., *Bioconj. Chem.* **2011**, *23*, 75-83.

[30] He J., Yan B., Tremblay L., Zhao Y., *Langmuir*. **2010**, *27*, 436-44.

[31] Kabanov AV., Vinogradov S., *Ange. Chem. Int. Ed.* **2009**, *48*, 5418-29.

[32] Shi L., Khondee S., Linz T., Berkland C., *Macromolecules.* **2008**, *41*, 6546-54.

[33] Lou S., Gao S., Wang W., Zhang M., Zhang J., Wang C., *Nanoscale*. **2015**.

[34] Klinger D., Landfester K., *J. Poly. Sci. Part A*: *Poly. Chem.* **2012**, *50*, 1062-75.

[35] Schwartz A., Fridovich S., Knowles B., Lodish H., *J. Bio. Chem.* **1981**, *256*, 8878-81.

[36] Kumar P., McQuarrie S., Zhou A., McEwan A., Wiebe L., *Nuc.Med. Bio.* **2005**, *32*, 647-53.

[37] Creixell M., Peppas N., *Nano Today*. **2012,** *7*, 367-79.

[38] Schwartz A., Fridovich S., Lodish H., *J. Bio. Chem.* **1982,** *257*, 4230-7.

[39] Stoorvogel W., Geuze H., Griffith J., Schwartz A., Strous G., *J. Cell Bio.* **1989**, *108*, 2137-48.

[40] Volz B., Orberger G., Porwoll S., Hauri H., Tauber R., *J. Cell Bio*. **1995,** *130*, 537-51.

[41] Strous G., Du Maine A., Zijderhand-Bleekemolen J., Slot J., Schwartz A., *J. Cell Bio*. **1985**, *101*, 531-9.

[42] Tao Y., He J., Zhang M., Hao Y., Liu J., Ni P., *Poly. Chem.* **2014**, *5*, 3443-52.

[43] Jiang H-L., Kim Y-K., Lee S., Park M., Kim E., Jin Y., *Arch. Pharm. Res.* **2010**, *33*, 551-6.

[44] Hu J., Liu J., Yang D., Lu M., Yin J., *Prot. Pep. Letters.* **2014**, *21*, 1025-30.

[45] Zhou X., Zhang M., Bryant Yung L., Zhou C., Lee L., Lee R.. *J. Int. Nanomed.* **2012**, *7*, 5465.

[46] Ahmed M., Narain R., *Biomaterials.* **2012,** *33*, 3990-4001.

[47] Li Y., Huang G., Diakur J., Wiebe L., *Curr. Drug Del.* **2008**, *5*, 299-302.

[48] KyungáKim S., MináPark K., JongáKim W., *Chem. Comm.* **2010**, *46*, 692-4.

[49] Harris AL., *Nature Rev. Can.* **2002**, *2*, 38-47.

[50] Welsh R., Jensen F., Cooper N., Oldstone M., Banapour B., Sernatiriger J., *Nature*. **1996,** *3*, 79-84.

[51] Nunn A., Linder K., Strauss HW., *J. Euro. Nuc. Med.* **1995**, *22*, 265-80.

[52] Höckel M., Vaupel P., *J. Nat. Can. Institute*. **2001**, *93*, 266-76.

[53] Dewey D., *Nature*. **1960**, *186*, 780-2.

[54] Fleming I., Manavaki R., Blower P., West C., Williams K., Harris A., *J. Brit. Can.* **2014**.

[55] Edwards D., *J. Antimicro. Chemo.* **1993**, *31*, 9-20.

[56] Biaglow J., Varnes M., Roizen-Towle L., Clark E., Epp E., Astor M. *Biochem. Pharm.* **1986**, *35*, 77-90.

[57] Takasawa M., Moustafa R., Baron J., *Stroke*. **2008**, *39*, 1629-37.

[58] Fowler J., *J. Int. Rad. Onc.* **1985**, 11, 665-74.

[59] Monney H., Parrick J., Wallace R., *Pharm. Thera.* **1981**, *14*, 197-216.

[60] Wardman P., *Clin. Onc.* **2007**, *19*, 397-417.

[61] Wiebe L., McEwan A., *Braz. Arch. Bio.Tech.* **2002**, *45*, 69-81.

[62] Kumar P., Bacchu V., Wiebe L., *Sem. Nuc. Med.* **2015,** 122-35.

[63] Mannan R., Somayaji V., Lee J., Mercer J., Chapman J., Wiebe L. *J. Nuc. Med.* **1991**, *32,* 1764-70.

[64] Urtasun R., Parliament M., McEwan A., Mercer J., Mannan R., Wiebe L., *J. Brit. Can. Supp.* **1996**, *27*, S209.

[65] Ye, J., *J. Int. Obesity.* **2009***, 33,* 54-66.

[66] Hajer, G., Timon W., Visseren F., *J. Euro. Heart.* **2008***, 29,* 2959-2971.

[67] Mannan R., Mercer J., Wiebe L., Kumar P., Somayaji V., Chapman J., *J. Nuc. Bio. Med.* **1991**, *36*, 60-7.

[68] Parliament M., Chapman J., Urtasun R., McEwan A., Golberg L., Mercer J., *J. Brit. Can.* **1992**, *65*, 90.

[69] Groshar D., McEwan A., Parliament M., Urtasun R., Golberg L., Hoskinson M., *J. Nuc. Med.* **1993**, *34*, 885.

[70] Vinjamuri S., O'Driscoll K., Maltby P., McEwan A., Wiebe L., Critchley M., *Clin. Nuc. Med*. **1999**, *24*, 891.

[71] Koehler L., Gagnon K., McQuarrie S., Wuest F., *Molecules*. **2010,** *15*, 2686-718.

[72] Mercer J., McEwan A., Wiebe L. *Curr. Radiopharm.* **2013**, *6*, 87-91.

[73] Reischl G., Dorow D., Cullinane C., Katsifis A., Roselt P., Binns D., *J. Pharm.Sci.* **2007,** *10*, 203-11.

[74] Al-Arafaj A., Ryan E., Hutchison K., Mannan R., Mercer J., Wiebe L., *J. Euro. Nuc. Med.* **1994**, *21*, 1338-42.

[75] Wiebe L. *Noujaim Inst. Pharm. Onc. Res.* **1997**. 189-94.

[76] Mercer J., Mannan R., Somayaji V., Wiebe L., Lee J., Chapman J., *Adv. Radiopharm.* **1990**.

Chapter 2

[1] Moore, J., *J. Poly. Sci. Part A.* **1964**, *2*, 835-843.

[2] Gulrez I., Syed K., Glyn O., Phillips S., Saphwan A., *Intech Open Acc. Pub.* **2011**.

[3] Viscotek Setting the Standard for GPC. Complete Guide for GPC/SEC/GFC Instrumentation and Detection Technologies, 2006. Retrieved from: http://s3.amazonaws.com/zanran_storage/md-scientific.dk/ContentPages/993457484.pdf

[4] Lin Y., Barron, Rm *Size Exc. Chroma. App. Poly. Sci.* **2015**.

[5] Agilent Technologies. A Guide to Multi-Detector Gel Permeating Chromatography. 2006, Retrieved from: https://www.chem.agilent.com/Library/primers/Public/5990-7196EN.pdf

[6] Malvern. GPC/SEC Theory: Universal Calibration. 2013, Retrieved from: http://www.malvernkorea.co.kr/labeng/technology/gel_permeation_chromatography_theory/universal_calibration_gpc_theory.htm

[7] Holzgrabe, U., Wawer, I., Diehl, B., *Elsevier*, **2011**.

[8] O'Reilly, R. NMR spectroscopy for polymer chemists. 2014, Retrieved from:

http://www2.warwick.ac.uk/fac/sci/chemistry/masters/courses/polymchem/polyintra/ch968/nmr_spectroscopy2.pdf

[9] Sartor, M. Dynamic light scattering to determine the radius of small beads in Brownian motion in a solution. Retrieved from: http://216.92.172.113/courses/phys39/light%20scattering/DLS%20LabView%20UCSD.pdf

[10] LS Instruments. Dynamic Light Scattering: Measuring the Particle Size Distribution. 2015, Retrieved from: http://www.lsinstruments.ch/technology/dynamic_light_scattering_dls/

[11] Brown M., Wittwer C. *Clin. Chem.* **2011,** *46*, 1221-1229.

[12] BD Biosciences. Introduction to Flow Cytometry: A Learning Guide. 2000, Retrieved from: http://www.d.umn.edu/~biomed/flowcytometry/introflowcytometry.pdf

[13] PCMB. Retrieved from: http://www.biosci.ohio-state.edu/~plantbio/osu_pcmb/pcmb_lab_resources/pcmb102_activities/biotech/biotech_gels.htm

[14] Ebada S.,Edrada R., Lin, W., Proksch, P., *Nature Proto.* **2008**, *3*, 1820-1831.

[15] Life Technologies. Secondary Antibodies as Probes. 2015, Retrieved from: https://www.lifetechnologies.com/ca/en/home/life-science/protein-biology/protein-biology-learning-center/protein-biology-resource-library/pierce-protein-methods/secondary-antibodies-probes.htm

Chapter 3

[1] Dykxhoorn D., Palliser D., Lieberman J., *Gene Thera.* **2006**, *13*, 541-52.

[2] Li J., Zacharek S., Chen X., Wang J., Zhang W., Janczuk A., *Bioorg. Med. Chem.* **1999**, *7*, 1549-58.

[3] Chapman J., Engelhardt E., Stobbe C., Schneider R., Hanks G., *Radio. Onc.* **1998**, *46*, 229-37.

[4] Harris A., *Nature Rev. Can.* **2002**, *2*, 38-47.

[5] Lundquist J., Toone E., *Chem. Rev.* **2002**, *102*, 555-78.

[6] Mishra V., Kumar R., *J. Sci. Res.* **2012**, *56*, 141-76.

[7] Hrzenjak A., Frank S., Wo X., Zhou Y., Vanberkel T., Kostner G., *J. Biochem.* **2003**, *376*, 765-71.

[8] Yu J-M., Li W-D., Lu L., Zhou X., Wang D., Li H., *J. Mat. Sci.* **2014**, *25*, 691-701.

[9] Zheng D., Duan C., Zhang D., Jia L., Liu G., Liu Y., *J. Int. Pharm.* **2012**, *436*, 379-86.

[10] Jain D., Kumar A., J. *Biomed. Pharm. Res.* **2013**, *2*.

[11] Eichman J., Bielinska A., Kukowska-Latallo J., Baker J., *Pharm. Sci. Tech. Today.* **2000**, *3*, 232-45.

[12] Kabanov A., Vinogradov S., *Ange. Chemie Int. Ed.* **2009,** *48*, 5418-29.

[13] Hector A., Schmid B., Beierkuhnlein C., Caldeira M., Diemer M., Dimitrakopoulos P., *Science*. **1999**, *286*, 1123-7.

[14] Yoo H., Mok H., *Arch. Pharm. Res.* **2015**, *38*, 129-36.

[15] Ramos J., Imaz A., Forcada J., *Poly. Chem.* **2012**, *3*, 852-6.

[16] Semsarilar M., Perrier S., *Nature Chem.* **2010**, *2*, 811-20.

[17] Takasawa M., Moustafa R., Baron J., *Stroke*. **2008**, *39*, 1629-37.

[18] Nunn A., Linder K., Strauss H., *J. Euro. Nuc. Med.* **1995**, *22*, 265-80.

[19] Fleming I., Manavaki R., Blower P., West C., Williams K., Harris A., *J. Brit. Cancer*. **2014**.

[20] Baio J., Schach D., Fuchs A., Schmüser L., Billecke N., Bubeck C., *Chem. Comm.* **2015**, *51*, 273-5.

[21] Richardson S., Kolbe H., Duncan R., *J. Int. Pharm.* **1999**, *178*, 231-43.

[22] El-Sayed A., Futaki S., Harashima H., *J. Amer. Assoc. Pharm. Res.* **2009**, *11*, 13-22.

[23] Benns J., Choi J., Mahato R., Park J., Kim S., *Bioconj. Chem.* **2000**, *11*, 637-45.

[24] Wang F., Wang Y., Wang H., Shao N., Chen Y., Cheng Y., *Biomaterials*. **2014**, *35*, 9187-98.

[25] Benaglia M., Rizzardo E., Alberti A., Guerra M., *Macromolecules*. **2005,** *38,* 3129-40.

[26] Deng Z., Li S., Jiang X., Narain R., *Macromolecules*. **2009,** *42*, 6393-405.

[27] Deng Z., Bouchackif H., Babooram K., Housni A., Choytun N,. Narain R., *J. Poly. Sci. Part A.* **2008**, *46*, 4984-96.

[28] Deng Z., Ahmed M., Narain R., *J. Poly. Sci. Part A.* **2009**, *47*, 614-27.

[29] Sunasee R., Wattanaarsakit P., Ahmed M., Lollmahomed F., Narain R., *Bioconj. Chem.* **2012**, *23*, 1925-33.

[30] Ahmed M., Narain R., *Mole. Pharm.* **2012**, *9*, 3160-70.

[31] Detampel P., Witzigmann D., Krähenbühl S., Huwyler J., *J. Drug Targ.* **2013**, *22*, 232-41.

[32] Kumar P., Naimi E., McEwan A., Wiebe L., *Bioorg. Med. Chem.* **2010**, *18*, 2255-64.

[33] Lee J., Jung J., Kim Y., Lee E., Choi J., *J. Int. Pharm.* **2014**, *459*, 10-8.

[34] Yang Y., Yang Y., Xie X., Wang Z,. Gong W,. Zhang H., *Biomaterials*. **2015**, *48*, 84-96.

[35] Plummer, R., Hill D., Whittaker, A., *Macromolecules*. **2006**, *39*, 8379-8388.

[36] Wang Y., Kotsuchibashi Y., Liu Y., Narain R., *Langmuir*. **2014**, *30*, 2360-2368.

[37] Liu X., Liu C., Zhou J., Chen C., Qu F., Rossi J., *Nanoscale.* **2015**.

[38] Aujard I., Benbrahim C., Gouget M., Ruel O., Baudin J., Neveu P., *J. Euro. Chem. A.* **2006**, *12*, 6865-79.

[39] Pack D., Hoffman A., Pun S., Stayton P., *Nature Rev. Drug Disc.* **2005**, *4*, 581-93.

[40] Chacko R., Ventura J., Zhuang J., Thayumanavan S., *Adv. Drug Del. Rev.* **2012**, *64*, 836-51.

[41] Booth A., Coxon T., Gough J., Webb S. *Cambridge Univ Press*. **2014**. mrss14-1688-y05-14.

[42] Park I., Kim T., Kim Y., Choi Y., Nah J., Cho C., *Key Eng,. Mat.* **2007**, *342*, 437-40.

[43] Gonçalves C., Berchel M., Gosselin M., Malard V., Cheradame H., Jaffrès P., *J. Int. Pharm.* **2014**, *460*, 264-72.

[44] Rigopoulou E., Roggenbuck D., Smyk D., Liaskos C., Mytilinaiou M., Feist E., *Autoimm. Rev.* **2012**, *12*, 260-9.

[45] Striegel A., Yau W., Kirkland J., Bly D., *John Wiley & Sons.* **2009**.

[46] Trathnigg B., *Prog. Poly. Sci.* **1995**, *20*, 615-50.

[47] Cheng C., Saltzman W., *Biomaterials*. **2011**, *32*, 6194-203.

[48] Chen P., Jafari M., Xu W., Chen B., Pan R., Karunaratne N., *US Patent 20,140,350,082*, **2014**.

Chapter 4

[1] Soutschek J., Akinc A., Bramlage B., Charisse K., Constien R., Donoghue M., Elbashir S., Geick A., Hadwiger P. Harborth, J., *Nature.* **2004**, *432*, 173-178.

[2] de Fougerolles A., Vornlocher H., Maraganore J., Lieberman J., *Nature Rev. Drug Disc.* **2007**, *6*, 443-453.

[3] Dykxhoorn D., Palliser D., Lieberman J. *Gene Ther.* **2006**, *13*, 541-552.

[4] Creixell M., Peppas N., *Nano Today.* **2012**, *7*, 367-379.

[5] Schiffelers R., Ansari A., Xu J., Zhou Q., Tang Q., Storm G., Molema G., Lu P., Scaria P., Woodle M., *Nucl. Acids Res.* **2004**, *32*, e149-e149.

[6] Kim S., Garg H., Joshi A., Manjunath N., *Trends Mole. Med.* **2009**, *15*, 491-500.

[7] Chen S., Zhaori G., *J. Euro. Clin. Invest.* **2011**, *41*, 221-232.

[8] Mintzer M., Simanek, E., *Chem. Rev.* **2008**, *109*, 259-302.

[9] Li J. Zacharek S., Chen X., Wang J., Zhang W., Janczuk A., Wang P., *Bioorg. Med. Chem.* **1999**, *7*, 1549-1558.

[10] Smith E., Sizovs A., Grandinetti G., Xue L. Reineke T., *Biomacromolecules.* **2011**, *12*, 3015-3022.

[11] Christian D., Cai S., Bowen D., Kim Y., Pajerowski J., Discher D., *J. Euro. Pharm. Biopharm.* **2009**, *71*, 463-474.

[12] Lundquist J., Toone E., *Chem. Rev.* **2002**, *102*, 555-578.

[13] Narla S., Nie H., Li Y., Sun X., *J. Carb. Chem.* **2012**, *31*, 67-92.

[14] Deng Z., Li S., Jiang X., Narain R., *Macromolecules.* **2009**, *42*, 6393-6405.

[15] Ahmed M., Jawanda M., Ishihara K., Narain R., *Biomaterials.* **2012**, *33*, 7858-7870.

[16] Ahmed M., Narain R., *Eng. Carb. Mat. Biomed. App. Wiley, Hoboken.* **2011**, 167-188.

[17] Chen J., Ahmed M., Liu Q., Narain, R., *J. Biomed. Mat. Res. Part A.* **2012**, *100*, 2342-2347.

[18] Adokoh C., Quan, S., Hitt M., Darkwa J., Kumar P., Narain R., *Biomacromolcules.* **2014**, *15*, 3802-3810.

[19] Quan S., Wang Y., Zhou A., Kumar P., Narain R., *Biomacromolecules.* **2015**.

[20] Steichen S., Caldorera-Moore M., Peppas N., *J. Euro. Pharm. Sci.* **2013**, *48*, 416-427.

[21] Diaz-Padilla I., Monk B., Mackay H., Oaknin A., *Crit. Rev. Onc. Hema.* **2013**, *85*, 303-314.

[22] Garofalo M., Romano G., Di Leva G., Nuovo G., Jeon Y., Ngankeu A., Sun J., Lovat F. Alder H., Condorelli G., *Nature Med.* **2012**, *18*, 74-82.

[23] MacEwan S., Chilkoti A., *Wiley Interdisc. Rev. Nanomed. Nanobio.* **2013**, *5*, 31-48.

[24] Kigawa, J., *Yonago acta medica.* **2013**, *56*, 43.

[25] Ahmed M., Wattanaarsakit P., Narain R., *Poly. Chem.* **2013**, *4*, 3829-3836.

[26] Ahmed M., Ishihara K., Narain R., *Chem. Commun.* **2014**, *50*, 2943-2946.

[27] Bhuchar N., Sunasee R., Ishihara K., Thundat T., Narain R., *Bioconj. Chem.* **2011**, *23*, 75-83.

[28] Ahmed M., Narain R., *Mole. Pharm.* **2012**, *9*, 3160-3170.

[29] Sizovs A., Xue L., Tolstyka Z.,Ingle N., Wu Y., Cortez M., Reineke, T., *J. Amer. Chem. Soc.* **2013**, *135*, 15417-15424.

[30] Canine B., Wang Y., Ouyang W., Hatefi A., *J. Cont. Rel.* **2011**, *151*, 95-101.

[31] Kobayashi S., Boggon T., Dayaram T., Jänne P., Kocher O., Meyerson M., Johnson B., Eck M., Tenen D., Halmos B., *New Eng. J. Med.* **2005**, *352*, 786-792.

[32] Sebastian S., Settleman J., Reshkin S., Azzariti A., Bellizzi A., Paradiso A., *Biochem. Biophy. Acta. Rev. Can.* **2006**, *1766*, 120-139.

Appendix A

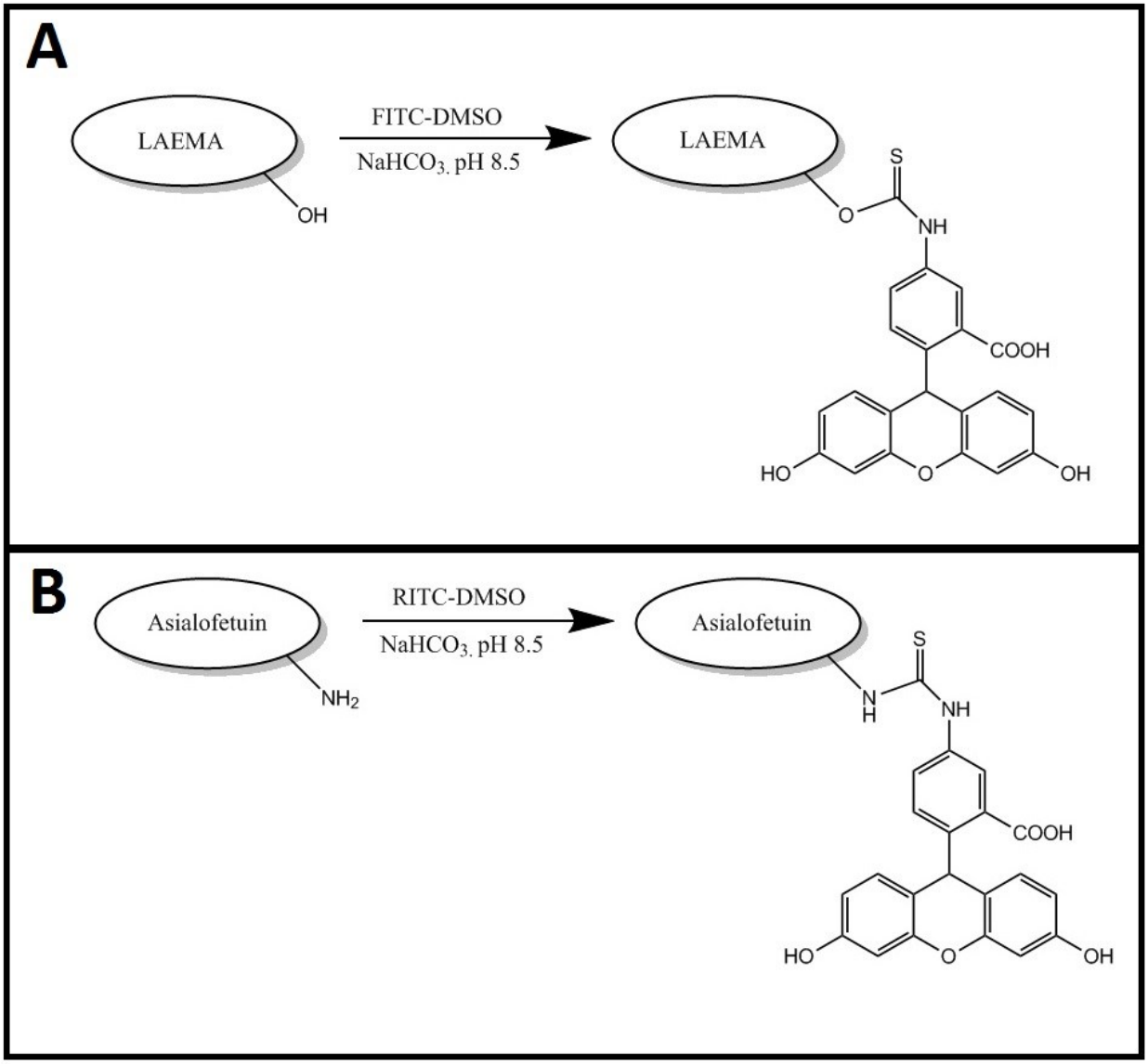

Figure S1. Schematic for conjugation of A) Fluorescein isothiocyanate on LAEMA and B) Rhodamine isothiocyanate on Asialofetuin

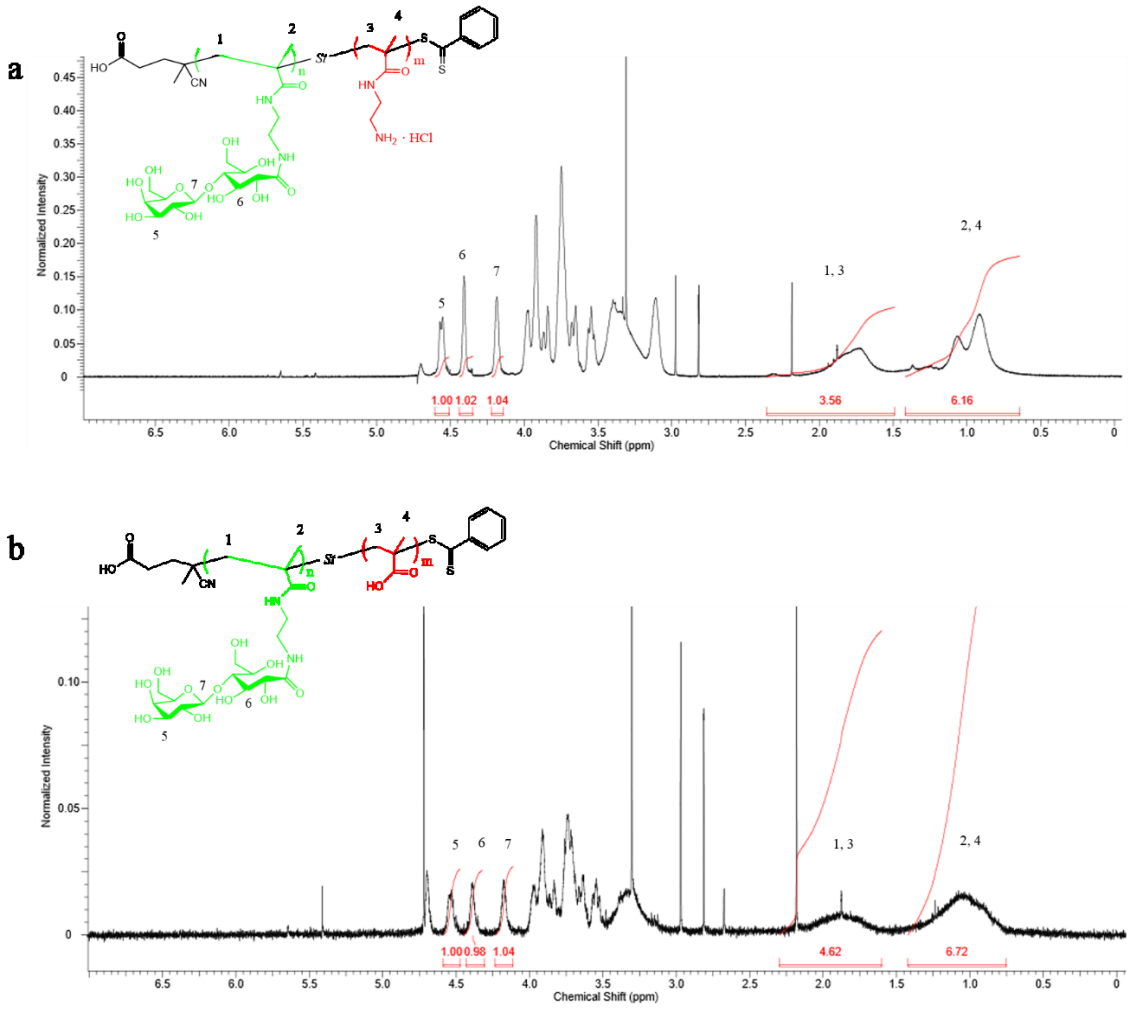

Figure S2. ^{1}H NMR spectra (D_2O) for poly(LAEMA$_{19}$-*st*-AEMA$_{19}$) (a) and poly(LAEMA$_{19}$-*st*-MA$_{24}$) (b) macro-CTAs.

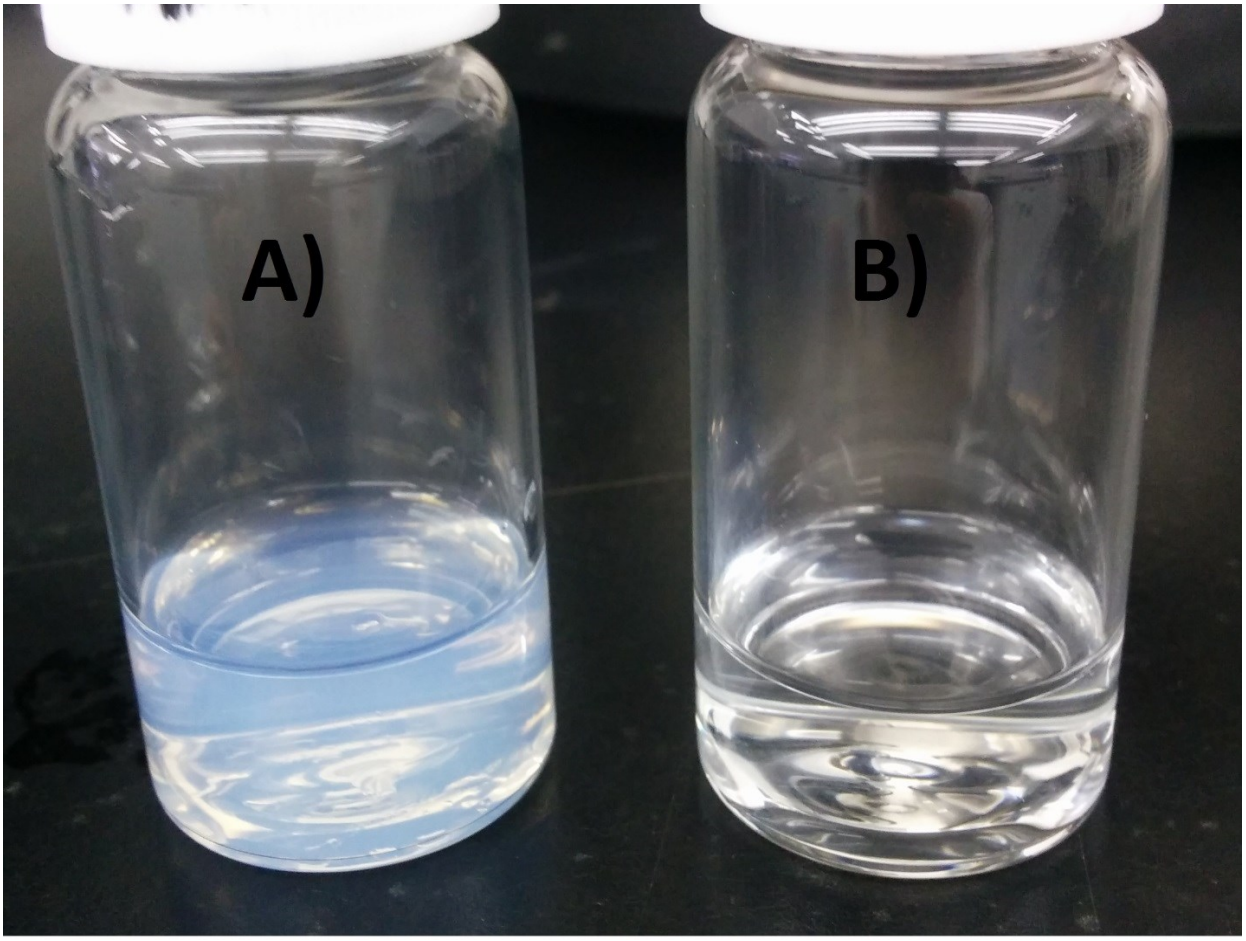

Figure S3. Digital photograph of 5 mg/mL aqueous solution of NG6 on a) heating above LCST and b) cooling below LCST.

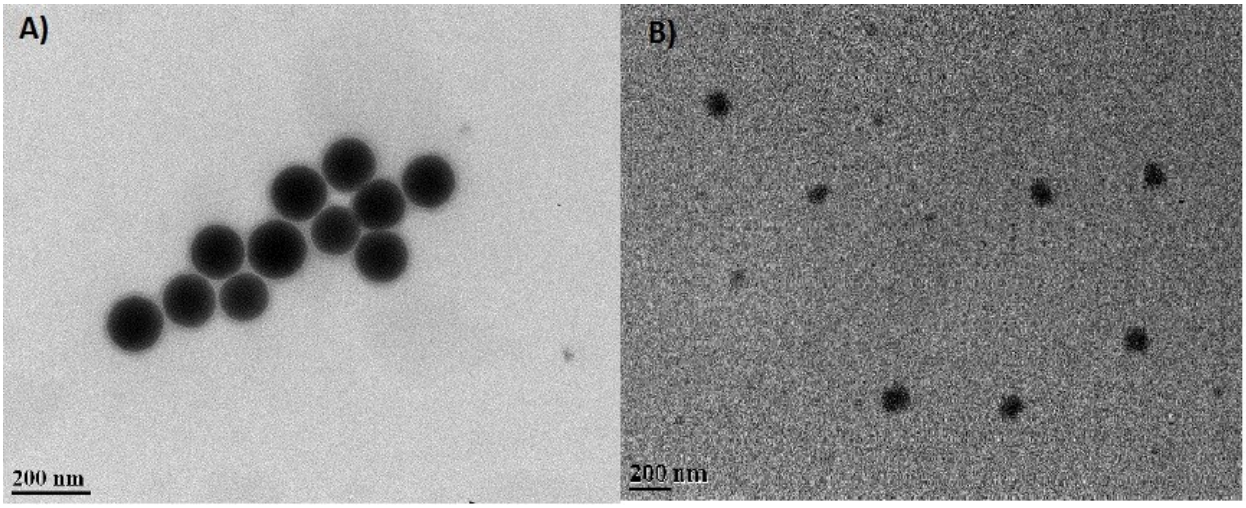

Figure S4. Transmission electron microscopy images of A) NG4 and B) NG6 synthesized via RAFT process. Scale bar = 200 nm.

Appendix B

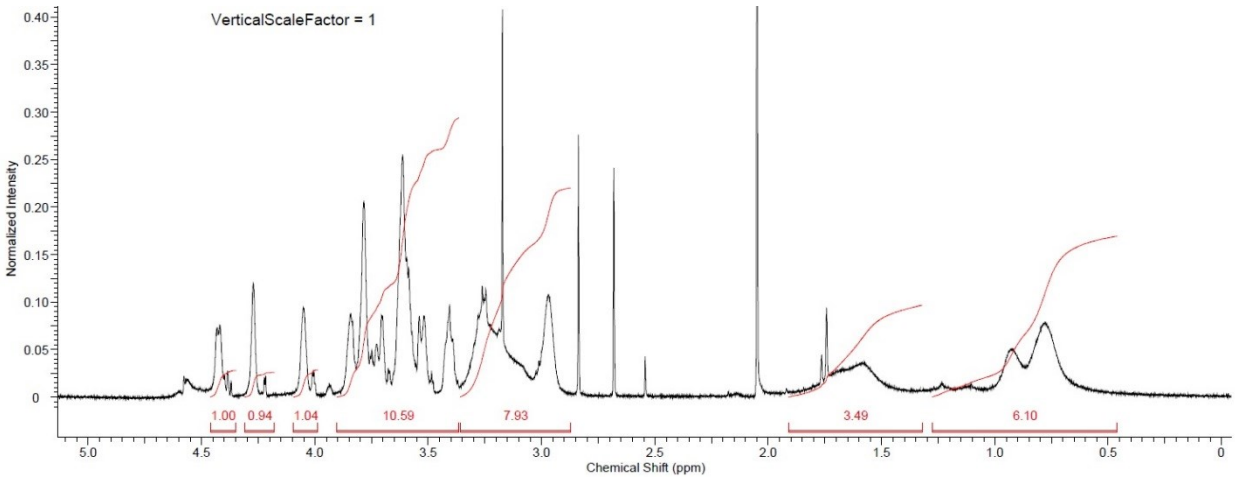

Figure S1. ^{1}H NMR (D_20) spectrum for P($AEMA_{50}$)-*st*-($LAEMA_{45}$).

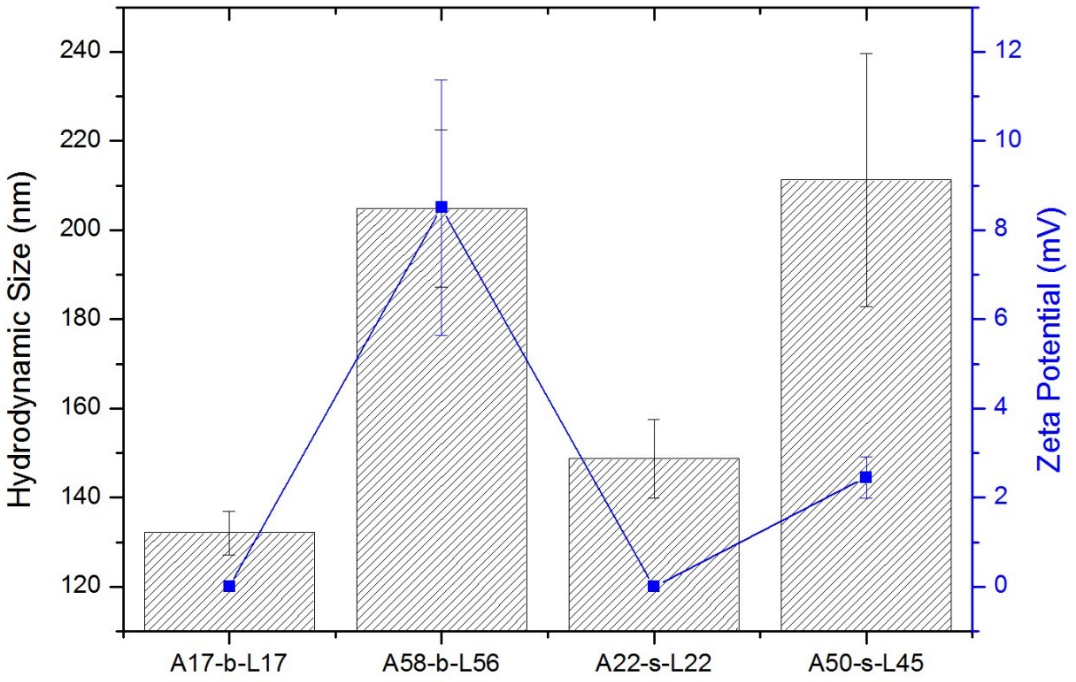

Figure S2. Hydrodynamic size and charges of glycopolymer-siRNA complexes in OMEM with 10% FBS determined by DLS and zeta potential instrumentation.

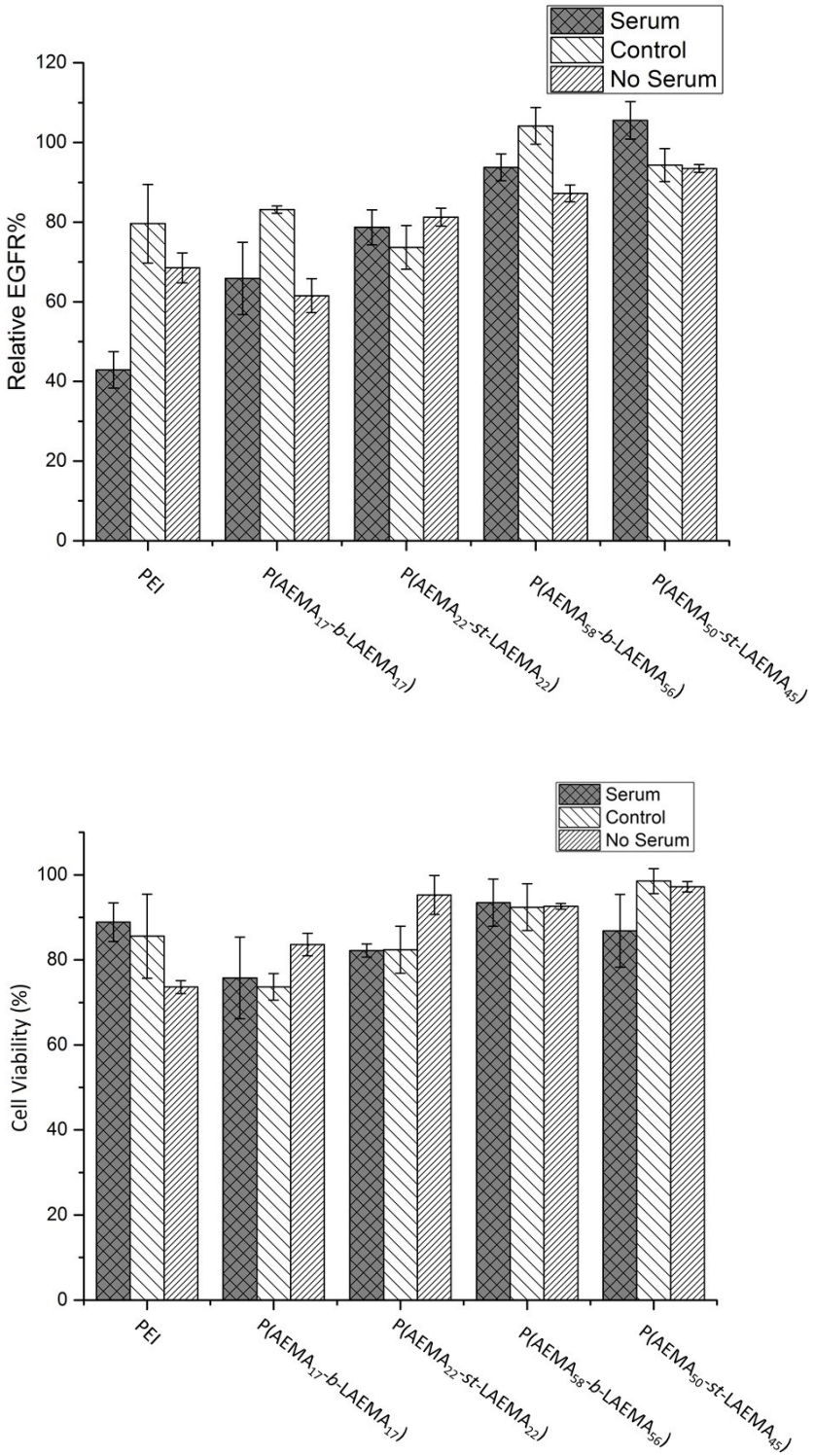

Figure S3. Relative percent of EGFR expression on cell surface of HeLa cells 48 h post-transfection with EGFR or control siRNA (250 ng or 0.2 nmol) and cell viability of HeLa cells 48 h post-treatment with siRNA of control polyplexes in OMEM with 10% FBS, as determined by Janus Green assay.

Table S1. Determination of molecular weight (*Mw*) and polydispersity (PDI) of macroCTAs by gel permeation chromatography (GPC).

MacroCTA	GPC (g/mol)	PDI (Mn/Mw)
P($AEMA_{58}$)	9705	1.159
P($AEMA_{17}$)	2943	1.23